Formation and disruption of tonotopy in a large-scale model of the auditory cortex

Tomková, M., Tomek, J., Novák, O., Zelenka, O., Syka, J., & Brom, C.

Note:

This is the authors' version of the manuscript, which may differ from the article's final version.

Please, cite this work as:

Tomková, M., Tomek, J., Novák, O., Zelenka, O., Syka, J., & Brom, C. (2015). Formation and disruption of tonotopy in a large-scale model of the auditory cortex. *Journal of computational neuroscience*, *39*(2), 131-153.

The final publication is available at Springer via http://dx.doi.org/10.1007/s10827-015-0568-2.

First online: 07 September 2015

Journal of Computational Neuroscience manuscript
The final publication is available at Springer via http://dx.doi.org/10.1007/s10827-015-0568-2

Formation and disruption of tonotopy in a large-scale model of the auditory cortex

Markéta Tomková · Jakub Tomek · Ondřej Novák · Ondřej Zelenka · Josef Syka · Cyril Brom

Received: date / Accepted: date

Abstract There is ample experimental evidence describing changes of tonotopic organisation in the auditory cortex due to environmental factors. In order to uncover the underlying mechanisms, we designed a large-scale computational model of the auditory cortex. The model has up to 100 000 Izhikevich's spiking neurons of 17 different types, almost 21 million synapses, which are evolved according to Spike-Timing-Dependent Plasticity (STDP) and have an architecture akin to existing observations. Validation of the model revealed alternating synchronised/desynchronised states and different modes of oscillatory activity. We provide insight into these phenomena via analysing the activity of neuronal subtypes and testing different causal interventions into the simulation. Our model is able to produce experimental predictions on a cell type basis. To study the influence of environmental factors on the tonotopy, different types of auditory stimulations during the evolution of the network were modelled and compared. We found that strong white noise resulted in completely disrupted tonotopy, which is consistent with *in vivo* experimental observations. Stimulation with pure tones or spontaneous activity led to a similar degree of tonotopy as in the initial state of the network. Interestingly, weak white noise led to a substantial increase in tonotopy. As the STDP was the only mechanism of plasticity in our model, our results suggest that STDP is a sufficient condition for the emergence and disruption of tonotopy under various types of stimuli. The presented large-scale model of the auditory cortex and the core simulator, SUSNOIMAC, have been made publicly available.

Keywords Auditory cortex · Large-scale model · Spiking neuron · Oscillation · STDP · Tonotopy

M. Tomková (✉) · J. Tomek · C. Brom
Faculty of Mathematics and Physics, Charles University in Prague, Czech Republic
E-mail: marketa.tomkova@stcatz.ox.ac.uk

O. Novák (✉) · O. Zelenka · J. Syka
Department of Auditory Neuroscience, Institute of Experimental Medicine, Academy of Sciences of the Czech Republic, Prague, Czech Republic
E-mail: ondrej.novak@biomed.cas.cz

M. Tomková · J. Tomek
Life Sciences Interface Doctoral Training Centre, University of Oxford, United Kingdom

1 Introduction

Much energy has been invested into the research of neural plasticity in the auditory cortex (AC). One aspect of this has been aimed at addressing changes in tonotopy (the spatial organisation of the AC according to sound frequency) during the critical period and its dependence on the acoustical environment and external stimulation (de Villers-Sidani et al., 2007; Nelken, 2014; Zhou et al., 2008; Zhang et al., 2001; Kim and Bao, 2009). The AC of animals reared under normal laboratory conditions (including a normal acoustical environment) develops properly, however under certain artificial acoustical conditions, the arrangement of the AC fails to develop normally, especially under relatively loud continual white noise (Zhang et al., 2002; Chang and Merzenich, 2003; Insanally et al., 2010). As the outcomes of *in vivo* research in this field are still more descriptive than explanatory, the fundamental mechanisms underlying such observations remain poorly understood.

What are the principles underlying the development of tonotopy under normal conditions and its disruption during noise rearing? How does tonotopy emerge in the non-input layers of the AC? Does it emerge inherently based on the network architecture, or is it dependent on some specific stimuli? Is it that the noise present in rearing actually disrupts tonotopy, or is it that it is merely preventing its formation? What mechanisms are responsible for the disruption of

tonotopy? Can we replicate *in silico* the lack of tonotopy as a consequence of noise rearing using simple learning rules (such as Spike-Timing-Dependent Plasticity)?

In order to address these questions, we designed a computational spiking neuron model of the primary auditory cortex (A1), presented several different inputs to the main input layer (layer IV, further referred to as L4) and observed the resulting tonotopy of the network. Besides the study of the development of tonotopy, we also investigated basic principles of functioning of a cortical network with a possibility to perturb the system and observe the causal consequences. Further we wanted our results to be straightforwardly comparable with the observations from *in vivo* experiments on a neuronal type basis. We emphasise that our model is not intended to be a minimal model replicating the studied phenomena, but rather a universal and extensible model that can be used to study a wide range of phenomena and give new hypotheses that can be later tested *in vivo*.

Computational modelling of the AC is a rather unexplored topic. Despite the existence of several published models, there are far fewer in comparison to visual cortex models or models of the lower stages of the auditory pathway. To the best of our knowledge, there are currently only four spiking neuron models of A1 as summarised in Table 1, all of which have very limited sizes and variety of neuronal types and connectomes. In their particular case, the models seem appropriate and sufficient. Three of the models use the Leaky Integrate and Fire (LIF, I&F) model of the neuron (Lapicque, 1907; Knight, 1972) which is considered to be one of the least plausible spiking neuron models, unable to replicate the most fundamental properties of cortical spiking neurons (Izhikevich, 2004). Of the four, only the model by Pinho et al. (de Pinho and Roque-da Silva, 1999; de Pinho et al., 2006) was used to observe tonotopy, but the description of their experiments and results seems incomplete and leads to very difficult reproducibility.

Our proposed model differs from the previous works in several aspects. It adopts the Izhikevich neuron model (Izhikevich, 2003, 2007), considered to be one of the most plausible models applicable in the modelling of large-scale neural networks (Izhikevich, 2007; Schutter, 2009). In addition, the model contains synapses with axonal conduction delays and synaptic weights that evolve according to long term plasticity in a form of the Spike-Timing-Dependent Plasticity (STDP) learning rule (Markram et al., 1997; Yuste and Denk, 1995; Song et al., 2000). The network architecture of our model was adapted from the *large-scale model of the mammalian cortex* proposed by Izhikevich and Edelman (2008), in which the numbers and probabilities of particular synaptic connections were based on real observations from cat visual cortex (Binzegger et al., 2004). Throughout our experiments, we used networks with at least 50 000 neurons in order to obey the numbers and types of synaptic connections as described in (Izhikevich and Edelman, 2008). On the other hand, as we focused on experiments with development, we also needed rather long simulations. Altogether, we decided to use a spiking neuron model (with the basic units being synapses and neurons) as an ideal trade-off between level of detail and computational efficiency. Up to 100 000 neurons with almost 21 million synapses and 17 neuronal types are included in the model.

Our main experiments focus on the arrangement of the developing neural network during the critical period, which in real rodents can take up to two weeks (de Villers-Sidani et al., 2007; Chang and Merzenich, 2003). Therefore, the length of simulation was maximised within our capabilities. We modelled evolutions as long as 12 hours of simulated time. Although this might seem too short, we observed strong differences in degree of tonotopy due to the different types of stimulation.

Our model also proved to be robust enough to enable observing the individual cortical mechanisms at a cellular level. As a proof of concept we performed two types of network perturbations and discuss their consequences. In the first case, we manipulate the conduction delays between basket cells in the layer L2/3 and discuss the effects of this perturbation on gamma oscillations. In the second case, we switch off one of the cell types and show that this perturbation substantially changes the behaviour of the system both on second and millisecond time scales.

To make our findings reproducible, we conform to the guidelines suggested by Nordlie et al. (2009) when describing the model. In addition all the used code and parameters are open source. A simulator SUSNOIMAC (Simulator Using Spiking Neurons Originally Intended for Modelling Auditory Cortex) was developed for simulating and analysing spiking neural networks. SUSNOIMAC can be used for further experiments with the presented model of A1 via user-friendly parameterisation. The simulator is designed in a way that more modules can be later connected. New models can be developed and simulated using the simulation core of SUSNOIMAC with only intermediate knowledge of Java.

2 Methods

2.1 Model architecture

Our proposed A1 model is divided into five layers: L1, L2/3, L4, L5 and L6. The thicknesses of the layers (69, 235, 208, 248 and 451 μm) are set according to experimental observations from mouse somatosensory cortex (DeFelipe et al., 2002). The area of the modelled network, 2000 $\times$ 3000 μm, is taken as a maximal estimation of the real A1 together with the ultrafield, a neighbouring auditory cortical area of the A1 often considered a continual extension of the A1 (Stiebler et al., 1997). The model contains several

Table 1 An overview of published models of the AC. Number of neurons refers to the number of neurons in the AC part of the model (some models contained other parts as well). HH-type is a model based on Hodgkin and Huxley (1952) model of neuron.

Model	Number of neurons	Neuronal types	Model of neuron	Synaptic plasticity	Experiment duration	Biological motivation
(de Pinho and Roque-da Silva, 1999; de Pinho et al., 2006)	4512	2	HH-type	-	≤ 10 s	Tonotopic organisation
(Larson et al., 2009, 2010)	20	1	LIF	STDP	≤ 10 s	Songbird recognition
(Chrostowski et al., 2011)	268	2	LIF	Homeostatic	≤ 30 s	Travelling waves and their relation to hearing loss
(Zhou et al., 2012)	2400	3	LIF	-	≤ 10 s	Spike latency tuning
This article	up to 100 000	17	Izhikevich	STDP	up to 12 h	Tonotopic organisation disrupted by noise

types of neurons, including excitatory pyramidal (p) regular spiking (RS) neurons, excitatory spiny stellate (ss) RS neurons, inhibitory basket (b) interneurons with fast spiking (FS) firing patterns and inhibitory non-basket (nb) interneurons, which morphologically include double-bouquet cells, neurogliaform cells, and Martinotti cells (Binzegger et al., 2004). The nb interneurons can exhibit low threshold spiking (LTS) firing pattern (Beierlein et al., 2003), latent spiking (LS) and other firing patterns (Kawaguchi, 1995; Kawaguchi and Kubota, 1997; Markram et al., 2004). The architecture and the connectome are based on the cortical part of the large-scale model of mammalian thalamocortical systems by Izhikevich and Edelman (2008). We distinguish 17 types of neurons: p2/3, ss4(L4), ss4(L2/3), p4, p5(L2/3), p5(L5/6), p6(L4), p6(L5/6), nb1, nb2/3, b2/3, nb4, b4, nb5, b5, nb6, b6, where the name is based on the morphology, the layer of the soma and the layer of the main target in parentheses. Since the detailed connectome of A1 is still unknown, we use data published by Binzegger et al. (2004) from area 17 of the visual cortex in cats, as used in (Izhikevich and Edelman, 2008). The connectome is generated according to a three-dimensional table that sets the numbers of synapses from different presynaptic neuronal types that each neuron should receive within a certain layer (Izhikevich and Edelman, 2008). Nearer neurons have a higher probability of connection than distant ones (Izhikevich and Edelman, 2008; Levy and Reyes, 2012). A synapse can be created only between such neurons where the soma of a postsynaptic neuron is reached by the axonal area of a presynaptic neuron. These axonal areas are specified for each neuronal type as the axonal radii for each layer of the network, as shown in Fig. 1. The axonal areas represent the area reached by the axon and its terminals. We use the same values as Izhikevich and Edelman (2008). The details of the connectome (as well as possible boundary effects) are described in the Supplementary materials (Section 1.3).

The same model has been explored with different numbers of neurons: 50 000 and 100 000 (with 10 053 066 and 20 815 126 synapses, respectively). We note that no scaling of synapses was necessary, since the planned number of synapses per postsynaptic neuron is constant in the algorithm of generating synapses, i.e., each neuron of a given type receives on average an equal number of synapses, independently of the network size. However, if the network is too sparse, a synapse can fail to be created (because no suitable presynaptic neuron of a given type exists within an allowed distance). For this reason, we found networks smaller than 50 000 neurons ill-suited for our purposes. In a network with 1 000 neurons, only 43.8% of planned synapses would be created, or 75.2% in the case of a network with 10 000 neurons. The omission of so many synapses can severely affect the balance of the planned connectome, which would go against our aim of building a model using established experimental data whenever possible. In networks with 50 000 and 100 000 neurons, 95.1% and 98.5% of planned synapses were created, which we deemed sufficient.

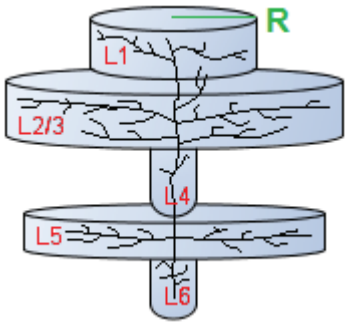

Fig. 1 An example of axonal areas. In each layer, the axonal area is specified by its radius R.

The approximate number of neurons in the real A1 is estimated to be $\approx 300\,000$–$500\,000$ (Ouda et al., 2011) with the upper limit of 500 000–1 000 000 based on densities in the mouse cerebral cortex (even though not only AC) (DeFelipe et al., 2002). Compared to these numbers, our largest neural network is only three to ten times smaller than in real mice.

2.2 Model architecture

Izhikevich's neuron model (Izhikevich, 2007) is used in the following form:

$$\begin{aligned} C\frac{dv}{dt} &= k(v-v_r)(v-v_t)-u+I_{syn}(t) \\ \frac{du}{dt} &= a(b(v-v_r)-u) \end{aligned} \tag{1}$$

with the auxiliary after-spike resetting:

$$\text{if} \quad (v \geq v_p) \quad \text{then} \quad v \leftarrow c, \quad u \leftarrow u+d, \tag{2}$$

where v is the membrane potential, u represents a membrane recovery current, C is the membrane capacitance, $I_{syn}(t)$ is the input current, v_r is the resting membrane potential, v_t is the instantaneous threshold potential, v_p is a spike cut-off value (the peak) and a, b, c and d are parameters of the model, specified for each neuronal type. Depending on the parameter values, the neuron model reproduces the dynamics of all neuronal types used in our network. Parameter values as listed in Table 2 are taken from (Izhikevich and Edelman, 2008).

The input current $I_{syn}(t)$ of a given neuron N_{post} in time step t is computed as:

$$I_{syn}(t) = I_{ext}(t) + \sum_{i=1,\ldots,k} w_{s_i}, \tag{3}$$

where $I_{ext}(t)$ represents external stimulation (only relevant in input layer neurons, when stimulation is present), $s_1,\ldots,s_k$ are synapses via which an action potential arrived at time step t to the neuron N_{post}, and w_{s_i} is the weight of synapse s_i.

Table 2 The used values of the parameters of the neuron model based on the type of the neuron: RS pyramidal and spiny-stellate neurons, FS basket interneurons, LS non-basket interneurons in L1, and LTS non-basket interneurons in the other layers.

Label	C	k	v_r	v_t	v_p	a	b	c	d
LS (nb1)	20	0.3	-66	-40	30	0.17	5	-45	100
RS (p)	100	3	-60	-50	50	0.01	5	-60	400
FS (b)	20	1	-55	-40	25	0.15	8	-55	200
LTS (nb)	100	1	-56	-42	40	0.03	8	-50	20

Each synapse has a given conduction delay that represents the time required for signal transmission along the axon. The delays are set and fixed when the network is first initialised. The values are proportional to the distances of the somata of presynaptic and postsynaptic neurons and are perturbed by a random number of milliseconds (ms) from a uniform distribution ranging from 0 to 5 (further written as Uniform(0, 5)). The resulting delays are truncated to the range 1–20 ms. The synaptic weights (efficacies) of neurons are initiated randomly; for excitatory neurons from Uniform(0, 100) and inhibitory neurons from Uniform(-50, 0) with units of picoamperes (pA). The inhibitory synaptic weights are constant. The excitatory synaptic weights develop according to constant Spike-Timing-Dependent-Plasticity (STDP).

The weight of a synapse between presynaptic and postsynaptic neurons is increased by the value of $G(\Delta t)$:

$$G(\Delta t) = \begin{cases} A_+ \cdot e^{\Delta t/\tau_+} & \text{if } \Delta t < 0 \quad \{ \text{ LTP part } \} \\ -A_- \cdot e^{-\Delta t/\tau_-} & \text{if } \Delta t > 0 \quad \{ \text{ LTD part } \}, \end{cases} \tag{4}$$

where Δt is an interval between presynaptic spike arrival and postsynaptic spike, τ_+ and τ_- are 20 ms, A_+ is 1 and A_- is 1.2, as it is in (Izhikevich, 2006). See Supplementary materials (Section 1.3) for a detailed description of the initialisation of delays and weights.

Real brain neocortical networks produce activity even in the absence of any sensory stimuli (Arieli et al., 1995). One of the mechanisms underlying this spontaneous activity is the phenomenon of miniature postsynaptic currents (mPSCs) called "minis" (Timofeev et al., 2000), which correspond to the spontaneous release of neurotransmitters independent of presynaptic spikes. Modelling minis is a classical approach to introduce spontaneous activity and reach homeostasis (Izhikevich and Edelman, 2008; Phoka et al., 2012; Muresan and Savin, 2007; Timofeev et al., 2000). In our model, minis are simulated to occur on each synapse with frequency F (Hz) and amplitude A (pA). Values used were F = `scalingFactor`$\cdot$ 3 Hz, A = 13 pA[1] corresponding to measured physiological values in the AC: $F = 3.3 \pm 0.2$ Hz and $A = 12.7 \pm 1.4$ pA (Kotak et al., 2005).

The time step of the simulation is set to 1 ms. To ensure numerical stability, each neuron is simulated with a time step of 0.5 ms using the first-order Euler method of integration (as in, e.g., Izhikevich, 2003, 2004, 2006).

2.3 Sensory stimulation

The main input sources from the lower stages of the auditory pathway to the real A1 are inputs from the auditory thalamus (ventral and dorsal medial geniculate bodies) and their major recipient is the layer L4 (Watson, 2012; Wu et al., 2011; Cruikshank et al., 2002; Kimura et al., 2003; Romanski and LeDoux, 1993; Winer and Lee, 2007; Barbour and Callaway, 2008). These inputs are topographically organised to form a gradient of frequency representation, reflecting the tonotopic organisation within the auditory thalamus

[1] The `scalingFactor` is equal to 20 and corresponds to scaled density of synapses in comparison to the real cortex and is adopted from (Izhikevich and Edelman, 2008).

(Watson, 2012; Schreiner et al., 2000; Winer, 2006). Our model incorporates these facts. Each neuron in the L4 layer can get, in each time step, an external input $I_{ext}(t)$, see eq. 3. This represents stimulation from neurons in the thalamus. In the following text, this stimulation is referred to as *external stimulation*.

Since we did not model the thalamus and any lower stage of the auditory pathways explicitly, a simplified approximation of how the original sound stimulus is processed in these stages was used. We only focus on two main characteristics of the sound: amplitude and frequency. We are truly aware of how important and extensive the subcortical processing in the auditory system is (Šuta et al., 2013, 2007; Syka et al., 2005; Šuta et al., 2003), however, we decided to use this level of simplification in order to have an easy-to-analyse model with clear interpretation of its input. However, the architecture of the model is modular and lower stages of the auditory pathways can be added later.

The modelled layer L4 is divided into 50 bands. Each band corresponds to a specific frequency of the sound stimulus. Since the exact values of these frequencies are not important, only their order, we will refer to them in this article by the indices of the bands (1–50).

The input of a given frequency is modelled as a set of independent and identically distributed (i.i.d.) constant-rate Poisson processes (one for each neuron in the respective frequency band) with its rate parameter reflecting the amplitude of the stimulation. Again, the exact values of the amplitude are not important and the strength of external input can be expressed as a probability that each input neuron in a band representing the used frequency will be stimulated in a given time step. When stimulation occurs to an input neuron, the strength of stimulation has been chosen as 1 500 pA, representing an input from several thalamic neurons.

In the presented experiments, three types of inputs were used: *spontaneous activity*, *pure tones* and *noise*.

During spontaneous activity, neurons receive no input from the thalamus and minis are the sole source of activity.

During pure tones, neurons in selected bands in L4 are stimulated with a certain probability representing the strength of stimulation. In our experiments, we tested development of the network with 5 (*pureTones5*) and 25 (*pureTones25*) pure tones, each lasting 500 ms.

During noise, each neuron in L4 is stimulated with a given probability (i.e., modelled as a set of i.i.d. constant-rate Poisson processes). In our experiments, a range of probability parameters of the noise input (ranging from 0.01 to 0.5) was tested.

2.4 Computer implementation

For all experiments, our network simulator SUSNOIMAC was used (Popelová, 2013). The simulator is freely available[2] along with the model and parameters used in the experiments presented in this publication. The whole software package consists of two parts: the simulator itself (written in Java, using parallelisation) and a Matlab toolbox for analysis of the simulator's outputs. As a pseudorandom number generator, the Mersenne Twister method (Matsumoto and Nishimura, 1998) was used, as one of the best PRNGs in terms of its combination of high degree of randomness and efficiency. The implementation of this method was provided by the Colt Parallel Java library (Wendykier and Nagy, 2010; Wendykier, 2013).

An important feature of SUSNOIMAC is the possibility to suspend a simulation and compute an experiment on the current state of the network in an "alternative reality" and then continue with the original experiment. This is particularly useful for "measuring experiments" that measure the network states several times during development. In these experiments, it is often necessary to present given stimuli to the network and measure the corresponding reaction. The alternative reality solution ensures that the simulation is not affected by any measuring experiment.

A simulation of one second of the model with 100 000 neurons (and $\approx$ 21 million of synapses) requires $\approx$ 33.73 s of computational time on a single-processor PC[3]. In total, we have computed ca. 180 experiments of more than 300 h of simulated time, taking more than 300 days of computational time.

3 Results

First, we performed validation of the model and analysis of its basic properties: development of the network under spontaneous activity (3.1), analysis of network oscillations and reactions of the network to perturbations (3.2) and how network reactions spread across layers in response to external stimulation (Supplementary materials, Section 2.1.1). Then we performed experiments studying tonotopic organisation after development under different acoustic stimuli (3.3).

3.1 Evaluation of spontaneous activity

First, we analysed network behaviour under spontaneous activity only. In these experiments, STDP was activated during the entire development and the sole source of activity was spontaneous activity with no external stimuli. We compared two different network sizes: 50 000 and 100 000 neu-

[2] Licenced under Creative Commons Attribution-NonCommercial-ShareAlike 4.0 International Public Licence. The code is at `https://sites.google.com/site/susnoimac`, last accessed: September 7, 2015.

[3] Processor: Intel(R) Core(TM) i7 930 @ 2.80 GHz, RAM: 16 GB, OS: Windows 7.

rons, which we are referring to as 50k and 100k later in the text.

3.1.1 The network activity

The network activity of the first 30 min of development under spontaneous activity of a 50k network is shown in Fig. 2. As we can see in Fig. 2A, after an initial period of stabilisation (ca. 8 min), the network reaches a "stereotypical dynamic state", in which the mean activity of individual neuronal types regularly rises and falls. This stereotypical activity is sometimes (e.g., after ca. 7 and 25 min in the 50k network (2A)) interrupted with a distinct "bump" of increased activity of nb cells, but then the original activity is reestablished. In other words, we did not see any persistent deviation from the "stereotyped dynamical state" in all our experiments with a complete unperturbed network.

An example of two types of firing rate activity is shown in Fig. 2B. In the first type (referred to as state H), the activity of b2/3 and b5 cells decreases, whereas the activity of the other cells increases. These intervals last approximately 10–20 s. The other type of activity (state L) lasts approximately twice as long as H.

Fig. 2C shows a comparison of the average firing rate of individual neuronal types. The values were similar in both tested networks (see Supplementary materials, Section 2.1). The most active neuronal type was b2/3 with a mean firing rate of between 30 and 40 Hz (spikes/second) and the second most active neuronal type was b5 with a mean firing rate of between 10 and 15 Hz. The other neuronal types showed mean firing rates of between 1 and 5 Hz. The higher spontaneous firing rate of the basket cells is in agreement with observations from the real AC (Sakata and Harris, 2012); however, the absolute spontaneous firing rate of basket cells in our model nearly twice outnumbers the values from the real AC. This may be for several reasons, see Discussion (Section 4) for more details.

A comparison of the development of absolute values of mean firing rates of individual neuronal types during the first 15 min of development are shown in Fig. 2D. We can see that after the initial ca. 8 min, the network stabilises in the alternating H and L states and that this alternating activity is present in nearly all the neuronal types.

In order to get better insight into the course of the H and L states and a potential role of individual neuronal types in it, we computed and visualised derivatives of firing rates of individual neuronal types as follows: first, we found centres of the H states in the given period (ca. 10–25 min); then we overlaid the centres, computed the derivatives of the firing rates, and averaged them over all the H states (21 in this period). As we can see in the results (2E), the H state is initiated by increasing activity of nb cells and decreasing activity of b2/3 cells. Further investigation of the phenomenon of alternating states is given in Section 3.2 and Discussion (Section 4).

3.1.2 Reaching stereotypical dynamical state

In an intrinsically rhythmically behaving system, such as our model, the behaviour of the network does not stabilise absolutely, e.g., having constant firing rates and synaptic weights of cells. Instead, we use the expression "stereotypical dynamical state" to describe the phase of network development where a limited number of types of state occurs and there is no global trend in development of firing rates.

In both network sizes, the network reached a stereotypical dynamical state at most after eight minutes. The method used for this was to record a 30 minutes long simulation of networks, when no external input was applied. This recording was binned into minute-long segments and within each segment the mean firing rate of all the neurons was computed, along with the standard deviation of firing rates within the minute[4].

To test if there was not a trend in firing rates, suggesting a lack of stabilisation, a line was fitted through the 23 points of the mean firing rate, from the 8th to 30th minute, and the significance of its slope was tested using a regression slope test. In the networks sized 50 000 and 100 000, the mean firing rate was 4.22 Hz and 4.24 Hz respectively; the maximum standard deviation was 0.33 Hz, 0.32 Hz respectively, suggesting a rather small spread of firing rates. The regression slope test returned p value > 0.05 in both networks (i.e., no significant difference was found between the slope of the fitted lines and zero-slope line). Even though this does not show that the slope is significantly similar to zero, it nevertheless suggests that there is no global shift in firing rates. The results are visualised in the Supplementary materials in Section 2.1.

3.2 Network oscillations

For measurement of oscillations present in the network we again used a 50k network which had been evolved for 12 hours with spontaneous activity and then simulated this network for 8 min of spontaneous activity. Network oscillations were mostly measured from simulated probes. For i-th probe at time t, we define the recorded signal $p_i(t)$ at location l as:

$$p_i(t) = \frac{\sum_{\forall n \in N_{p_i}} u(n) \frac{1}{dist(n,l)}}{\sum_{\forall n \in N_{p_i}} \frac{1}{dist(n,l)}} \tag{5}$$

[4] The minute-long window contains sixty values of firing rate, one for each second in the window. The mean and standard deviation are computed from these sixty values.

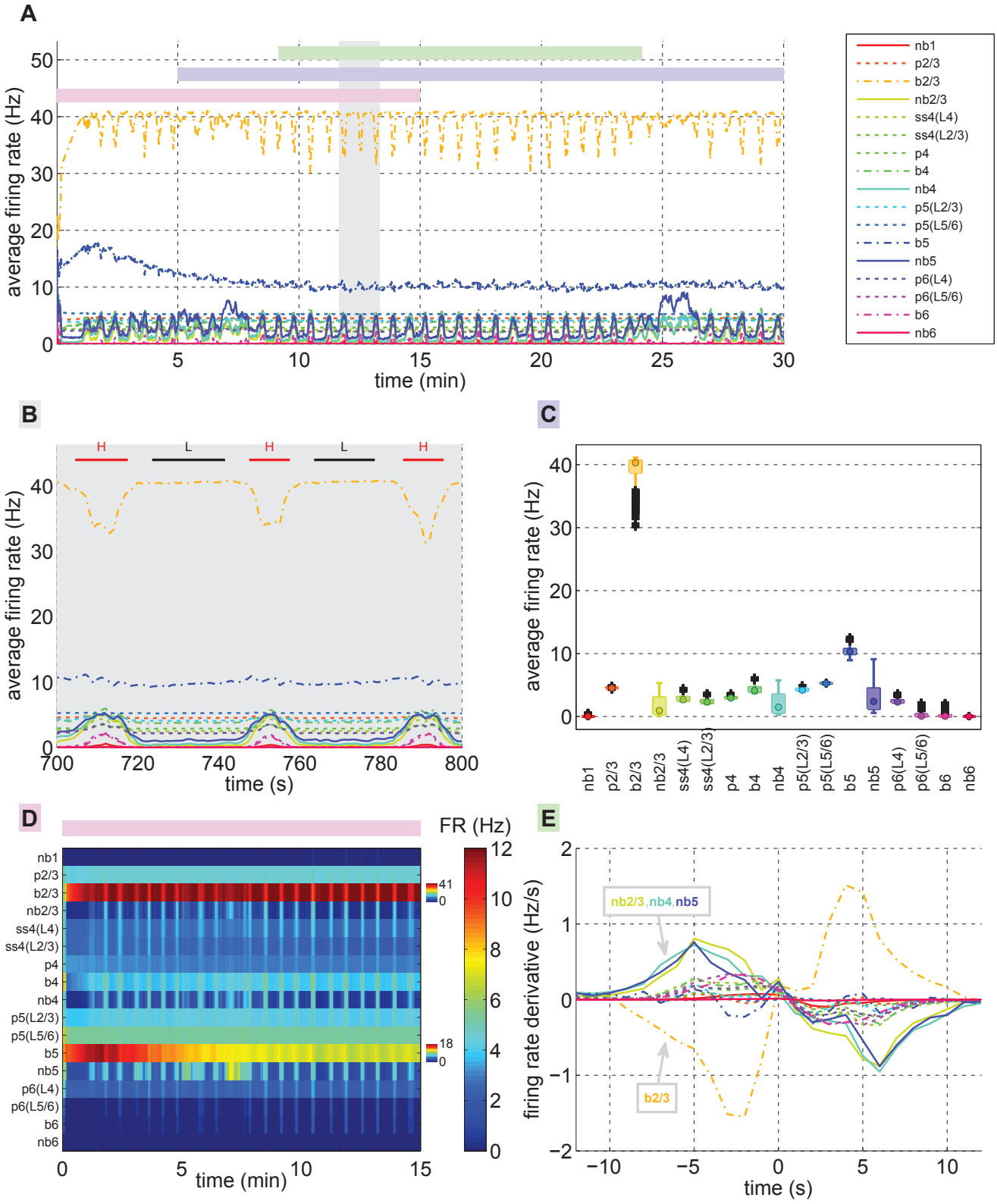

Fig. 2 Network activity of a 50k network during an experiment lasting of 30 minutes. **(A):** Mean activity of neuronal types over time. For each type, the mean activity was computed as the number of spikes of neurons of the given type in each second, divided by the number of neurons of this type. The neuronal types are coded by colour and line style (nb: solid line, b: dash-dotted line, p and ss: dotted line). The coloured stripes represent time intervals used for computation of the following parts of the image: (B): grey, (C): violet, (D): pink, (E): green. **(B):** An enlarged section of (A) with marked intervals of two types of firing rate activity (H, red) and (L, black). **(C):** A boxplot visualisation of firing rates of individual neuronal types (during 5–30 min). **(D):** Another visualisation of the stabilisation period of the network as in (A). The firing rate of individual cell types are colour-coded so that the behaviour of sparsely firing neuronal types can be clearly seen. Note individual colour bars for b2/3 and b5 types. **(E):** Averaged derivatives of firing rates during 21 H states (during 550–1450 s).

where N_{p_i} is the set of neurons within 75 µm of the probe, $u(n)$ is the potential of the neuron and *dist* is 3D Euclidean distance. Therefore, the recorded signal is essentially a weighted average of potentials of neurons near the probe with the weights being inversely proportional to the Euclidean distance of the cell to the probe. The signals from probes were further analysed using the Fourier transform of sliding time windows (each window of length 1 s; window shift 100 ms).

Various rhythms arose in the network: predominantly a theta-like oscillation (4–6 Hz), an alpha-like oscillation (8–12 Hz) and a spectrum of gamma oscillations (40–60 Hz). To reveal how these oscillations change during simulation, power spectra of the signal on the probes were analysed throughout time. In Fig. 3A, we show a spectrogram of a signal from one of the probes (each column represents a power spectrum for one time window, where the power is coded by colour). In Fig. 3B, summed power spectra in bands 3–7, 8–12, and 40–60 Hz are plotted (for each time step). In Fig. 3C, evolution of the mean of the excitatory weights over time is shown. Evolution of the (log) firing rates is shown in Fig. 3D. Finally, four examples of spike times, raster plots and power spectra from four different time windows are shown in 3E, F.

Three different states were present in the recorded data: *desynchronised*, and two types of synchronised: *theta-like* and *alpha-like*. Interestingly, theta-like states corresponded to the earlier mentioned H states and desynchronised states corresponded to the L states. Finally, alpha-like oscillations were measured in the "bumps" of increased activity of nb cells.

In a desynchronised state, any discernible network oscillations were suppressed (see, e.g., 300–301 s in Fig. 3E, F). During a theta-like state, strong theta-frequency oscillations were present (see, e.g., 30–31 s in Fig. 3E, F). The third, and least common state, alpha-like state is characterised by a strong alpha frequency component and generally happens in place of the more common theta-like state and not only as higher harmonic mode of the theta-like oscillation (see, e.g., 360–361 s in Fig. 3E, F). Similar alternations of synchronised and desynchronised states were observed *in vivo* in the AC in both anaesthetised (Sakata and Harris, 2012; Clement et al., 2008; Sakata and Harris, 2009) and unanaesthetised (Sakata and Harris, 2012) animals.

The low activity frequencies (theta and alpha) arose both as local (measuring using the probes as described earlier) and global oscillations (summing up the potentials of all cells in the network for each time step, not weighting them by distance). However, high activity frequencies (gamma) were present mostly as local oscillations. This is consistent with experimental observations that report gamma rhythms being weaker in global EEG recordings than in local recordings, such as LFPs and intracranial EEGs (Nunez and Srinivasan, 2006). These observations are also consistent with a large-scale model of the mammalian cortex by Izhikevich and Edelman (2008).

The plots in Fig. 3C, D suggest that changes in firing rates of certain neuronal types and synaptic weights are aligned with the synchronised/desynchronised states. We noticed in the Fig. 2E that the derivatives of firing rates seem to return to their original values, i.e., the theta-like state seems like it could restart immediately after it ends, while it is obviously not the case in our data when a desynchronised state occurs. We believe that this phenomenon is linked to the development of synaptic weights and non-linearity of the entire system, as shown in Fig. 3C, D, where synaptic weights slowly grow in desynchronised states, and then drop during a theta-like state.

3.2.1 Network perturbations

An advantage of studying network dynamics in a model as opposed to reality, is the option to easily adjust the model and observe the consequential changes in the network dynamics with the aim of deciphering the underlying mechanisms. As a proof-of-concept and an example of such an approach, we performed several simple perturbations and used them to observe changes in network dynamics. First, we focused on oscillations of the potential in the gamma band. The largest contribution to the global gamma oscillation power[5] is comprised of basket cells oscillations (Supplementary materials, Section 2.1.2). Out of the basket cells in our model, the strongest gamma pacemakers are the b2/3 cells (Fig. 4A). Other basket cells (b4, b5 and b6 cells) contribute much less. The gamma power is centred around ca. 50 Hz frequency. Relative contributions to basket oscillations in the gamma band (40–60 Hz) are depicted in Fig. 4A (89.9 %, 4.7 %, 5.2 % and 0.2 % for b2/3, b4, b5 and b6 cells, respectively).

Several theories concerning the source of gamma oscillations in cerebral circuits exist and often differ substantially, e.g., intrinsic basket cell oscillation (I) models, inhibitory-inhibitory (I-I) models or inhibitory-excitatory (I-E) models (Buzsáki and Wang, 2012).

In order to contribute to this discussion, we focused on the I-I model and performed some perturbations of the synaptic conduction delays between b2/3 cells (Fig. 4B). We started three experiments from a completely identical time point of a 50k network, which had been already evolved for 12 h under spontaneous activity evolution. Besides the new control run (blue line, delays 5.1 $\pm$ 1.6 ms; mean $\pm$ standard deviation) we let the network run with two different perturbations of the delays on connections between b2/3

[5] We focused only on desynchronised states and nearly desynchronised states in this analysis in order to have the largest oscillations in the gamma band.

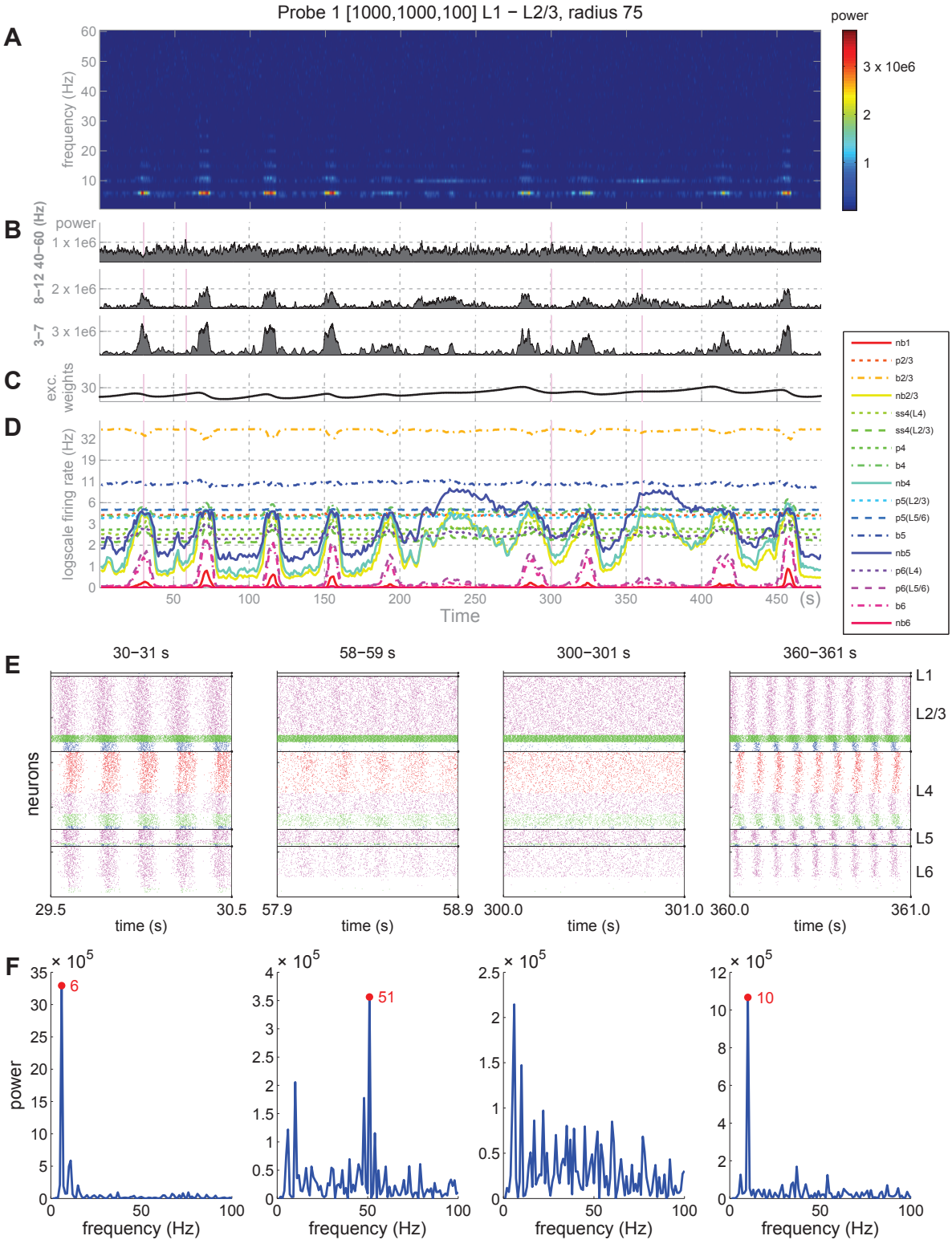

Fig. 3 The Fourier analysis of the signal from a single probe placed in L2/3 of the modelled cortex, aligned with firing rates and development of synaptic weights. **(A):** Powers of frequencies across time. **(B):** Summed powers of selected frequency bands. **(C):** Development of synaptic weights. **(D):** Development of firing rates (note the log-scale y-axis). **(E):** Visualisation of firings of the whole network in selected second-long time windows (these windows are marked by a pink vertical line in (B)–(D)). The neuronal types are colour-coded (p: magenta, ss: red, b: green, nb: blue). **(F):** Power spectra computed from the time windows above them. Note the different scales of the y-axes.

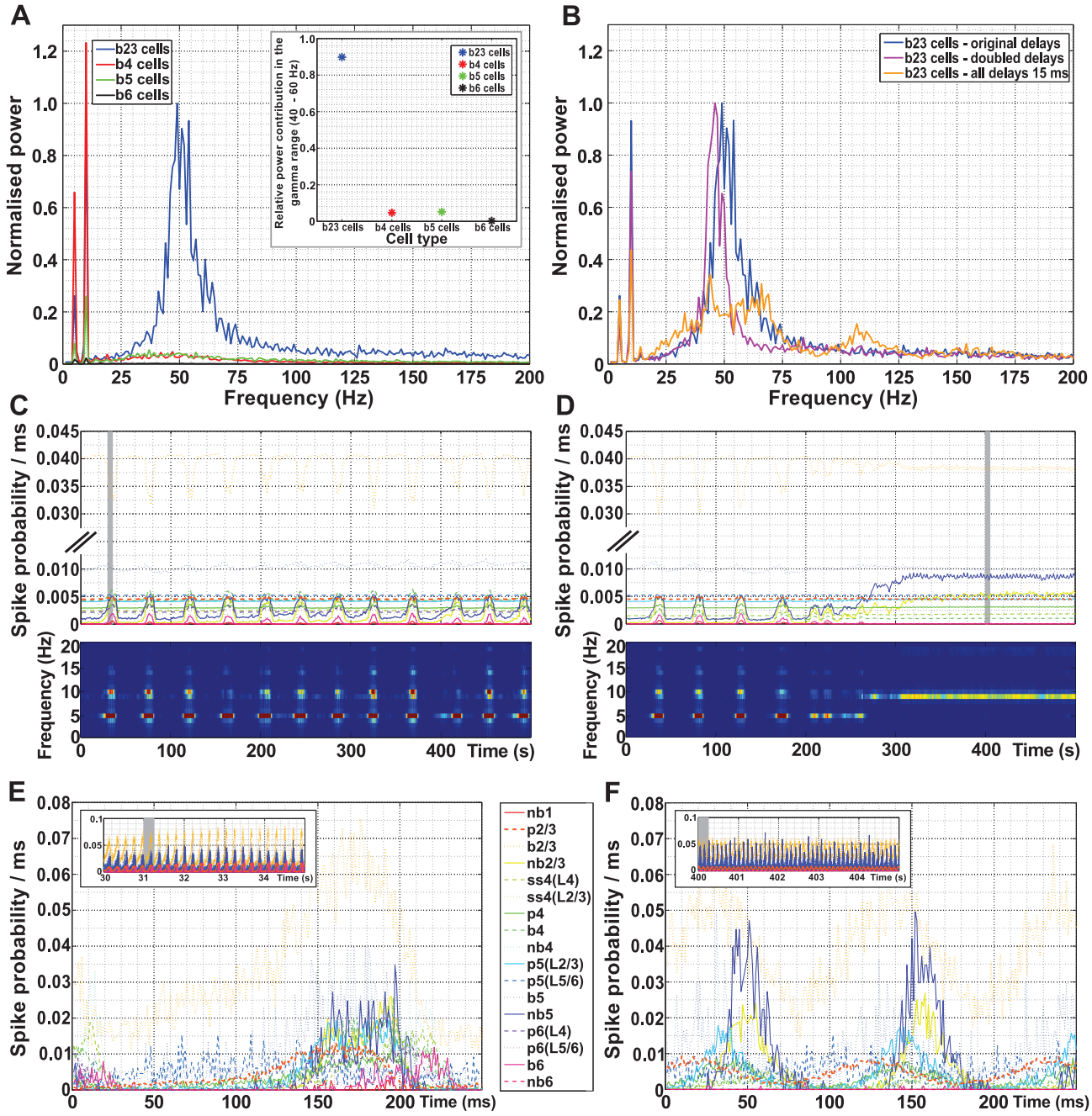

Fig. 4 Characterisation of normal and perturbed evolution of a matured 50k network. **(A):** Normalised potential power spectra of basket cells from different cortical layers; the potentials were averaged over all b cells in particular layer and the spectra were normalised in such a way that they were divided by the maximal value in the power spectrum of b2/3. Inset: Summed power of the spectra in the gamma range (40–60 Hz). **(B):** Power spectra of the averaged potential of b2/3 cells with original and perturbed mutual conduction delays. The original delays 5.1 ± 1.6 ms (mean ± standard deviation), blue line, were in one case changed to double values 10.2 ± 3.2 ms, magenta line, and in the second case all the delays were set to 15 ms, orange line. **(C):** Firing activity of different cell types on a large time scale (firing averaged over each second; neuronal types colour-coded: see legend in between (E) and (F)) and a spectrogram of the firing rate containing the three principal oscillatory states. **(D):** The same plot and spectrogram as in (C), but the p6(L4) cells were turned off at the beginning (time = 0). Note the interrupted y-axis in the upper parts of the two latest figures. **(E):** Firing activity of different cell types during with 1 ms resolution (a grey area in the inset). Inset: Zoomed grey area from (C), where the activity is averaged over each second. **(F):** Firing activity of different cell types with 1 ms resolution from a simulation with turned off p6(L4) cells (a grey area in the inset). Inset: Zoomed grey area from (D), where the activity is averaged over each second.

cells: First, all the original delays were doubled (magenta line, delays 10.2 ± 3.2 ms). Second, all the delays were set to 15 ms (orange line). Doubling the delays led to a ca. 5 Hz decrease of the centre frequency of the gamma peak (Gaussian fit of the gamma peak: for original delays, blue line, centre = 51 Hz, sigma = 8.3 Hz; for doubled delays, red line, centre = 46 Hz, sigma = 5.6 Hz). Setting all the delays to 15 ms led to a disintegration of the gamma peak and three separated local maxima appeared instead. These data suggest that coupling between b2/3 cells plays an important role in the process of generating gamma oscillations and the mechanism is somewhat resistant to a moderate perturbation of the connection delays (see Discussion, i.e., Section 4). To exemplify the potential to investigate the impact of silencing a certain cell type, we turned off a specific cell type, p6(L4). As a control, an evolved 50k network was allowed to run unperturbed. In Fig. 4C a regularly oscillating stereotypical dynamic state of the network can be seen. In the case of turning the p6(L4) cells off in the beginning of the run (Fig. 4D), the system evolved normally only at the beginning and then collapsed into the alpha-like state, suggesting the importance of p6(L4) neurons for normal function. Differences in firing activity between the two experiments (control and p6(L4) turned off) can also be studied on a finer time scale (see Fig. 4E and 4F).

The important principle of our simulator is that it enables the investigation of contribution made by individual cell types to the networks behaviour, e.g., cortical oscillations. The use of the alternative reality enables such experiments to be performed in a casual manner.

3.3 Tonotopy-related experiments

The tonotopy-related experiments researched network development under different external sound stimuli. First, we designed and ran 20 experiments: all combinations of five types of input, two sizes of network and two randomisation seeds. In the following text these experiments are referred to as *main tonotopy-related experiments*. Based on the results, we designed and ran seven *additional tonotopy-related experiments* that explored seven additional intensities of the noise input. Below, we describe the methodology common to all experiments and the results from both groups of tonotopy-related experiments.

3.3.1 Methodology of analysis of results

Each experiment and analysis of its results have the same structure as depicted in Fig. 5.

First, the development of the network is simulated. In given times during development, the degree of tonotopy is measured in an alternative reality. In this measurement, a battery of 250 pure tones (all 50 bands, each with five intensities: 0.2, 0.35, 0.5, 0.65 and 0.8) is presented to the network ten times. Each pure tone lasts 100 ms and is followed by 400 ms of silence (only spontaneous activity is present). The pure tones in the battery are ordered randomly, but the same permutation is used for each of the ten repetitions. Each tonotopy measurement lasts $10 \cdot 250 \cdot 500$ ms = 1 250 000 ms of the simulated time. During the measurement the synaptic weights are fixed. The spike trains from all neurons are recorded during the entire measurement.

Subsequently the *receptive field* (RF) and the *summed receptive field* (summedRF) are computed for each neuron from the recorded spike trains. The RF is a matrix of 50 bands $\times$ 5 intensities, containing spike counts for the given inputs. The summedRF refers to the RF summed over all intensities. According to the summedRF, it is determined which neurons will be called *tuned* and what will be their *best frequency* (BF). To be labelled as tuned, a neuron had to fulfil two conditions. First, it had to fire at least once during the measurement. Second, it had to prefer only one band or an interval of neighbouring bands. To determine this, *relativeThreshold* was defined as `percentage` $\cdot$ maxVal, where `percentage` is a parameter and maxVal is the highest number in summedRF. In our analysis, `percentage` = 90% was used. Then, the indices of bands with a summedRF value greater than the relativeThreshold formed an interval (in other words, a contiguous set of indices).

If a neuron was tuned, its BF was taken as a mean value of bands above relativeThreshold. For examples of tuned and untuned neurons, see Fig. 6.

To visualise the BFs of the tuned neurons in the entire network, a *spatial visualisation* was used. The tuned neurons were plotted as a 2D projection of the modelled cortex with colours corresponding to their BFs (blue being band 1 and red band 50). In a totally tonotopic network, we would see a clear colour gradient from blue on the left to red on the right.

In order to compare the state of tonotopy in the network, we designed and used an *average distance metric* (ADM) defined as:

$$\mathrm{ADM}(network) = \frac{\sum_{n \in T} |B_n - BF_n|}{|T|} \tag{6}$$

where T is the set of tuned noninput[6] neurons, B_n is the band where the n-th neuron from T is placed and BF_n is the best frequency of the n-th neuron. In a totally tonotopic network, ADM would be zero. In contrast a completely chaotic network (where the BF of neurons is selected randomly)

[6] Input neurons (i.e., neurons from layer L4) are not accounted because they are trivially tonotopic and would skew the results by enforcing that every network has a large quantity of perfectly tonotopic neurons.

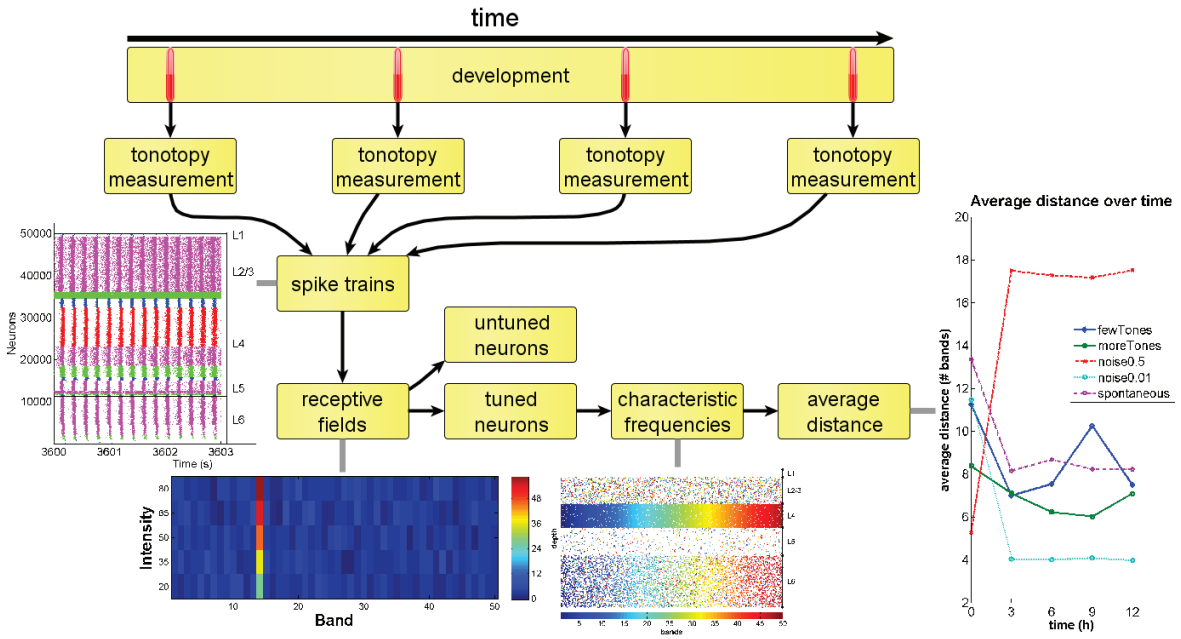

Fig. 5 A diagram of steps done in the analysis of results. Each experiment consists of development and measurement of tonotopy in several time slices during development. From each measurement, the spike trains were recorded and used to compute receptive fields of all neurons. Then, the tuned neurons were selected and their characteristic frequencies determined. Finally, the state of tonotopy was measured using average distance metric (ADM).

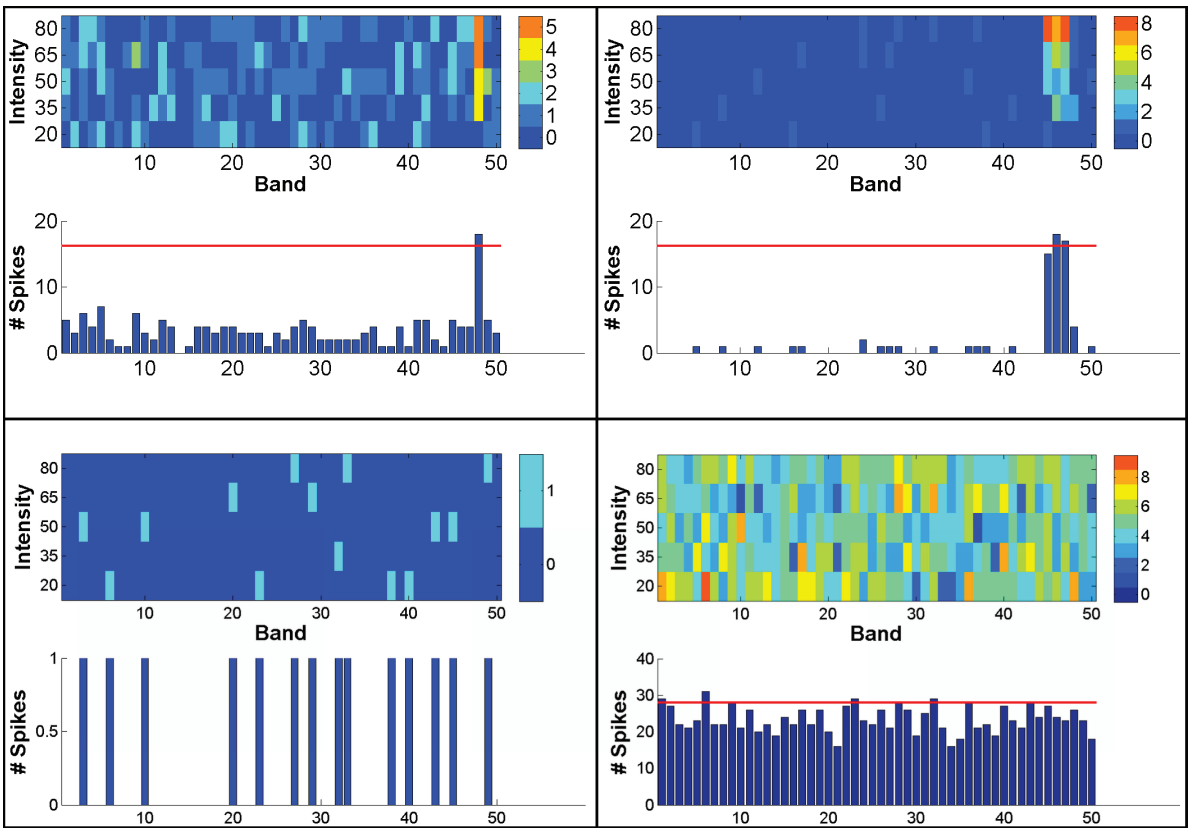

Fig. 6 Examples of RFs (top in each quadrant) and summedRF (bottom in each quadrant) in four different neurons. The two top neurons are tuned. The top left neuron has only one band above the relativeThreshold (red horizontal line in summedRF). The top right neuron has two but neighbouring bands above the relativeThreshold. The two bottom neurons are untuned because the bottom left one is not active enough and the bottom right one has several not connected bands above relativeThreshold.

with 50 bands would have an ADM of 16.67, the mean difference of two independent variables from Uniform(1, 50). These numbers were used as the baseline for measuring the degree of tonotopy of networks after rearing under various stimuli.

There is one potential theoretical case in which the values of ADM could give misleading information about tonotopy, when one network, has low number of tuned neurons (but well tuned neurons) and another network has high number of tuned neurons (but on average less well tuned neurons). In this case the first network would have much lower ADM, even though it is not clear, whether we should call this network tonotopic (especially when the number of tuned neurons is extremely low). Therefore, apart from measuring ADM, we also measured the percentage of tuned neurons in the network and verified that the networks with low ADM have also relatively high percentage of tuned neurons and vice versa.

3.3.2 Effects of different types of stimuli on the development of tonotopy (main tonotopy-related experiments)

We explored 12 h simulated time of development of the network under 5 different external stimuli: *spontaneous*, *pureTones5*, *pureTones25*, *noise0.5* and *noise0.01*. All the experiments contained the same amount of minis, but differed in their external stimulation. In the *spontaneous input* condition, neurons did not receive any external input. In the *pureTones5* condition, the network was stimulated by pure tones presented to the input layer (L4). Each pure tone lasted 500 ms and had an intensity of 0.5[7]. The index of the next stimulated band was always randomly selected from the set of bands 2, 14, 26, 38 and 50. In the *pureTones25* input condition, the set of stimulated bands contained all the odd bands (25 bands in total). In the *noise0.5* condition, the external stimulation consisted of noise with an intensity of 0.5 (i.e., each neuron in the input layer was in each time step stimulated with probability 0.5) and in the *noise0.01* condition, the noise had an intensity of 0.01.

Each of these 5 input conditions was run on two network sizes of 50 000 and 100 000 neurons, with two different random seeds, 20 main experiments in total[8]. For each of these 20 experiments, the state of tonotopy was measured at 5 different times during the development: after 10 s of stabilisation, after 3 h, 6 h, 9 h and 12 h. All the values of ADM in this section are written in the form of (mean value $\pm$ standard deviation for the smaller network; mean value $\pm$ standard deviation for the larger network), computed from both seeds and all the time slices except the initial one.

Comparison of effects of different inputs. The results of the main tonotopy-related experiments are shown in Fig. 7 and 8. In all the experiments, the input layer L4 was completely tonotopic (in Fig. 7, the neurons of L4 form a clear colour gradient). This is not surprising, because this layer directly receives tonotopically ordered external input causing the neurons to fire primarily when their band is stimulated. Therefore, a comparison of tonotopy between networks was performed using only non-input neurons.

Already the initial network was tonotopic to a certain extent (ADM 11–12). From the second measurement (3 h) on, there was a marked difference between the experiments (see Figure 8A for development of ADM over time and 8C for summarising visualisation of these values). The *noise0.5* input condition led to the lowest tonotopy (ADM 17.2 $\pm$ 0.3; 18.4 $\pm$ 0.2), whilst the network stimulated under the *noise0.01* condition became the most tonotopic one (ADM 4.3 $\pm$ 0.4; 5.6 $\pm$ 0.7). The other inputs led to intermediate values of tonotopy (ADM 8.4 $\pm$ 1.2; 8.7 $\pm$ 0.7 for the *pureTones5* condition, 7.0 $\pm$ 0.6; 8.0 $\pm$ 0.3 for the *pureTones25* condition and 8.3 $\pm$ 0.2; 8.3 $\pm$ 0.5 for the *spontaneous* condition).

Percentages of tuned neurons were in agreement with the results based on ADM (see Supplementary materials, Section 2.2). The *noise0.5* condition led to a network with the lowest percentage of tuned neurons (13.2 $\pm$ 0.5%; 14.5 $\pm$ 0.3%) and the *noise0.01* condition led to a network with the highest percentage of tuned neurons (28.5 $\pm$ 0.5%; 27.8 $\pm$ 2.8%), confirming that the network reared with *noise0.5* had much lower tonotopy than the network reared with *noise0.01*.

The measurements of tonotopy (both ADM and percentage of tuned neurons) were relatively stable over time from 3 h on (with standard deviation ≤ 1.2 in all the cases) keeping the following order: *noise0.01* being the most tonotopic one, *noise0.5* being the least tonotopic one, and the other three conditions being in between these two.

In order to compare the significance of the difference in tonotopic organisation within each network, we performed a Kruskal-Wallis ANOVA[9] on the networks after 12 h of simulation. The test was performed on values of $|B_n - BF_n|$ for each tuned non-input neuron in each input condition, where the notation is the same as in equation 6, using Matlab functions `kruskalwallis` and `multcompare` (with the default parameters, i.e., Tukey-Kramer multiple comparison test). The results are given in Fig. 8B, showing that in all the four networks, *noise0.5* led to significantly disrupted tono-

[7] This means intensity corresponding to the probability 0.5, i.e., each neuron in the input layer has, in each time step, a probability 0.5 to be externally stimulated, as defined in Section 2.2.

[8] Note that computation of a single 12 h development of a 50k network, along with the measurement of tonotopy, takes circa 10 days; we therefore could not compute more repetitions with different seeds.

[9] The reason for using Kruskal-Wallis ANOVA (instead of standard ANOVA) is the fact that it does not require normally distributed data.

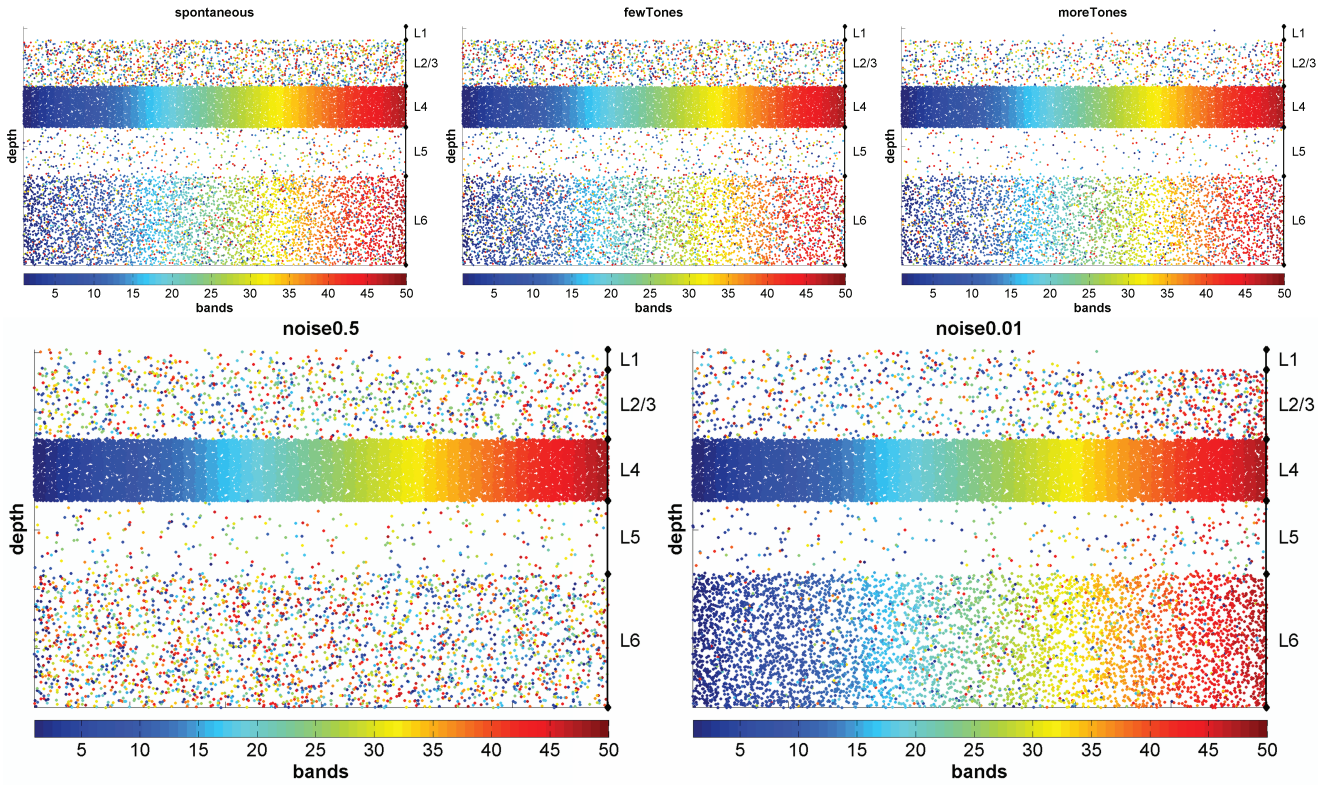

Fig. 7 Spatial visualisation of 50k networks after 12 h of experiments. Only the tuned neurons are plotted, with the colour representing their BF. The main difference is in layer L6, where the *noise0.5* condition led to a much less tonotopic state than the other input conditions. The other seed and network size can be found in the Supplementary materials in Section 2.2.

topic organisation, whereas *noise0.01* led to significantly increased tonotopy.

Comparison of layers. Apart from L4, the most tonotopic layer was L6. The other layers were rather heterogeneous, with an exception of L2/3 and L5 in the *noise0.01* condition, which were mildly tonotopic (ADM 12.3 $\pm$ 0.9; 11.6 $\pm$ 0.7 for L2/3 and 9.9 $\pm$ 0.6; 10.9 $\pm$ 0.7 for L5). A table with ADM computed separately for each layer can be found in the Supplementary materials (Section 2.2).

Comparison of excitatory and inhibitory neurons. When the tonotopy results were grouped according to neuronal type, inhibitory basket (b) neurons in all layers were observed to exhibit a greater tonotopic tendency than the other neuronal types (Fig. 8D). With the exception of the *noise0.5* condition, where the tonotopy was disrupted in general, the mean ADM was 0.9–1.9 for basket neurons, whereas it was 3.3–8.9 for non-basket and 2.6–6.4 for pyramidal neurons. Nevertheless, even in the case of the *noise0.5* condition, the inhibitory basket neurons were nearly two times more tonotopic than the other types. A table with ADM computed separately for each neuron type can be found in the Supplementary materials (Section 2.2).

3.3.3 Relationship between tonotopy and intensity of noise rearing (additional tonotopy-related experiments)

In the main tonotopy-related experiments, it emerged that strong noise disrupted tonotopy, weak noise led to clear tonotopy and spontaneous activity (which is the same as noise with intensity 0) resulted in values in between the two noise experiments. Similarly, observations from *in vivo* experiments show that both overstimulation (Zhang et al., 2002; Chang and Merzenich, 2003; Insanally et al., 2010) and acoustic deprivation during development (Stanton and Harrison , 2000) lead to altered tonotopic organisation and that an intermediate amount of afferent stimulation is necessary for correct maturation of the sensory system (Reale et al., 1987; Nahmani and Turrigiano, 2014). Therefore we hypothesised that an intermediate level of input stimulation could lead to higher tonotopy than both the absence of stimulation (only spontaneous activity) and stimulation with strong noise.

We were interested in what would happen for noises with intensities between 0.01 and 0.5. We hypothesised that the tonotopy for this range of intensities could have a shape similar to that depicted in the Fig. 8E. We were also interested in where the peak could be found, namely what intensity of

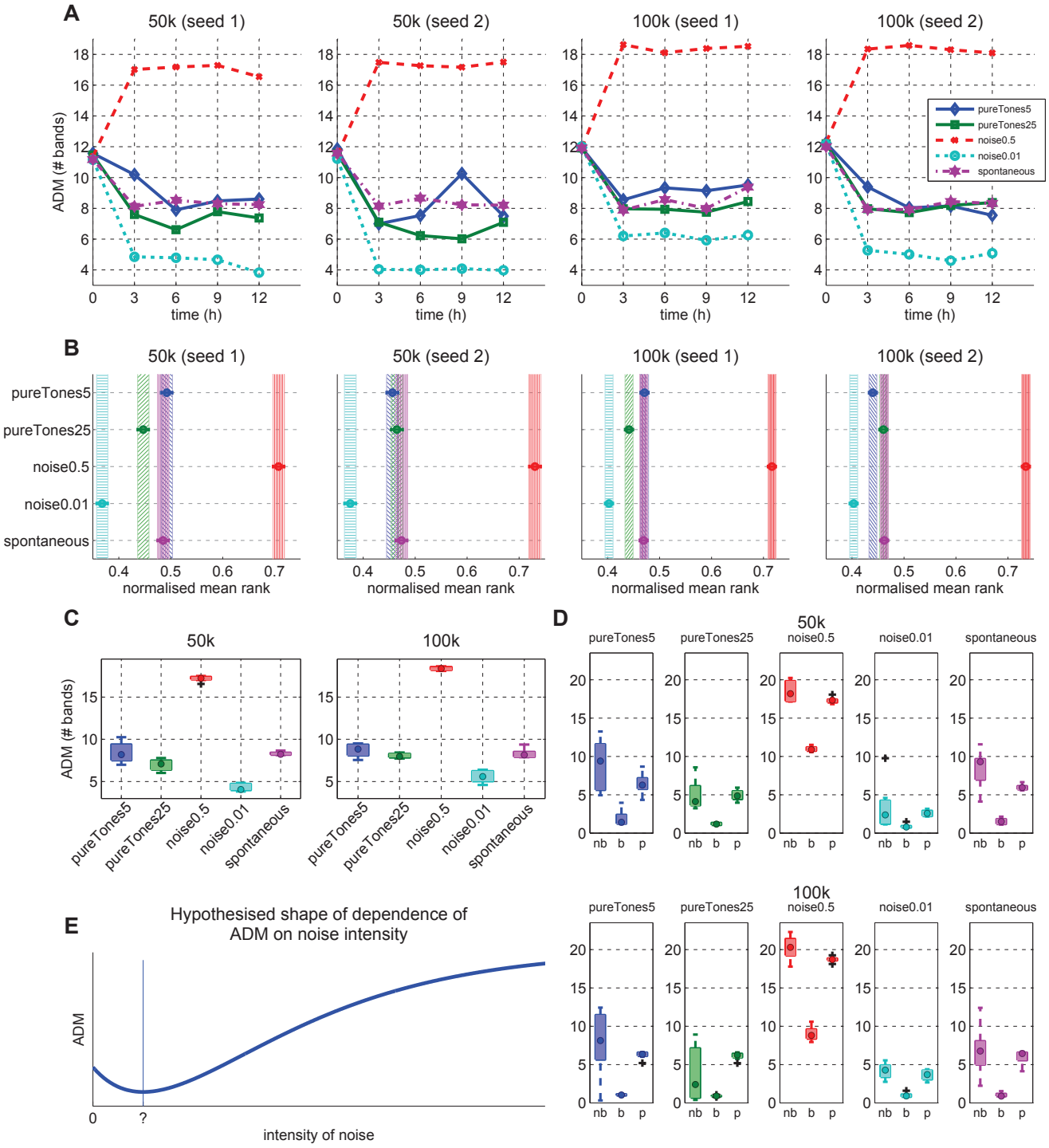

Fig. 8 Development of ADM of tuned non-input neurons. Note that the lower ADM, the higher tonotopy. **(A):** Development of ADM over time, separately for each network size (50k, 100k) and random seed. Except at the beginning, *noise0.5* condition has clearly the highest ADM (therefore the lowest tonotopy), whereas *noise0.01* condition has the lowest ADM (therefore the highest tonotopy). **(B):** Visualisation of Kruskal-Wallis test and following Tukey-Kramer multiple comparison test performed on neuron-wise ADM from the last time slice (i.e., after 12 h of development) separately for each input condition. The y-axis contains the five input conditions (their order does not matter). The x-axis corresponds to normalised mean rank (i.e., instead of numeric values, only ranking of neurons in all the networks by their distance from their best frequency is used; then this ranking is converted to 0–1 scale). For each input condition, the estimated mean rank is plotted with a circle and the estimated 95% confidence interval is plotted as a vertical band. Those pairs of input conditions that have non-overlapping bands are significantly different (with p-value < 0.01). **(C):** Boxplot visualisation of the distribution of ADM computed from both random seeds and all the time slices except the initial one. On each box, the central dot line is the median and the edges of the box are the 25th and 75th percentiles. The black crosses represent outliers and whiskers extend to the most extreme data points, which were not considered outliers. **(D):** Same as in (C), but the neurons are grouped by their type: non-basket (nb), basket (b), and pyramidal (p). **(E):** Dependence of ADM on the intensity of noise, according to our hypothesis. The zero intensity of noise corresponds to the spontaneous input condition. The question mark represents potential intensity of noise, which leads to the lowest ADM (i.e., the highest tonotopy).

noise would lead to the highest tonotopy. In addition, would the peak change during the network's evolution?

To answer these questions, seven additional experiments were performed on the 50k network with the first seed. The simulations were run for 2 h of simulated time. All the networks were externally stimulated by a noise input with varied noise intensity: 0.0075, 0.02, 0.03, 0.1, 0.2, 0.3 and 0.4 (from previous experiments, we already had results for noise with intensity 0, 0.01 and 0.5).

The state of tonotopy was measured after 1 s, after 15 s, 30 min, 1 h and at the end of the simulation. The results are shown in Fig. 9. In Fig. 9A, we can see a standard visualisation of ADM over time for the three original intensities (0, 0.01 and 0.5) for 12 h and for selected new intensities (namely 0.02 and 0.03) for 2 h. In Fig. 9B, ADM is plotted against intensity of the noise, separately for each time slice. At the beginning (after 1 s), there is no clear trend. Already after 15 s, low intensities led to a visible increase in tonotopy. During the following 30 min, very low intensities

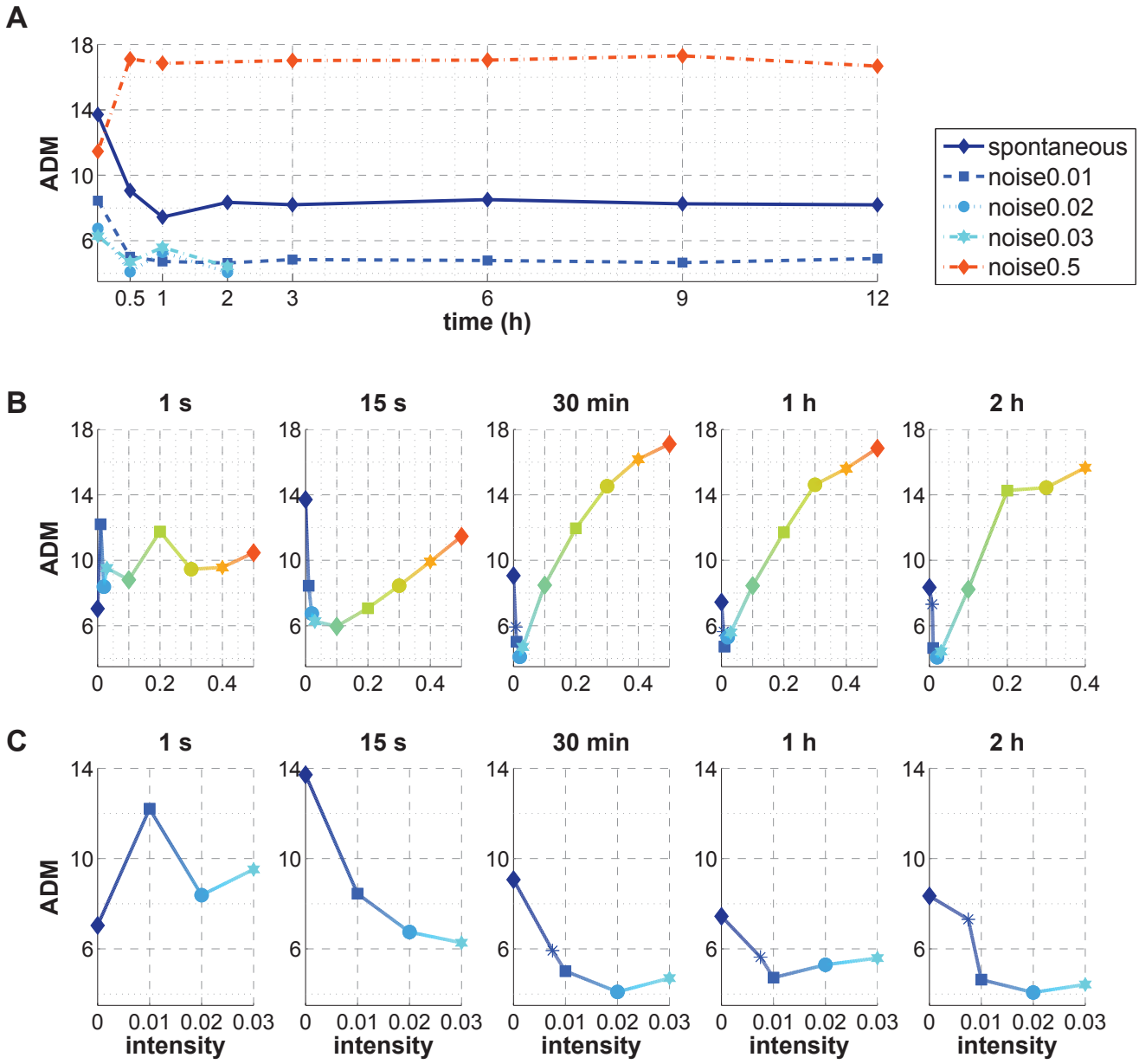

Fig. 9 The tonotopy for different values of noise intensity. **(A):** Comparison of development of ADM over time for five different conditions: spontaneous activity (i.e., zero noise) and four intensities of noise. The intensity of noise is colour-coded (from 0 (dark blue) to 0.5 (red)) and is consistent with the colour-coding in (B) and (C). **(B):** ADM vs. intensity of noise in five time slices (after 1 s, 15 s 30 min, 1 h, and 2 h of development). **(C):** Zoom of (B) in each time slice. Note that the smaller the value of ADM, the higher the tonotopy. According to the tested intensities, the intensity leading to the lowest ADM (i.e., the highest tonotopy) is between values 0.01 and 0.02.

(0.075–0.03) led to even increased tonotopy, whereas high intensities led to visibly decreased tonotopy. Moreover, the curve is relatively smooth, very much resembling the shape of the curve given by our hypothesis in Fig. 8E. In the next two time slices (1 h and 2 h), the shape remained similar as in the 30 min time slice.

In each of the time slices from 15 s on, there was a clear global optimum (see Fig. 9C for an inset with low intensities). The intensity of the global optimum differed between the time slices (started as 0.1 in the 15 s time slice and moved to 0.01–0.02 in the following time slices).

In summary, the additional tonotopy-related experiments supported the idea that noise with low intensity can increase the degree of tonotopy, whilst noise with high intensity disrupts the tonotopy and the higher the intensity, the lower the tonotopy. The intensity of noise that caused the strongest tonotopy seemed to stabilise between 0.01 and 0.02. Even though we cannot measure the exact value of the global optimum (since we have only several discrete measurements) and we cannot prove that it will not move during time, we can conclude that at least during the first 12 h of simulation, intensity 0.01 was more tonotopic than intensity 0 (9A) and therefore the optimum would probably not move to 0. Therefore, these results support the hypothesised shape in 8E.

4 Discussion

We constructed a large-scale model of the A1, evaluated its main characteristics and performed several tonotopy-related experiments to simulate and research the development of a tonotopic arrangement of the model. Each neuron was simulated according to the Izhikevich's spiking neuron model (Izhikevich, 2003, 2007).

The architecture of our model is based on the available data from the cat primary visual cortex (Binzegger et al., 2004). Although there can be some differences in cortical architecture between visual and auditory cortices (Barbour and Callaway, 2008; Smith and Populin, 2001), detailed data for the AC are not yet available. There is evidence that the differences are not fundamental (Harris and Shepherd, 2015). In our model, the excitatory synaptic weights developed according to STDP (Markram et al., 1997; Yuste and Denk, 1995; Song et al., 2000). The inhibitory weights were kept constant as experimental evidence suggests that in the AC the inhibitory tuning profile is formed to a large extent prior to the onset of hearing experience and is not substantially modified during further development (Sun et al., 2010). In actual real organisms, the inhibitory and excitatory weights can also be modified during active conditioning paradigms. Such learning is mediated by nucleus basalis and interneurons in the first layer of the AC (Froemke et al, 2007; Letzkus et al., 2011). The simulator is prepared to be connected with a module, to mimic the inputs from the nucleus basalis, which should enable us to perform simulations with conditioning paradigms. For computational reasons we did not model some more detailed aspects of the cortex, namely short-term synaptic plasticity (Zucker, 1989; Buonomano and Maass, 2009), dendritic spikes (Gasparini et al., 2004), all long-distance cortico-cortical connections coming from the other parts of the neocortex (Iurilli et al., 2012; Zingg et al., 2014), cortico-thalamic and non-specific thalamo-cortical connections (Wu et al., 2011), and gap junctions among the same neuronal type and within the same cortical layer (Galarreta and Hestrin, 1999).

To evaluate the basic plausibility of our model, the spontaneous activity of the network was analysed. We measured the mean spontaneous firing rate of each type of modelled neuron in our model. In accordance with *in vivo* data (Sakata and Harris, 2009, 2012; Moore and Wehr, 2013), we observed higher firing rates in basket cells compared to pyramidal cells. However, the absolute spontaneous firing rates of superficial basket cells in our model was higher than in the experimental data; ≈ 5 Hz for p2/3 and 30–40 Hz for b2/3 in our model vs. 2.2 ± 0.5 Hz for superficial pyramidal cells and 7.5 ± 4.4 for superficial fast-spiking cells (Sakata and Harris, 2012). This discrepancy could be attributed to many reasons, such as the fact that we used only two different ranges for the evolution of synaptic weight (for excitatory and inhibitory synapses). In a real neocortical network, some synapses are stronger or weaker based on the position and cell type of the presynaptic or postsynaptic neuron (Richardson et al., 2009; Barbour et al., 2007; Holmgren et al., 2003; Feldmeyer et al., 1999; Song et al., 2005). However, the most straightforward explanation comes from neglecting the long-distance connections coming from outside the modelled area, especially the connections ending on the L1 interneurons that in turn inhibit the b2/3 interneurons. As the connections to L1 interneurons are largely excitatory (Christophe et al., 2002) and more than 90% of L1 interneurons are inhibitory (Hestrin and Armstrong, 1996), there could be a consequent lack of inhibition in the supragranular layers of our model resulting in higher spontaneous firing rates in the p2/3 and b2/3.

When evaluating the development of the model, we also assessed local and global oscillations within the network and the spontaneous firing rate of each neuronal type. Low frequency activity (theta and alpha) arose globally, however, high frequency activity (gamma) was present mostly locally. This is consistent with the experimental observation that gamma rhythms are weaker in global EEG recordings than in local recordings (Nunez and Srinivasan, 2006).

Interestingly, we observed two main alternating states of the network during the network development: theta-like synchronised and desynchronised states. Similar alternations of synchronised and desynchronised states were observed in the sensory cortices; the visual cortex of awake rats (Xu

et al., 2012) and the AC *in vivo* in both anaesthetised (Sakata and Harris, 2012; Clement et al., 2008; Sakata and Harris, 2009) and awake (Sakata and Harris, 2012) animals. In the synchronised state in the model, the frequency of the oscillation was either around 5 Hz corresponding to theta waves, or around 10 Hz corresponding to alpha waves. In the theta-like state, there were always higher harmonic frequencies in the corresponding spectrograms raising the question as to whether or not the alpha band is just a higher harmonic mode. However, in parts of the spontaneous evolution of the network the alpha-like band was present alone as the fundamental frequency of the network global oscillation. Although the EEG theta oscillations are often mentioned in the context of hippocampal theta cells (O'Keefe and Recce, 1993; Huxter et al., 2003) and alpha oscillations are supposed to be generated by thalamo-cortical interactions (Bollimunta et al., 2011), they emerged solely from the cortex in our model. This implies that there could also be a cortical origin of these oscillations as indicated by some experimental evidences (Raghavachari et al., 2006; Liebe et al., 2012; Bollimunta et al., 2011). In general, our results show that our network is capable of producing such oscillatory modes.

As a proof of concept that our model enables the investigation of inner mechanisms of the network, we focused on gamma oscillations and the behaviour of the system on cell-type resolution. The gamma oscillations were clearly observable from the virtual potential probe within the network. In our model we showed that the strongest pacemaker of gamma oscillations are the b2/3 cells (Fig. 4A and Supplementary materials, Section 2.1.2). Indeed, basket cells are supposed to be crucial for gamma oscillations (Buzsáki and Wang, 2012; Cardin et al., 2009). We further investigated the mechanism of the gamma oscillation. Prolonging the synaptic conduction delays between b2/3 cells resulted in substantial changes in the b2/3-cell spectra. Doubling the delays led only to a ca. 5 Hz decrease (ca. 50 Hz $>$ ca. 45 Hz) of the centre frequency of the gamma peak, but the spectrum remained relatively similar. However, further prolonging the delays led to disintegration of the gamma-centred part of the spectrum. Our results suggest that connections between b2/3 cells play a role in the process of firing synchronisation, as suggested in (Bartos et al., 2002), and that the generation of the gamma oscillation is rather an intrinsic property of basket cells (doubling the delays did not lead to halving the oscillatory frequency), in agreement with (Traub et al., 1998).

Even very sophisticated physiological mechanisms can be studied using rather simple, but well-designed models (Wagatsuma et al., 2011). However, the correspondence of these results with the real neuronal networks needs careful extrapolation and the individual building blocks cannot be straightforwardly compared to their real counterparts. We developed a pseudo-realistic model which could produce experimental predictions on a single-neuronal-type basis that could be straightforwardly tested *in vivo*. The model enables the study of its inner structure and motifs (Haeusler et al., 2009). The spike trains of individual cell types can be readily exported from our model and the causal link between the activities of individual cell types can be discussed. Inspired by (Wagatsuma et al., 2011; Haeusler et al., 2009) we focused on several mechanisms governing the behaviour of the network. The plots in Fig. 3C, D suggest that changes in firing rates of certain neuronal types (and synaptic weights) are aligned with the synchronised/desynchronised states. Interestingly, at the beginning of the transition into the oscillatory theta-like state in Fig. 2E, the first cells to increase their activity are all active types of non-basket (nb) cells; nb2/3, nb4 and nb5. The activity of the b2/3 cells decreases at the same time. After that, the activity of the remaining cells increases with an approximately two-second delay. Concerning the sequence of the activation of nb2/3 and b2/3 cells, one may speculate about a causal relation of the sequence, such as the rise of nb cells causing the decrease of b2/3 activity, allowing the remaining cells to become more active. Indeed, according to (Cottam et al., 2013; Xu et al., 2013), interactions between nb (somatostatin+) and b cells (parvalbumin+) were recently observed experimentally.

We also evaluated evoked activity in the network. Tonal stimulation of L4 was propagated to L23 and to subgranular layers. This is in correspondence with experimental data, except the delayed activation of L6 (Sakata and Harris, 2012). This discrepancy is probably caused by the omission of thalamo-cortical projections to L5/6 in our model.

Finally, we used the model to research cortical plasticity and changes in tonotopic organisation after the presentation of different types of stimuli to the system during development. In order to compare the degree of tonotopy of the network (all layers except L4), we measured the average distance metric (ADM). This ADM was calculated both from excitatory and inhibitory neurons as both of them can be tuned to a certain frequency (Moore and Wehr, 2013; Li et al., 2014a,b). The ADM metric gives 0 for a completely tonotopic network and 16.67 for a network with random best frequencies; the higher the ADM, the lower the tonotopy.

Immediately after the initiation of the network, some degree of tonotopy (11–12) was found, solely due to the local interconnections with layer L4. After development under spontaneous (no input from the thalamus) or pure tone conditions, the tonotopy remained similar (ADM 8.4 $\pm$ 1.2 (for 50k network); 8.7 $\pm$ 0.7 (for 100k network) for the *pureTones5* condition, 7.0 $\pm$ 0.6; 8.0 $\pm$ 0.3 for the *pureTones25* condition and 8.3 $\pm$ 0.2; 8.3 $\pm$ 0.5 for the *spontaneous* condition).

However, noise rearing changed the degree of tonotopy considerably. High-intensity noise completely disrupted the tonotopy giving an ADM of 17.2 $\pm$ 0.3; 18.4 $\pm$ 0.2. Such disruption of tonotopy by noise is consistent with experi-

mental observations (Chang and Merzenich, 2003; Froemke and Jones, 2011; Zhang et al., 2002; Insanally et al., 2010). A possible underlying mechanism could be that strong noise stimulation weakens synapses between the input layer and other layers of the network due to STDP and the fact that LTD is higher than LTP (1.2 vs 1.0). Thus during the measurement of tonotopy, fewer neurons respond to the frequency corresponding to the band they are in.

Interestingly, low-intensity noise rearing led to an increase in tonotopy (ADM 4.3 ± 0.4; 5.6 ± 0.7), compared to both initial state and spontaneous activity. Such values of ADM represent clear but not perfectly smooth tonotopy. This corresponds to observations from real AC, especially in smaller mammals, where tonotopy was observed, but also was not perfectly smooth (Rothschild et al., 2010; Bandyopadhyay et al., 2010; Issa et al., 2014).

The fact that spontaneous activity (i.e., no external stimulation) led to lower tonotopy than weak white noise could correspond to the observation that acoustic deprivation in real animals seems to alter tonotopy. It was observed that all sensory modalities need a certain amount of stimulation during development; otherwise they develop improperly (Reale et al., 1987; Nahmani and Turrigiano, 2014). A total acoustic deprivation in congenitally deaf cats leads to disrupted synaptic activity and functional deficits in the AC (Kral et al., 2006). It can be expected that altered synaptic activity will lead to abnormal receptive field formation and thus to deteriorated tonotopy. Moreover, restricted neonatal cochlear lesions result in altered tonotopy in the AC (Stanton and Harrison , 2000).

Based on these observations we hypothesised that there could be a continuous relationship between intensity of noise stimulation and resulting tonotopy and that an intermediate level of input stimulation could lead to higher tonotopy than both absence of stimulation (only spontaneous activity) and stimulation with strong noise. Therefore, we measured tonotopy after development under 10 different intensities of noise between 0 (spontaneous activity only) and 0.5 (strong noise). The resulting ADM plotted against the level of noise (Fig. 9) had a surprisingly smooth "U" shape. From 30 min of simulation on, this shape remained relatively stable, with an optimum between intensities 0.01 and 0.02.

Another interesting prediction made by our model is the difference between tonotopy of the different neuronal types. According to our results, inhibitory basket neurons were clearly more tonotopically ordered than excitatory pyramidal and inhibitory non-basket neurons. This is an example of a prediction that can be verified experimentally.

It is important to point out that based on our results STDP seems to be a sufficient mechanism to explain the above described phenomena observed *in vivo*. At the same time, we are aware of some limitations of our model. Firstly, the omission of the thalamus can influence network dynamics and oscillations; especially in subgranular layers (Steriade et al., 1993; Lee and Winer, 2008). The modular structure of our model allows us to add the thalamus in future work. Secondly, we stimulated only layer L4 although thalamocortical projections in real AC terminate both in supra- and to a lesser extent even subgranular layers (Huang and Winer, 2000). This could affect the tonotopy and response latency of these layers.

The model differed from real observations in tonotopy of layers L2/3 and L5. The corresponding ADM values were quite high in the model. This may be due to several reasons. The most straightforward reason is the omission of the inputs from the thalamus to other layers aside from L4 (Binzegger et al., 2004; Izhikevich and Edelman, 2008). These inputs especially innervate L3 relatively densely, and to a lesser extent also L5 in the AC (Smith et al., 2012; Huang and Winer, 2000). However, the reason may also be the inputs presented to the network. We hypothesise that to develop tonotopy in these layers, a correct "natural" environment is necessary (such as more tones together, with various intensities, durations, frequencies etc).

This reasoning presents suggestions for future work. In terms of making the model more complex and precise, more details could be incorporated into it (however, the simpler and more concise the model, the easier and clearer the analysis of its results). On the other hand, there are many interesting questions to ask about the network mechanisms; for example the relationship between excitation and inhibition in sharpening a neuronal receptive field (Wu et al., 2008; de la Rocha et al., 2008), the role of input timings on a neuron when sharpening its receptive field (Oswald et al., 2006; Happel et al., 2010), or the role of different types of interneurons in sharpening a neuronal receptive field (Wilson et al., 2012). Some questions will require an extension of the model and more sophisticated analysis. Our model is designed in such a way that additional modules running on the same simulation core (e.g., thalamus, inferior colliculi) can be readily connected. We are convinced that this type of model could answer at least some of these kinds of questions.

In order to facilitate implementation of further modifications of the model and other neuronal modelling in general, the presented model and software have been made publicly available at `https://sites.google.com/site/susnoimac/`.

Acknowledgements We would like to thank Elisa Brann, Martin Popel and Felix Zhou for help with polishing the manuscript and The Bakala Foundation for financial support of the two first authors during their studies. This work was supported by the Grant Agency of the Czech Republic (P303/12/1347), by PRVOUK "P46 – Informatika", and by Engineering and Physical Sciences Research Council (EP/F500394/1). This work made use of the Open Science Data Cloud (OSDC) which is an Open Cloud Consortium (OCC)-sponsored

project (Grossman et al., 2012); which is a work supported in part by grants from Gordon and Betty Moore Foundation and the National Science Foundation and major contributions from OCC members like the University of Chicago.

References

Arieli A, Shoham D, Hildesheim R, Grinvald A (1995) Coherent spatiotemporal patterns of ongoing activity revealed by real-time optical imaging coupled with single-unit recording in the cat visual cortex. *Journal of Neurophysiology* **73**(5):2072–2093

Bandyopadhyay S, Shamma SA, Kanold PO (2010) Dichotomy of functional organization in the mouse auditory cortex. *Nature Neuroscience* **13**(3):361–368

Barbour B, Brunel N, Hakim V, Nadal JP (2007) What can we learn from synaptic weight distributions? *Trends in Neuroscience* **30**(12):622–9, DOI 10.1016/j.tins.2007.09.005, URL `http://www.ncbi.nlm.nih.gov/pubmed/17983670`

Barbour DL, Callaway EM (2008) Excitatory local connections of superficial neurons in rat auditory cortex. *The Journal of Neuroscience* **28**(44):11,174–11,185

Bartos M, Vida I, Frotscher M, Meyer A, Monyer H, Geiger JRP, Jonas P (2002) Fast synaptic inhibition promotes synchronized gamma oscillations in hippocampal interneuron networks. *Proceedings of the National Academy of Sciences of the United States of America* **99**(20):13,222–13,227

Beierlein M, Gibson JR, Connors BW (2003) Two dynamically distinct inhibitory networks in layer 4 of the neocortex. *Journal of Neurophysiology* **90**(5):2987–3000

Binzegger T, Douglas RJ, Martin KAC (2004) A quantitative map of the circuit of cat primary visual cortex. *The Journal of Neuroscience* **24**(39):8441–8453

Bollimunta A, Mo J, Schroeder CE, Ding M (2011) Neuronal mechanisms and attentional modulation of corticothalamic α oscillations. *The Journal of Neuroscience* **24**(39):8441–8453

Buonomano DV, Maass W (2009) State-dependent computations: spatiotemporal processing in cortical networks. *Nature Reviews Neuroscience* **10**(2):113–125

Buzsáki G, Wang XJ (2012) Mechanisms of gamma oscillations. *Annual review of neuroscience* **35**:203–225

Cardin JA, Carlén M, Meletis K, Knoblich U, Zhang F, Deisseroth K, Tsai LH, Moore CI (2009) Driving fast-spiking cells induces gamma rhythm and controls sensory responses. *Nature* **459**(7247):663–667, DOI 10.1038/nature08002, URL `http://www.ncbi.nlm.nih.gov/pubmed/19396156`

Chang EF, Merzenich MM (2003) Environmental noise retards auditory cortical development. *Science* **300**(5618):498–502

Christophe E, Roebuck A, Staiger JF, Lavery DJ, Charpak S, Audinat E (2002) Two types of nicotinic receptors mediate an excitation of neocortical layer I interneurons. *Journal of Neurophysiology* **88**(3):1318–27, URL `http://www.ncbi.nlm.nih.gov/pubmed/12205153`

Chrostowski M, Yang L, Wilson HR, Bruce IC, Becker S (2011) Can homeostatic plasticity in deafferented primary auditory cortex lead to travelling waves of excitation? *Journal of Computational Neuroscience* **30**(2):279–299

Clement EA, Richard A, Thwaites M, Ailon J, Peters S, Dickson CT (2008) Cyclic and sleep-like spontaneous alternations of brain state under urethane anaesthesia. *PLoS One* **3**(4):e2004

Cottam JC, Smith SL, Häusser M (2013) Target-specific effects of somatostatin-expressing interneurons on neocortical visual processing. *The Journal of Neuroscience* **33**(50):19567–19578

Cruikshank SJ, Rose HJ, Metherate R (2002) Auditory thalamocortical synaptic transmission in vitro. *Journal of Neurophysiology* **87**(1):361–384

DeFelipe J, Alonso-Nanclares L, Arellano JI (2002) Microstructure of the neocortex: comparative aspects. *Journal of Neurocytology* **31**(3-5):299–316

Feldmeyer D, Egger V, Lubke J, Sakmann B (1999) Reliable synaptic connections between pairs of excitatory layer 4 neurones within a single barrel of developing rat somatosensory cortex. *Journal of Physiology* **521 Pt 1**:169–90, URL `http://www.ncbi.nlm.nih.gov/pubmed/10562343`

Froemke RC, Merzenich MM, Schreiner CE (2007) A synaptic memory trace for cortical receptive field plasticity. *Nature* **450**(7168):425–429

Froemke RC, Jones BJ (2011) Development of auditory cortical synaptic receptive fields. *Neuroscience & Biobehavioral Reviews* **35**(10):2105–2113

Galarreta M, Hestrin S (1999) A network of fast-spiking cells in the neocortex connected by electrical synapses. *Nature* **402**(6757):72–75

Gasparini S, Migliore M, Magee JC (2004) On the initiation and propagation of dendritic spikes in Ca1 pyramidal neurons. *The Journal of Neuroscience* **24**(49):11,046–11,056

Grossman RL, Greenway M, Heath AP, Powell R, Suarez R, Wells W, White KP, Atkinson M, Klampanos I, Alvarez H, Harvey C and Mambretti J (2012) The Design of a Community Science Cloud: The Open Science Data Cloud Perspective. doi:10.1109/SC.Companion.2012.127, URL `https://www.opensciencedatacloud.org/`

Happel MF, Jeschke M, Ohl FW (2010) Spectral integration in primary auditory cortex attributable to temporally precise convergence of thalamocortical and intracortical input. *The Journal of Neuroscience* **30**(33):11,114–11,127

Haeusler S, Schuch K, Maass W (2009) Motif distribution, dynamical properties, and computational performance of two data-based cortical microcircuit templates. *Journal of Physiology Paris* **103**(1-2):73–87

Harris, KD, Shepherd, GM (2015) The neocortical circuit: themes and variations. *Nature neuroscience* **18**(2):170–181

Hestrin S, Armstrong WE (1996) Morphology and physiology of cortical neurons in layer I. *The Journal of Neuroscience* **16**(17):5290–5300

Hodgkin AL, Huxley AF (1952) A quantitative description of membrane current and its application to conduction and excitation in nerve. *The Journal of Physiology* **117**(4):500

Holmgren C, Harkany T, Svennenfors B, Zilberter Y (2003) Pyramidal cell communication within local networks in layer 2/3 of rat neocortex. *Journal of Physiology* **551**(Pt 1):139–53, DOI 10.1113/jphysiol.2003.044784, URL `http://www.ncbi.nlm.nih.gov/pubmed/12813147`

Huang CL, Winer JA (2000) Auditory thalamocortical projections in the cat: laminar and areal patterns of input. *Journal of Comparative Neurology* **427**(2):302–331

Huxter J, Burgess N, O'Keefe J (2003) Independent rate and temporal coding in hippocampal pyramidal cells. *Nature* **425**(6960):828–832

Insanally MN, Albanna BF, Bao S (2010) Pulsed noise experience disrupts complex sound representations. *Journal of Neurophysiology* **103**(5):2611

Issa JB, Haeffele BD, Agarwal A, Bergles DE, Young ED, Yue DT (2014) Multiscale optical Ca 2+ imaging of tonal organization in mouse auditory cortex. *Neuron* **83**(4):944–959

Iurilli G, Ghezzi D, Olcese U, Lassi G, Nazzaro C, Tonini R, Tucci V, Benfenati F, Medini P (2012) Sound-driven synaptic inhibition in primary visual cortex. *Neuron* **73**(4):814–828

Izhikevich EM (2003) Simple model of spiking neurons. *IEEE Transactions on Neural Networks* **14**(6):1569–1572

Izhikevich EM (2004) Which model to use for cortical spiking neurons? *IEEE Transactions on Neural Networks* **15**(5):1063–1070

Izhikevich EM (2006) Polychronization: Computation with spikes. *Neural Computation* **18**(2):245–282

Izhikevich EM (2007) Solving the distal reward problem through linkage of STDP and dopamine signaling. *Cerebral Cortex* **17**(10):2443–2452

Izhikevich EM, Edelman GM (2008) Large-scale model of mammalian thalamocortical systems. *Proceedings of the National Academy of Sciences* **105**(9):3593–3598

Kawaguchi Y (1995) Physiological subgroups of nonpyramidal cells with specific morphological characteristics in layer II/III of rat frontal cortex. *The Journal of Neuroscience* **15**(4):2638–2655

Kawaguchi Y, Kubota Y (1997) GABAergic cell subtypes and their synaptic connections in rat frontal cortex. *Cerebral Cortex* **7**(6):476–486

Kim H, Bao S (2009) Selective increase in representations of sounds repeated at an ethological rate. *The Journal of Neuroscience* **29**(16):5163–5169

Kimura A, Donishi T, Sakoda T, Hazama M, Tamai Y (2003) Auditory thalamic nuclei projections to the temporal cortex in the rat. *Neuroscience* **117**(4):1003–1016

Knight BW (1972) Dynamics of encoding in a population of neurons. *The Journal of General Physiology* **59**(6):734–766

Kotak VC, Fujisawa S, Lee FA, Karthikeyan O, Aoki C, Sanes DH (2005) Hearing loss raises excitability in the auditory cortex. *The Journal of Neuroscience* **25**(15):3908–3918

Kral A, Tillein J, Heid S, Klinke R, Hartmann R (2006) Cochlear implants: cortical plasticity in congenital deprivation. *Progress in Brain Research* **157**:283–313

Lapicque L (1907) Recherches quantitatives sur l'excitation électrique des nerfs traitée comme une polarisation. *Journal de Physiologie et de Pathologie Générale* **9**(1):620–635

Larson E, Billimoria CP, Sen K (2009) A biologically plausible computational model for auditory object recognition. *Journal of Neurophysiology* **101**(1):323–331

Larson E, Perrone BP, Sen K, Billimoria CP (2010) A robust and biologically plausible spike pattern recognition network. *The Journal of Neuroscience* **30**(46):15,566–15,572

Lee CC, Winer JA (2008) Connections of cat auditory cortex: I. Thalamocortical system. *Journal of Comparative Neurology* **507**(6):1879–1900

Letzkus JJ, Wolff SBE, Meyer EMM, Tovote P, Courtin J, Herry C, Luethi A (2011) A disinhibitory microcircuit for associative fear learning in the auditory cortex. *Nature* **480**(7377):331–335

Levy RB, Reyes AD (2012) Spatial profile of excitatory and inhibitory synaptic connectivity in mouse primary auditory cortex. *Journal of Neuroscience* **32**(16):5609–5619

Li LY, Ji XY, Liang FX, Li YT, Xiao ZJ, Tao HZW., Zhang, LI (2014a) A Feedforward Inhibitory Circuit Mediates Lateral Refinement of Sensory Representation in Upper Layer 2/3 of Mouse Primary Auditory Cortex. *Journal of Neuroscience* **34**(41):13670–13683

Li LY, Xiong XR, Ibrahim LA, Yan W, Tao H, Zhang LI (2014b) Differential Receptive Field Properties of Parvalbumin and Somatostatin Inhibitory Neurons in Mouse Auditory Cortex. *Cerebral Cortex* Epub ahead of print

Liebe S, Hoerzer GM, Logothetis NK, Rainer G (2012) Theta coupling between V4 and prefrontal cortex predicts visual short-term memory performance. *Nature Neuroscience* **15**(3):456–462

Markram H, Lübke J, Frotscher M, Sakmann B (1997) Regulation of synaptic efficacy by coincidence of postsynaptic APs and EPSPs. *Science* **275**(5297):213–215

Markram H, Toledo-Rodriguez M, Wang Y, Gupta A, Silberberg G, Wu C (2004) Interneurons of the neocortical inhibitory system. *Nature Reviews Neuroscience* **5**(10):793–807

Matsumoto M, Nishimura T (1998) Mersenne twister: a 623-dimensionally equidistributed uniform pseudo-random number generator. *ACM Transactions on Modeling and Computer Simulation (TOMACS)* **8**(1):3–30

Moore AK, Wehr M (2013) Parvalbumin-expressing inhibitory interneurons in auditory cortex are well-tuned for frequency. *The Journal of Neuroscience* **33**(34):13,713–13,723

Muresan RC, Savin C (2007) Resonance or integration? self-sustained dynamics and excitability of neural microcircuits. *Journal of Neurophysiology* **97**(3):1911–1930

Nahmani M, Turrigiano GG (2014) Deprivation-induced strengthening of presynaptic and postsynaptic inhibitory transmission in layer 4 of visual cortex during the critical period. *The Journal of Neuroscience* **34**(7):2571–2582

Nelken I (2014) Stimulus-specific adaptation and deviance detection in the auditory system: experiments and models. *Biological Cybernetics* pp 1–9, DOI 10.1007/s00422-014-0585-7, URL `http://dx.doi.org/10.1007/s00422-014-0585-7`

Nordlie E, Gewaltig MO, Plesser HE (2009) Towards reproducible descriptions of neuronal network models. *PLoS Computational Biology* **5**(8):e1000,456

Nunez PL, Srinivasan R (2006) *Electric fields of the brain: the neurophysics of EEG*. Oxford University Press, USA

O'Keefe J, Recce ML (1993) Phase relationship between hippocampal place units and the EEG theta rhythm. *Hippocampus* **3**(3):317–330

Oswald AMM, Schiff ML, Reyes AD (2006) Synaptic mechanisms underlying auditory processing. *Current Opinion in Neurobiology* **16**(4):371–376

Ouda L, Druga R, Syka J (2011). Distribution of SMI-32-immunoreactive neurons in the central auditory system of the rat. *Brain Structure and Function* **217**(1):19–36

Phoka E, Wildie M, Schultz SR, Barahona M (2012) Sensory experience modifies spontaneous state dynamics in a large-scale barrel cortical model. *Journal of Computational Neuroscience* **33**(2):323–339

de Pinho M, Roque-da Silva AC (1999) A realistic computational model of formation and variability of tonotopic maps in the auditory cortex. *Neurocomputing* **26**:355–359

de Pinho M, Mazza M, Roque AC (2006) A computational model of the primary auditory cortex exhibiting plasticity in the frequency representation. *Neurocomputing* **70**(1):3–8

Popelová M (2013) *Software tool for modelling coding and processing of information in auditory cortex of mice*. Master Thesis, Charles University in Prague, Faculty of Mathematics and Physics, URL `http://www.marketa.najevisti.info/dokumenty/master_thesis.pdf`

Raghavachari S, Lisman JE, Tully M, Madsen JR, Bromfield EB, Kahana MJ (2006) Theta oscillations in human cortex during a working-memory task: evidence for local generators. *Journal of Neurophysiololgy* **95**(3):1630–8, DOI 10.1152/jn.00409.2005, URL `http://www.ncbi.nlm.nih.gov/pubmed/16207788`

Reale RA, Breugge JF, Chan JC (1987) Maps of auditory cortex in cats reared after unilateral cochlear ablation in the neonatal period. *Brain Research* **431**(2):281–290

Richardson RJ, Blundon JA, Bayazitov IT, Zakharenko SS (2009) Connectivity patterns revealed by mapping of active inputs on dendrites of thalamorecipient neurons in the auditory cortex. *Journal of Neuroscience* **29**(20):6406–17, DOI 10.1523/JNEUROSCI.0258-09.2009, URL `http://www.ncbi.nlm.nih.gov/pubmed/19458212`

de la Rocha J, Marchetti C, Schiff M, Reyes AD (2008) Linking the response properties of cells in auditory cortex with network architecture: cotuning versus lateral inhibition. *The Journal of Neuroscience* **28**(37):9151–9163

Romanski LM, LeDoux JE (1993) Organization of rodent auditory cortex: anterograde transport of PHA-L from MGv to temporal neocortex. *Cerebral Cortex* **3**(6):499–514

Rothschild G, Nelken I, Mizrahi A (2010) Functional organization and population dynamics in the mouse primary auditory cortex. *Nature Neuroscience* **13**(3):353–360

Sakata S, Harris KD (2009) Laminar structure of spontaneous and sensory-evoked population activity in auditory cortex. *Neuron* **64**(3):404–418

Sakata S, Harris KD (2012) Laminar-dependent effects of cortical state on auditory cortical spontaneous activity. *Frontiers in Neural Circuits* **6**(109), DOI 10.3389/fncir.2012.00109

Schreiner CE, Read HL, Sutter ML (2000) Modular organization of frequency integration in primary auditory cortex. *Annual Review of Neuroscience* **23**(1):501–529

Schutter ED (2009) *Computational modeling methods for neuroscientists*. The MIT Press

Smith PH, Populin LC (2001) Fundamental differences between the thalamocortical recipient layers of the cat auditory and visual cortices. *Journal of Comparative Neurology* **436**(4):508–519

Smith PH, Uhlrich DJ, Manning KA, Banks MI (2012) Thalamocortical projections to rat auditory cortex from the ventral and dorsal divisions of the medial geniculate nucleus. *Journal of Comparative Neurology* **520**(1):34–51, DOI 10.1002/cne.22682, URL `http://www.ncbi.nlm.nih.gov/pubmed/21618239`

Song S, Miller KD, Abbott LF (2000) Competitive Hebbian learning through spike-timing-dependent synaptic plasticity. *Nature Neuroscience* **3**(9):919–26, DOI 10.1038/78829, URL `http://www.ncbi.nlm.nih.gov/pubmed/10966623`

Song S, Sjöström PJ, Reigl M, Nelson S, Chklovskii DB (2005) Highly nonrandom features of synaptic connectivity in local cortical circuits. *PLoS Biology* **3**(3):e68

Stanton SG, Harrison RV (2000) Projections from the medial geniculate body to primary auditory cortex in neonatally deafened cats. *Journal of Comparative Neurology* **426**:117–129

Steriade M, McCormick DA, Sejnowski TJ (1993) Thalamocortical oscillations in the sleeping and aroused brain. *Science* **262**(5134):679–685

Stiebler I, Neulist R, Fichtel I, Ehret G (1997) The auditory cortex of the house mouse: left-right differences, tonotopic organization and quantitative analysis of frequency representation. *Journal of Comparative Physiology A* **181**(6):559–571

Sun YJ, Wu GK, Liu Bh, Li P, Zhou M, Xiao Z, Tao HW, Zhang LI (2010) Fine-tuning of pre-balanced excitation and inhibition during auditory cortical development. *Nature* **465**(7300):927–931

Syka J, Šuta D, Popelář J (2005) Responses to species-specific vocalizations in the auditory cortex of awake and anesthetized guinea pigs. *Hearing research* **206**(1):177–184

Šuta D, Kvašňák E, Popelář J, Syka J (2003) Representation of species-specific vocalizations in the inferior colliculus of the guinea pig. *Journal of neurophysiology* **90**(6):3794–3808

Šuta D, Popelář J, Kvašňák E, Syka J (2007) Representation of species-specific vocalizations in the medial geniculate body of the guinea pig. *Experimental brain research* **183**(3):377–388

Šuta D, Popelář J, Burianová J, Syka J (2013) Cortical representation of species-specific vocalizations in Guinea pig. *PloS one* **8**(6):e65432

Timofeev I, Grenier F, Bazhenov M, Sejnowski TJ, Steriade M (2000) Origin of slow cortical oscillations in deafferented cortical slabs. *Cerebral Cortex* **10**(12):1185–1199

Traub RD, Spruston N, Soltesz I, Konnerth A, Whittington MA, Jefferys GR (1998) Gamma-frequency oscillations: a neuronal population phenomenon, regulated by synaptic and intrinsic cellular processes, and inducing synaptic plasticity. *Progress in Neurobiology* **55**(6):563–575

de Villers-Sidani E, Chang EF, Bao S, Merzenich MM (2007) Critical period window for spectral tuning defined in the primary auditory cortex (A1) in the rat. *The Journal of Neuroscience* **27**(1):180–189

Wagatsuma N, Potjans TC, Diesmann M, Fukai T (2011) Layer-Dependent Attentional Processing by Top-down Signals in a Visual Cortical Microcircuit Model. *Frontiers in Computational Neuroscience* **5**(31):1–15

Watson C (2012) *The mouse nervous system*. Academic Press

Wendykier P (2013) Parallel Colt. URL `https://sites.google.com/site/piotrwendykier/software/parallelcolt`

Wendykier P, Nagy JG (2010) Parallel colt: a high-performance Java library for scientific computing and image processing. *ACM Transactions on Mathematical Software (TOMS)* **37**(3):31

Wilson NR, Runyan CA, Wang FL, Sur M (2012) Division and subtraction by distinct cortical inhibitory networks in vivo. *Nature* **488**(7411):343–348

Winer JA (2006) Decoding the auditory corticofugal systems. *Hearing Research* **212**(1):1–8

Winer JA, Lee CC (2007) The distributed auditory cortex. *Hearing Research* **229**(1-2):3

Wu GK, Arbuckle R, Liu Bh, Tao HW, Zhang LI (2008) Lateral sharpening of cortical frequency tuning by approximately balanced inhibition. *Neuron* **58**(1):132–143

Wu GK, Tao HW, Zhang LI (2011) From elementary synaptic circuits to information processing in primary auditory cortex. *Neuroscience & Biobehavioral Reviews* **35**(10):2094–2104

Xu S, Jiang W, Poo M, Dan Y (2012) Activity recall in a visual cortical ensemble. *Nature Neuroscience* **15**(3):449–455

Xu H, Jeong HY, Tremblay R, Rudy B (2013) Neocortical somatostatin-expressing GABAergic interneurons disinhibit the thalamorecipient layer 4. *Neuron* **77**(1):155–167

Yuste R, Denk W (1995) Dendritic spines as basic functional units of neuronal integration. *Nature* **375**(6533):682–684

Zhang LI, Bao S, Merzenich MM (2001) Persistent and specific influences of early acoustic environments on primary auditory cortex. *Nature Neuroscience* **4**(11):1123–1130

Zhang LI, Bao S, Merzenich MM (2002) Disruption of primary auditory cortex by synchronous auditory inputs during a critical period. *Proceedings of the National Academy of Sciences* **99**(4):2309–2314

Zhou X, Nagarajan N, Mossop BJ, Merzenich MM (2008) Influences of un-modulated acoustic inputs on functional maturation and critical-period plasticity of the primary auditory cortex. *Neuroscience* **154**(1):390–396

Zhou Y, Mesik L, Sun YJ, Liang F, Xiao Z, Tao HW, Zhang LI (2012) Generation of spike latency tuning by thalamocortical circuits in auditory cortex. *The Journal of Neuroscience* **32**(29):9969–9980

Zingg B, Hintiryan H, Gou L, Song MY, Bay M, Bienkowski MS, Foster NN, Yamashita S, Bowman I, Toga AW (2014) Neural networks of the mouse neocortex. *Cell* **156**(5):1096–1111

Zucker RS (1989) Short-term synaptic plasticity. *Annual Review of Neuroscience* **12**(1):13–31

Supplementary Materials

Formation and disruption of tonotopy in a large-scale model of the auditory cortex

Journal of Computational Neuroscience

Markéta Tomková[1a,c], Jakub Tomek[a,c], Ondřej Novák[b], Ondřej Zelenka[b], Josef Syka[b], and Cyril Brom[a]

[a]Faculty of Mathematics and Physics, Charles University in Prague, Czech Republic
[b]Department of Auditory Neuroscience, Institute of Experimental Medicine, Academy of Sciences of the Czech Republic, Prague, Czech Republic
[c]Life Sciences Interface Doctoral Training Centre, University of Oxford, United Kingdom

9th May 2015

[1]marketa.tomkova@stcatz.ox.ac.uk

Chapter 1

Methods: Model of the Auditory Cortex

This section contains selected details of the presented model. The text is based on (Popelova, 2013). It follows the guidelines suggested by Nordlie et al. (2009), which, as we hope, will help to make the description comprehensible and reproducible. All the model parameters are written in the following `font`.

1.1 Model composition

The model consists of the layers L1, L2/3, L4, L5, and L6. The layer L4 is an input layer. The neurons are distinguished according to populations called `neuronal types`. All neurons of the same neuronal type lie in the same `layer` of the cortex and have the same parameters of the neuron model – the generalised form of the Izhikevich neuron model (Izhikevich, 2007; Izhikevich and Edelman, 2008). The number of neurons of each type is specified by the percentage with the name `cells`, i.e. the resulting number of neurons of this type is `cells`*`N_NEURONS / 100`, where `N_NEURONS` is the total number of neurons in the network and is a general parameter of the model.

Each neuronal type has a specified area reached by its axon (and its terminals). This area is specified as an axonal radius (in μm) for each layer of the network (see Figure 1.1). We will refer to these values as table **X0**, where **X0**[T][L] gives the value of axonal radius of neuronal type T in layer L. These values are used during the generation of synaptic connections: a synapse can be created only between such neurons where the soma of a postsynaptic neuron is reached by an axonal area of the presynaptic neuron. This is a simplification based on (Izhikevich and Edelman, 2008).

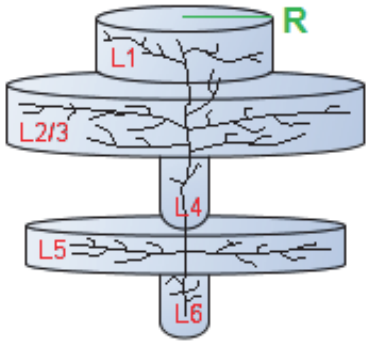

Figure 1.1: An example of axonal areas. In each layer, the axonal area is specified by its radius **R**.

The parameters of the 17 neuronal types used are listed in Section 1.8. The parameter `type` (additional information) is used to distinguish between 4 cell types:

1. pyramidal neurons (p): these exhibit regular spiking (RS), or sometimes chattering (CH), or intrinsically bursting (IB) firing patterns (Connors and Gutnick, 1990; Contreras, 2004)
2. spiny stellate neurons (ss): these exhibit RS firing patterns (Contreras, 2004)

3. basket interneurons (b): these exhibit fast spiking (FS) firing patterns (Connors and Gutnick, 1990; Contreras, 2004)

4. non-basket interneurons (nb), which morphologically include double-bouquet cells, neurogliaform cells, and Martinotti cells (Binzegger et al., 2004) and can exhibit low threshold spiking (LTS) firing pattern (Beierlein et al., 2003), latent spiking (LS) and other firing patterns (Kawaguchi, 1995; Kawaguchi and Kubota, 1997; Markram et al., 2004)

The `names` of neuronal types are based on nomenclature as in (Izhikevich and Edelman, 2008; Beierlein et al., 2003), where the first part is the cell type (b, nb, p, ss), the second part is the layer and the optional third part in brackets is the layer, to which the neuron projects (only in ss and p neurons); for example $p5_{(L2/3)}$ means pyramidal neurons in L5 that project (mainly) to L2/3.

The algorithm for initialising neurons, their locations and other parameters is described in the Pseudocode 1.1. The locations are generated randomly in the relevant layer, but in such a way that neurons do not overlap. Here, the general parameter `RADIUS` is used (all neuron use the same value). By neuron's location we mean the location of the neuron's soma. Other parameters are used according to the neuronal type.

```
1. i=0;
2. For each neuronal type T:
   (a) N_T ← T.cells * N_NEURONS / 100;
   (b) For j from 0 to N_T:
       i. Create a neuron with the following parameters:
          A. number i
          B. random location in the layer T.layer, which does not overlap with
             any soma of a previous neuron
          C. T.excitatory
          D. T.layer
          E. membrane potential T.vr and membrane recovery 0
          F. parameters T.Cap, T.cr, T.vt, T.vp, T.a, T.b, T.c and T.b
      ii. If (T.layer is input layer) then
          A. add the created neuron to a band neuron.location.y / BAND_WIDTH
     iii. i++;
```

Pseudocode 1.1: The algorithm of the generation of neurons in the model.

1.2 Coordinate systems and topology

All neurons are given numbers from interval ⟨0, N_NEURONS), each neuron having a unique number. We use the *anatomical coordinates* according to the coordinate systems listed in (Nordlie et al., 2009), because population (neuronal type) determines the layer within the AC and each neuron has a location that refers to a position in the AC.

1.3 Connectivity

The connectivity mechanism is based on the mechanism described in (Izhikevich and Edelman, 2008). However, their publication does not explain the connectivity in sufficient enough detail for reimplementation (this opinion has been voiced also by Nordlie et al. (2009)). Therefore we proposed additional mechanisms and algorithms to make a clearly defined connectivity.

1.3.1 Connectivity data

The connectivity mechanism uses two tables. The first table (table **X1**) defines, for each neuronal type T, the recommended number of synapses which lead to each neuron of this type. We will call this number **X1**[T].

The second table (table **X2**) has three dimensions: postsynaptic neuronal type T_post, presynaptic neuronal type T_pre, and layer L of the synapse location. The value **X2**[T_post][T_pre][L] means that each neuron of type T_post should receive **X2**[T_post][T_pre][L] % of its synapses from neurons of type T_pre in layer L. The range of the values in this table is $\langle 0, 100 \rangle$. The resulting number of synapses from T_pre neurons to a neuron of T_post type in layer L is:

X1[T_post] * **X2**[T_post][T_pre][L] / 100

1.3.2 Selecting presynaptic candidates

Selecting presynaptic candidates – description

In the algorithm that generates connectivity, it was necessary to solve the following situation. The tables **X1** and **X2** determine the number of synapses to neuron N_post (of type T_post) from neurons of type T_pre in the layer L. Let S be this number. Only near enough neurons may be chosen as presynaptic – for simplicity only those, radius of which in layer L reaches the soma of the neuron N_post. The nearer neurons should have a higher probability of connection than the distant ones (Izhikevich and Edelman, 2008; Levy and Reyes, 2012). For simplicity, we can consider that this probability decays linearly from the centre of the circle defined by the axonal radius to a zero value at the edge (as it is used in (Izhikevich and Edelman, 2008)). Distance d can be considered only two dimensional (in our coordinate system named as x and y) – not in the dimension of height (which goes through all layers). This is reasonable due to the fact that if an axon goes through a layer (its radius being nonzero in the layer), then the distance from the axis of the axon should be considered. As a metric, the Euclidean distance can be used. For simplicity of the model, axons are assumed to grow directly vertical. The situation is depicted in Figure 1.2, the relevant distance has the label d.

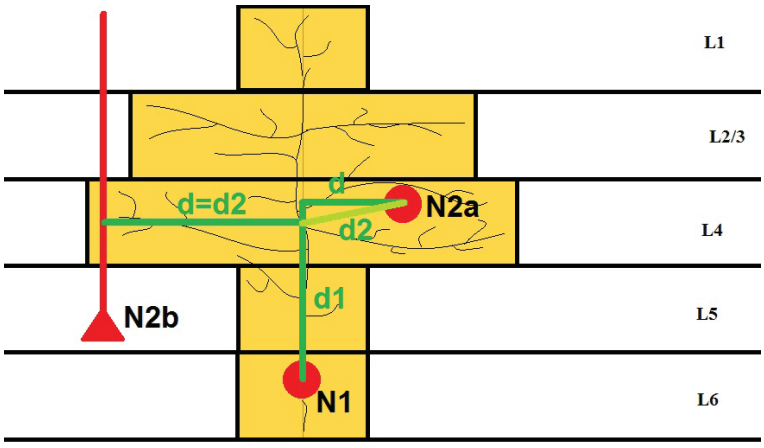

Figure 1.2: A schema of possible connections. The neuron N1 is a presynaptic neuron and N2a and N2b are postsynaptic neurons. (N2b is a pyramidal neuron.) Distances d1 and d2 will be used during initialisation of the conductance delays. Distance d is used in computation of probability of the connection.

This means that we have a set of candidates (K), from which a connection may lead to a neuron N_post and each candidate N_pre has a probability of forming a synapse to N_post depending on their distance d. We denote this probability by N_pre.P. Subsequently, we want to choose S candidates (presynaptic neurons) from the set K and create a synaptic connection from these chosen candidates to neuron N_pre.

Selecting presynaptic candidates – solution

Hence, the situation is simplified to an abstract mathematical problem defining how to select S elements from set of $|K|$ candidates, where each has a given probability of selection. One typical computer-science solution for this problem is the *Roulette Wheel Selection* (used in Genetic Algorithms (see, e.g., Goldberg, 1989)). We create a roulette with $|K|$ pockets, where pocket N_pre has a size N_pre.P. Subsequently, we throw a ball in the roulette and spin the wheel and the element (neuron) associated with the winning pocket is selected. The wheel is spun S times. Therefore we say that we throw (in sum) S balls in the roulette, which determines S winning candidates. The Roulette Wheel Selection is depicted in Figure 1.3.

It is obvious that larger pockets have larger probability to be selected. It is good to consider that we do not mind selecting one candidate more times (this means that more balls fell to the same pocket). In such a case, more synapses between one pair of neurons are created (we call it a multi-connection), which corresponds to real observations (see the Section 1.3.6). Besides, the algorithm could be easily adjusted to avoid multi-connections (e.g., when a pocket is selected, we remove the pocket from the roulette).

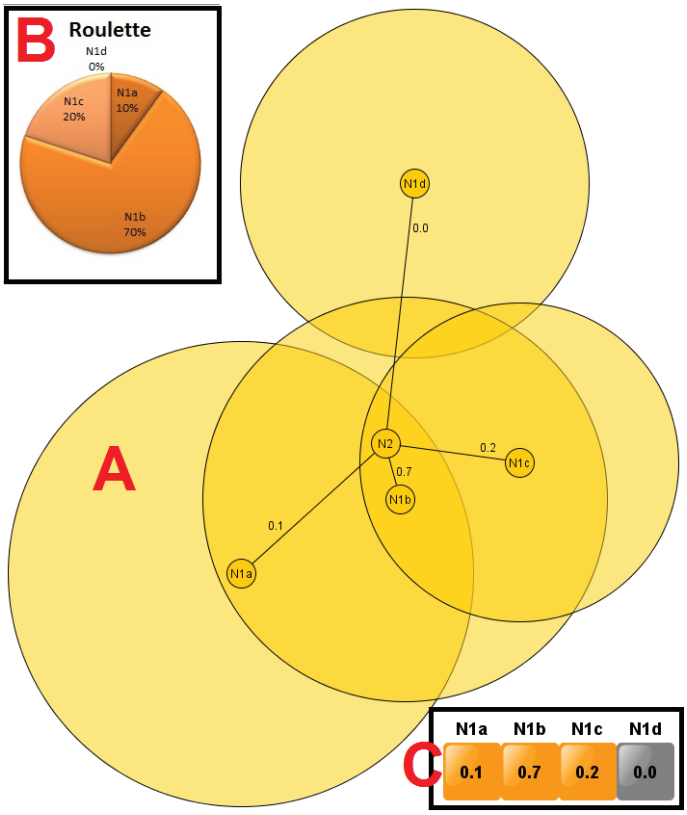

Figure 1.3: A schema of the Roulette Wheel Selection of presynaptic neurons. Part A of the figure: The view from above the network. N2 is a postsynaptic neuron (in the center) and N1a, N1b, N1c, N1d form a set K of possible presynaptic neurons. The probabilities of these connections are respectively: N1a: 0.1, N1b: 0.7, N1c: 0.2, N1d: 0.0 (the axonal area of N1d does not reach N2). Part B of the figure: a schema of the relevant roulette wheel with pockets corresponding to the presynaptic neurons (and sizes of the pockets corresponding to the probabilities of the connections from these neurons to N2). Part C of the figure: the resulting roulette represented as an array.

This algorithm can be easily and effectively implemented. The sizes of pockets are stored in an array (see part C of the Figure 1.3). Then a throw of a ball into the roulette means generating one (pseudo)random number from uniform distribution within an interval $\langle 0, \mathrm{SUM})$, where SUM means the sum of all pocket sizes. Subsequently, the relevant pocket (which corresponds to the generated number) is looked up and represents the index number of the first selected candidate. This procedure is repeated S times.

1.3.3 Setting synaptic conductance delays

The synaptic conductance delay should be dependent on the length of the connection and speed of transmission. For simplicity, we will consider the same transmission speed for all connections (even though the real speed depends on many factors, such as myelination, type of connection, distinction between transmission speed on axon and dendrite, etc.). The length of the connection consists of two parts: the vertical part along axon (called d1) and horizontal part to the axon bouton (d2); see Figure 1.2.

Let N_pre be the presynaptic neuron, N_post be the postsynaptic neuron and L be the layer, where the synapse lies. Distance d1 can be defined as the Manhattan distance (also called taxicab distance, city block distance, or rectilinear distance) between location of N_pre and location L, which is defined as an axis of the axon of N_pre in the middle of layer L. Distance d2 can be defined as the Manhattan distance between L and location of N_post.

Besides this deterministic component of the delay, we decided to add a stochastic component in the form of small (pseudo)random perturbation generated from the uniform distribution within an interval $\langle 0$, `DELAY_PERTURBATION`$)$, where `DELAY_PERTURBATION` is a general parameter of the model. The resulting value of delay is bounded from above by the value `MAX_DELAY`, which is also a general parameter of the model.

1.3.4 Setting synaptic weights

Excitatory synapses (the synapses from excitatory neurons) have non-negative weights and inhibitory synapses (the synapses from inhibitory neurons) have non-positive weights. Although in some models, the weight values are dependent on connection length (e.g., Bart et al., 2005), according to results obtained from recordings of the mouse primary auditory cortex (Levy and Reyes, 2012), the synaptic weight does not seem to be correlated with distance between somata. We therefore do not account for this factor in the initial values of synaptic weight. The resulting initial weight values were chosen as (pseudo)randomly generated from uniform distribution within an interval $\langle 0$, `PARAM_W_EXC`$)$ for excitatory synapses and (`-PARAM_W_INH`, $0\rangle$ for inhibitory synapses, where `PARAM_W_EXC` and `PARAM_W_INH` are general parameters of the model.

1.3.5 Connectivity algorithm

The resulting algorithm of generating synaptic connections is described in the Pseudocode 1.2. It is based on the mechanisms explained in the previous subsections. The algorithm contains just the main ideas. In terms of efficiency, it is worth skipping passages where one of the following values is zero:

- `AXONAL_RADIUS` (the axonal area of presynaptic neuron does not reach the layer L)
- S, i.e. number of balls (no such connection should be created)
- size of the set of candidates (any presynaptic neuron does not fulfil the condition of the connection)

It is important to realise that the set of candidates can be small or even empty. If the set is empty, it means that no presynaptic neuron of the right type reaches the postsynaptic neuron. Then no such connections will be created. This may be considered a reasonable result. However, if the set is non-empty but small (e.g., smaller than S, the number of balls thrown into the roulette), it may lead to enforced "mega-multi-connections", such as 100 connections between one pair of neurons. The resulting network may behave in a very inappropriate way, such as groups of neurons firing every time step for a long period of time (this is based on our observations). For the question of multi-connections, see Section 1.3.6.

Therefore we proposed a mechanism, which prevents the creation of mega-multi-connections, but does not avoid all multi-connections. This mechanism simply limits the number of balls S in a single roulette pocket to maximal value of $|K|$, the number of candidates (nonzero pockets in the roulette). Therefore, there is always a possibility of no multi-connections, but in practise a certain number of multi-connections are created.

1.3.6 Possible pitfalls and other features

Self-connections: "If the same neuron can be selected as pre- and post-synaptic neuron, is this connection allowed?"

The proposed model does not allow connection from one neuron to the same neuron. This restriction was decided upon in order to prevent negative and inappropriate effects on dynamics of the whole network.

```
1. For each postsynaptic neuronal type T_post, layer L, and presynaptic neuronal
   type T_pre:

   (a) S ← X1[T_post] * X2[T_post][T_pre][L] / 100

   (b) AXONAL_RADIUS ← X0[T_pre][L]

   (c) For each neuron N_post of type T_post:

        i. Create a roulette of possible presynaptic candidates:  each
           presynaptic neuron N_pre of type T_pre (other than N_post) will have
           a pocket of size max(0, AXONAL_RADIUS -d), where d is an Euclidean
           distance from N_pre to N_post in x and y coordinates

       ii. SUBPROGRAM(roulette, N_post)
```

Pseudocode 1.2: The algorithm of generating the connectome. The Roulette Wheel Selection is used to select the presynaptic neurons, which will be connected with `N_post`. Probability of these connections is based on the distance d (see Figure 1.2. When a roulette is created, the presynaptic neurons are selected via a process described in the SUBPROGRAM: 1.3.

```
SUBPROGRAM(roulette, N_post):

  1. S times:

     (a) Throw a ball into roulette and call N_pre the winning pocket.

     (b) delay ← max( MAX_DELAY, 1+round(d1+d2/VELOCITY) +
         rand(DELAY_PERTURBATION) ), where:

          i. d1 ← distance between N_pre.location.z and z_L, which is z coordinates
             of the centre of the layer L

         ii. d2 ← Manhattan distance between locations (N_pre.location.x,
             N_pre.location.y, z_L) and N_post

     (c) If (N_pre is excitatory)

          i. weight ← PARAM_W_EXC*randomDouble {from ⟨0,1)}

     (d) Else

          i. weight ← PARAM_W_INH*randomDouble {from ⟨0,1)}

     (e) Create a synapse from N_pre to N_post with parameters delay, weight and
         zero weightDerivate.
```

Pseudocode 1.3: The algorithm of selecting S presynaptic neurons (which will be connected with N_post), using a roulette created in the Pseudocode 1.2. When a presynaptic neuron is selected, the synaptic delay and weight are initialised. The distances d1 and d2 are depicted in Figure 1.2.

Recurrence, which is an important feature in both real and artificial neural networks, is present in the form of cycles longer than one edge, i.e. loops (using the terminology from theory of graphs, see (Matousek and Nesetril, 1998)).

Multi-connections: "If a pair of pre- and post-synaptic neurons can be chosen more than once, is this connection allowed?"

The proposed model allows such multi-connections between one pair of neurons, but prevents occurrence of "mega-multi-connections" (i.e. high number of connections between one pair of neurons).

Boundary effects: "How are boundary effects in topological connections handled?"

The proposed model does not treat the connections on borders differently than neurons in the centre of the network. The only difference is that neurons on borders might receive more multi-connections, because the set of presynaptic neurons is smaller. The resulting state is similar as if the weights would be adjusted (as it is used, e.g., in (Chrostowski et al., 2011)). The most common alternative prevention of the boundary effects is mapping of the network on a ring (Vida et al., 2006),(Tsodyks and Sejnowski, 1995), torus (Percha et al., 2005),(Mehring et al., 2003), or sphere (Izhikevich, 2004). However, in such a solution, neurons from one border of the network would be connected to neurons from the opposite border of the network, e.g., neurons from band 1 with neurons from band 50. This could have a significant negative influence on the resulting tonotopy. Therefore, we rejected this alternative as unsuitable for the case of the AC.

1.4 Neurons and synapses

All neurons are single-compartmental and are modelled by the generalised form of the Izhikevich neuron model (Izhikevich, 2007), described in the main text. The parameters of the equations are determined by the neuronal type (see the Section 1.1 for definition of the used neuronal types and the Section 1.8 for the used parameters). The synaptic conduction delays are static (they do not change over time). The synaptic weights evolve according to the STDP, described in the main text. All implementation details can be found in the (Popelova, 2013, Chapter 3). All neurons are single-compartmental and they are modelled by the generalised form of the Izhikevich neuron model (Izhikevich, 2007), described in the main text. The parameters of the equations are determined by the neuronal type (see the Section 1.1 for definition of the used neuronal types and the Section 1.8 for the used parameters). The synaptic conduction delays are static (they do not change over time). The synaptic weights evolve according to the STDP, described in the main text. All implementation details can be found in the (Popelova, 2013, Chapter 3).

1.5 Model input and output

The model has two kinds of inputs: first, the external inputs from the thalamus, and second, the internal inputs in the form of miniature postsynaptic currents (mPSCs). The latter are not exactly inputs, but an internal mechanism leading to spontaneous activity. The main feature measured as output of the model are spike of all the neurons and their times. These spike trains are plotted as spike-time raster plots and used for computation of average firing activity, local and global oscillations and receptive fields of the neurons and subsequent analysis of the network tontopy. Synaptic weights are a side feature measured as an output.

1.6 Model validation

Model validation can have several meanings. First (as it is meant in Nordlie et al., 2009), it can mean to provide information and partial results that will allow others to test and validate re-implementations of the model. The used models of neurons and synapses are well known and their behaviour can be found, e.g., in (Izhikevich, 2003, 2006).

Second, it can mean a comparison of the model and the reality in basic features. According to this meaning, we designed and ran a set of validation experiments, described in the main text.

1.7 Model implementation

We used the SUSNOIMAC simulator tool for the simulation and additional Matlab scripts for the results' analyses. All implementation details can be found in the (Popelova, 2013, Chapter 3).

1.8 Model parameters

In this section we list all used parameters, their description and values used. The parameters of the model are divided into five groups: the general model parameters, neuronal types, layers, and connectivity. In addition to this, each experiment has its own setting for input parameters and simulation parameters.

1.8.1 General model parameters

The general model parameters are listed in the Table 1.1.

Name	Unit	Description	Used values
WIDTH	μm	Width of the network.	2000
LENGTH	μm	Length of the network.	3000
N_NEURONS	-	Total number of neurons in the network.	50 000, 100 000
RADIUS	μm	Radius of a typical neuron (used to prevent overlapping).	10
VELOCITY	μm/ms	Speed of signal transmission along synaptic connection.	100
N_BANDS	-	Number of input bands in the input layers.	50
MAX_DELAY	ms	Maximal synaptic conductance delay.	20
MAX_WEIGHT	-	Maximal weight of excitatory synapses.	100
DELAY_PERTURBATION	ms	Each initial synaptic delay is perturbed by a random number from interval $\langle 0,$ DELAY_PERTURBATION$)$.	5
PARAM_W_EXC	-	Initial weight of an excitatory synapse is a random number from interval $\langle 0,$PARAM_W_EXC$)$.	100
PARAM_W_INH	-	Initial weight of an inhibitory synapse is a random number from interval $($PARAM_W_INH$,0\rangle$.	-50

Table 1.1: The **general** parameters of the model.

1.8.2 Layer parameters

The used layers and their parameters are listed in the Table 1.2.

Layer	Thickness (μm)	Is input layer
L1	69	No
L2/3	235	No
L4	208	Yes
L5	248	No
L6	451	No

Table 1.2: Parameters of the **layers** of the model.

1.8.3 Neuronal types parameters

The used neuronal types and their parameters are listed in the Table 1.3.

Label	T	L	Cells	C	k	v_r	v_t	v_p	a	b	c	d	exc.
nb1	nb	L1	1.512	20	0.3	-66	-40	30	0.17	5	-45	100	false
p2/3	p	L2/3	26.21	100	3	-60	-50	50	0.01	5	-60	400	true
b2/3	b	L2/3	3.125	20	1	-55	-40	25	0.15	8	-55	200	false
nb2/3	nb	L2/3	4.234	100	1	-56	-42	40	0.03	8	-50	20	false
$ss4_{(L4)}$	ss	L4	9.274	100	3	-60	-50	50	0.01	5	-60	400	true
$ss4_{(L2/3)}$	ss	L4	9.274	100	3	-60	-50	50	0.01	5	-60	400	true
p4	p	L4	9.274	100	3	-60	-50	50	0.01	5	-60	400	true
b4	b	L4	5.444	20	1	-55	-40	25	0.15	8	-55	200	false
nb4	nb	L4	1.512	100	1	-56	-42	40	0.03	8	-50	20	false
$p5_{(L2/3)}$	p	L5	4.839	100	3	-60	-50	50	0.01	5	-60	400	true
$p5_{(L5/6)}$	p	L5	1.31	100	3	-60	-50	50	0.01	5	-60	400	true
b5	b	L5	0.605	20	1	-55	-40	25	0.15	8	-55	200	false
nb5	nb	L5	0.806	100	1	-56	-42	40	0.03	8	-50	20	false
$p6_{(L4)}$	p	L6	13.71	100	3	-60	-50	50	0.01	5	-60	400	true
$p6_{(L5/6)}$	p	L6	4.839	100	3	-60	-50	50	0.01	5	-60	400	true
b6	b	L6	2.016	20	1	-55	-40	25	0.15	8	-55	200	false
nb6	nb	L6	2.016	100	1	-56	-42	40	0.03	8	-50	20	false

Table 1.3: Parameters of the **neuronal types** of the model. The units are: Cells (%), v_r, v_t, v_p (mV). Column exc. means whether the neuronal type is excitatory.

The used axonal radii of neuronal types in all layers (table called **X0** in the previous text) are listed in Table 1.4.

Label	L1	L2/3	L4	L5	L6
nb1	200	200	200	200	200
p2/3	550	1120	150	1000	150
b2/3	0	150	150	150	0
nb2/3	200	200	200	200	200
$ss4_{(L4)}$	0	300	1120	400	150
$ss4_{(L2/3)}$	150	400	500	150	150
p4	150	1120	150	550	150
b4	0	0	500	0	0
nb4	200	200	200	200	200
$p5_{(L2/3)}$	150	400	300	500	250
$p5_{(L5/6)}$	0	0	150	500	1000
b5	0	0	0	500	0
nb5	200	200	200	200	200
$p6_{(L4)}$	0	0	150	500	1000
$p6_{(L5/6)}$	0	150	1000	150	150
b6	0	0	0	0	500
nb6	200	200	200	200	200

Table 1.4: Parameters of the model related to the **axonal areas** (axonal radii in layers, in μm).

1.8.4 Connectivity parameters

The used parameters related to connectivity are listed in Figure 1.4 (in the previous text this table was called **X1** (the column Syn) and **X2** (the rest of the table)).

Label	Layer	Syn	nb1	p2/3	b2/3	nb2/3	ss4(L4)	ss4(L2/3)	p4	b4	nb4	p5(L2/3)	p5(L5/6)	b5	nb5	p6(L4)	p6(L5/6)	b6	nb6
nb1	L1	445	10.1	6.3	0.6	1.1	x	x	0.1	x	x	0.1	x	x	x	x	x	x	x
p2/3	L2/3	290	x	59.9	9.1	4.4	0.6	6.9	7.7	x	0.8	7.4	x	x	x	2.3	x	x	0.8
p2/3	L1	65	10.2	6.3	0.1	1.1	x	x	0.1	x	x	0.1	x	x	x	x	x	x	x
b2/3	L2/3	193	1.3	51.6	10.6	3.4	0.5	5.8	6.6	x	0.8	6.3	x	x	x	2.1	x	x	0.7
nb2/3	L2/3	165	1.7	48.6	11.4	3.3	0.5	5.5	6.2	x	0.8	5.9	x	x	x	1.8	x	x	0.6
ss4(L4)	L4	290	x	2.7	0.2	0.6	11.9	3.7	4.1	7.1	2	0.8	0.1	x	x	32.7	x	x	5.8
ss4(L2/3)	L4	249	x	5.6	0.4	0.8	11.3	3.8	4.3	7.2	2.1	1.1	0.1	x	x	31.1	x	x	5.5
p4	L4	252	x	4.3	0.2	0.6	11.5	3.6	4.2	7.2	2.1	1.2	0.1	x	x	31.4	0.1	x	5.9
p4	L2/3	43	x	63.1	5.1	4.1	0.6	7.2	8.1	x	0.6	7.8	x	x	x	2.5	x	x	0.8
p4	L1	40	10.2	6.3	0.1	1.1	x	x	0.1	x	x	0.1	x	x	x	x	x	x	x
b4	L4	162	x	5.8	0.5	0.8	11	3.8	4.2	8.4	2.4	1.1	x	x	x	30.3	x	x	5.4
nb4	L4	184	x	2.7	0.2	0.6	11.7	3.6	4	8.2	2.3	0.8	0.1	x	x	32.2	x	x	5.7
p5(L2/3)	L5	216	x	45.9	1.8	0.3	3.3	2	7.5	x	0.9	11.7	1	0.8	1.1	2.3	2.1	x	11.5
p5(L2/3)	L4	14	x	2.8	0.1	0.7	12.2	3.8	4.2	5.2	1.5	0.8	0.1	x	x	33.7	x	x	5.9
p5(L2/3)	L2/3	21	x	63.1	5.1	4.1	0.6	7.2	8.1	x	0.6	7.8	x	x	x	2.5	x	x	0.8
p5(L2/3)	L1	9	10.2	6.3	0.1	1.1	x	x	0.1	x	x	0.1	x	x	x	x	x	x	x
p5(L5/6)	L5	255	x	44.3	1.7	0.2	3.2	2	7.3	x	0.8	11.3	1.2	0.8	1.1	2.3	2.5	0.3	11.3
p5(L5/6)	L4	47	x	2.8	0.1	0.7	12.2	3.8	4.2	5.2	1.5	0.8	0.1	x	x	33.7	x	x	5.9
p5(L5/6)	L2/3	68	x	63.1	5.1	4.1	0.6	7.2	8.1	x	0.6	7.8	x	x	x	2.5	x	x	0.8
p5(L5/6)	L1	283	10.2	6.3	0.1	1.1	x	x	0.1	x	x	0.1	x	x	x	x	x	x	x
b5	L5	149	x	45.5	2.3	0.2	3.3	2	7.5	x	1.1	11.6	1	0.9	1.3	2.3	2	x	11.4
nb5	L5	149	x	45.5	2.3	0.2	3.3	2	7.5	x	1.1	11.6	1	0.9	1.3	2.3	2	x	11.4
p6(L4)	L6	163	x	2.5	0.1	0.1	0.7	0.9	1.3	x	0.1	0.1	4.9	x	0.3	1.2	13.2	7.7	7.7
p6(L4)	L5	53	x	46.8	0.8	0.3	3.4	2.1	7.7	x	0.6	11.9	1	0.6	0.8	2.3	2.1	x	11.7
p6(L4)	L4	96	x	2.8	0.1	0.7	12.2	3.8	4.2	5.2	1.5	0.8	0.1	x	x	33.7	x	x	5.9
p6(L4)	L2/3	6	x	63.1	5.1	4.1	0.6	7.2	8.1	x	0.6	7.8	x	x	x	2.5	x	x	0.8
p6(L5/6)	L6	279	x	2.5	0.1	0.1	0.7	0.9	1.3	x	0.1	0.1	4.9	x	0.3	1.2	13.2	7.8	7.8
p6(L5/6)	L5	13	x	46.8	0.8	0.3	3.4	2.1	7.7	x	0.6	11.9	1	0.6	0.8	2.3	2.1	x	11.7
p6(L5/6)	L4	12	x	2.8	0.1	0.7	12.2	3.8	4.2	5.2	1.5	0.8	0.1	x	x	33.7	x	x	5.9
p6(L5/6)	L2/3	14	x	63.1	5.1	4.1	0.6	7.2	8.1	x	0.6	7.8	x	x	x	2.5	x	x	0.8
p6(L5/6)	L1	3	10.2	6.3	0.1	1.1	x	x	0.1	x	x	0.1	x	x	x	x	x	x	x
b6	L6	161	x	2.5	0.1	0.1	0.7	0.9	1.3	x	0.1	0.1	4.9	x	0.4	1.2	13.2	7.7	7.7
nb6	L6	161	x	2.5	0.1	0.1	0.7	0.9	1.3	x	0.1	0.1	4.9	x	0.4	1.2	13.2	7.7	7.7

Figure 1.4: Parameters of the model related to the connectome. The column Syn defines a number of synapses from presynaptic neuron (rows, column Label)) to postsynaptic neuron (columns), which occur in a given layer (column Layer).

1.8.5 Input parameters

The parameters related to input of our modelled networks are listed in the Figure 1.5.

Name	Unit	Description	Used values
INPUT_TYPE	-	Type of input (0 ∼ nothing, 1 ∼ minis, 2 ∼ noise, 3 ∼ few pure tones, 4 ∼ more pure tones, 5 ∼ more normal sounds, 6 ∼ tonotopy experiment)	1, 2, 3, 4, 6
INPUT_VALUE	pA	Value of the input current.	1500
INPUT_DURATION	ms	Duration of one input.	500
BANDS	-	List of used bands separated by semicolons.	different values
INTENSITIES	-	List of used intensities expressed as probabilities in the range $\langle 0, 1\rangle$ separated by semicolons.	different values

Table 1.5: Input parameters.

1.9 Tabular description

Finally, an overall summarised description, as it is recommended in guidelines by Nordlie et al. (2009), is listed in the Table 1.6.

	Model Summary
Populations	Seventeen: nb1, p2/3, b2/3, nb2/3, $ss4_{(L4)}$, $ss4_{(L2/3)}$, p4, b4, nb4, $p5_{(L2/3)}$, $p5_{(L5/6)}$, b5, nb5, $p6_{(L4)}$, $p6_{(L5/6)}$, b6, nb6
Topology	3D coordinates within a network
Connectivity	Generated according to probabilities of connections between all pairs of neuronal types
Neuron model	Generalised Izhikevich neuron model (Izhikevich, 2007)
Channels models	-
Synapse model	Fixed synaptic conduction delays and changeable synaptic weights
Plasticity	STDP
Input	Tonotopic inputs from thalamus
Measurements	Spike trains (and from them spike-time raster plot and global and local waves); development of: mean activity (within a network and individual neuronal types), weights and their distribution, tonotopic features (receptive fields, best frequencies and measure of tonotopy)

Table 1.6: A summarised tabular description of the presented model.

Chapter 2

Results

2.1 Validation Experiments

This section contains additional figures depicting results from the validation experiments: development of the excitatory weights in Fig. 2.1, development of the firing rate in Fig. 2.2 and 2.3. The remainder of this section is focused on brief evaluation of evoked activity and testing of inhibitory-excitatory (I-E) models as a possible source of gamma oscillations.

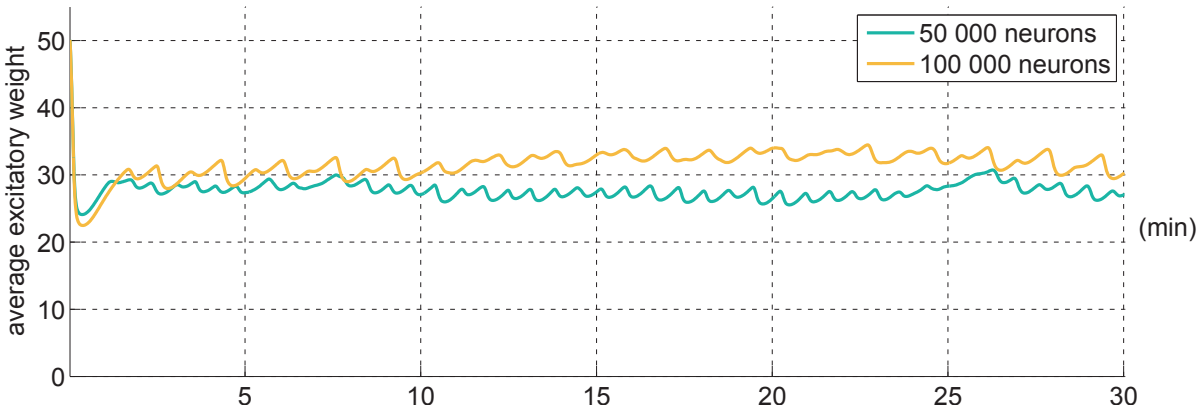

Figure 2.1: A comparison of the development of the mean excitatory weights between the network sizes: 50 000 (green) and 100 000 (yellow). As we can see, the weights in both networks reach a stable stereotypical dynamic state. The fact that the larger network has slightly higher average values than the smaller network could be explained by the sparseness of the smaller network, because in the sparse network, there is a higher probability that a synapse will die out (when a postsynaptic neuron does not receive sufficient input).

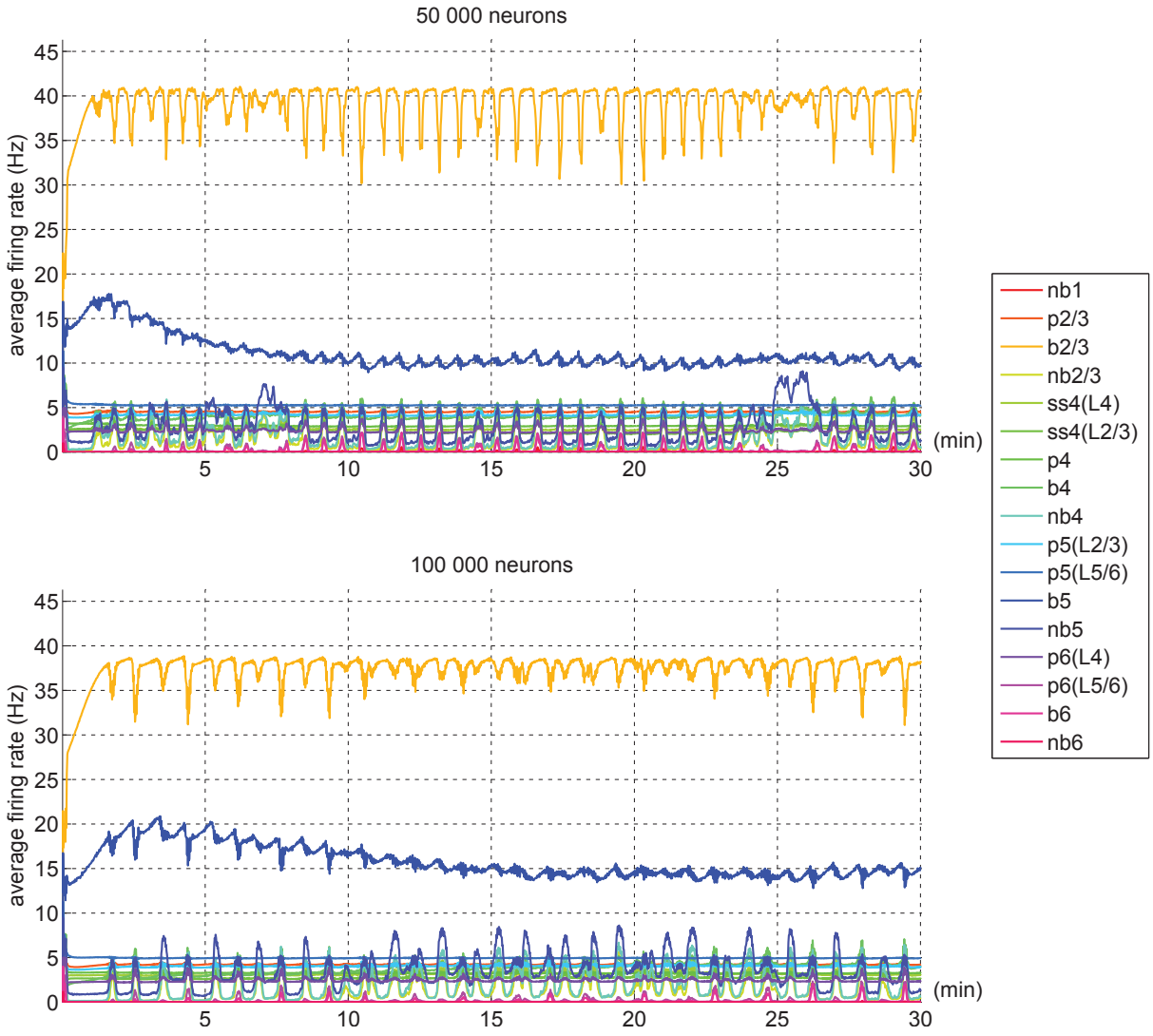

Figure 2.2: The mean firing rate activity of individual neuronal types in single runs of networks with 50 000 neurons (top) and 100 000 neurons (bottom).

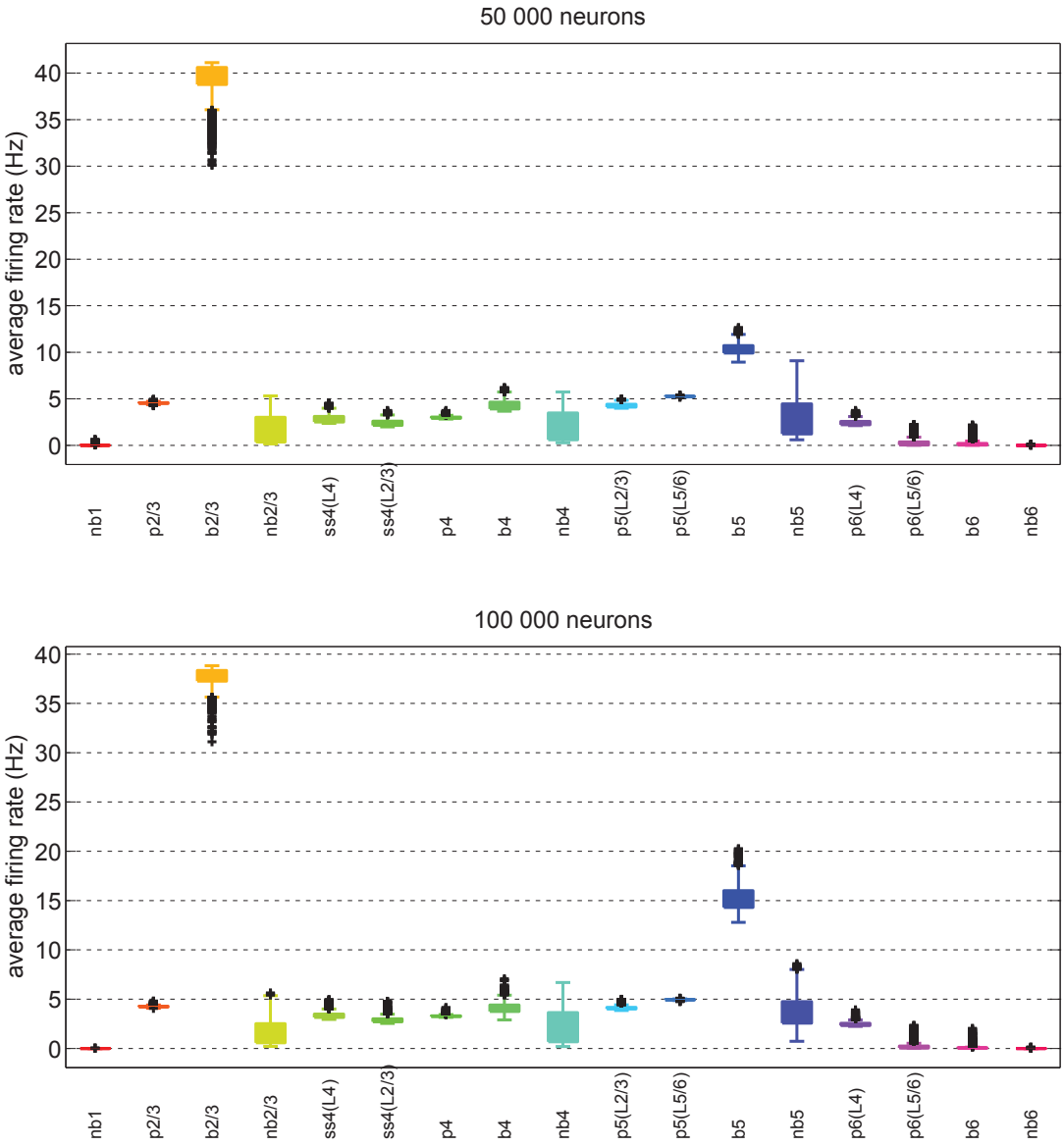

Figure 2.3: Boxplot of mean firing rate activity of individual neuronal types in networks with 10 000 neurons (first row), 50 000 neurons (second row) and 100 000 neurons (third row).

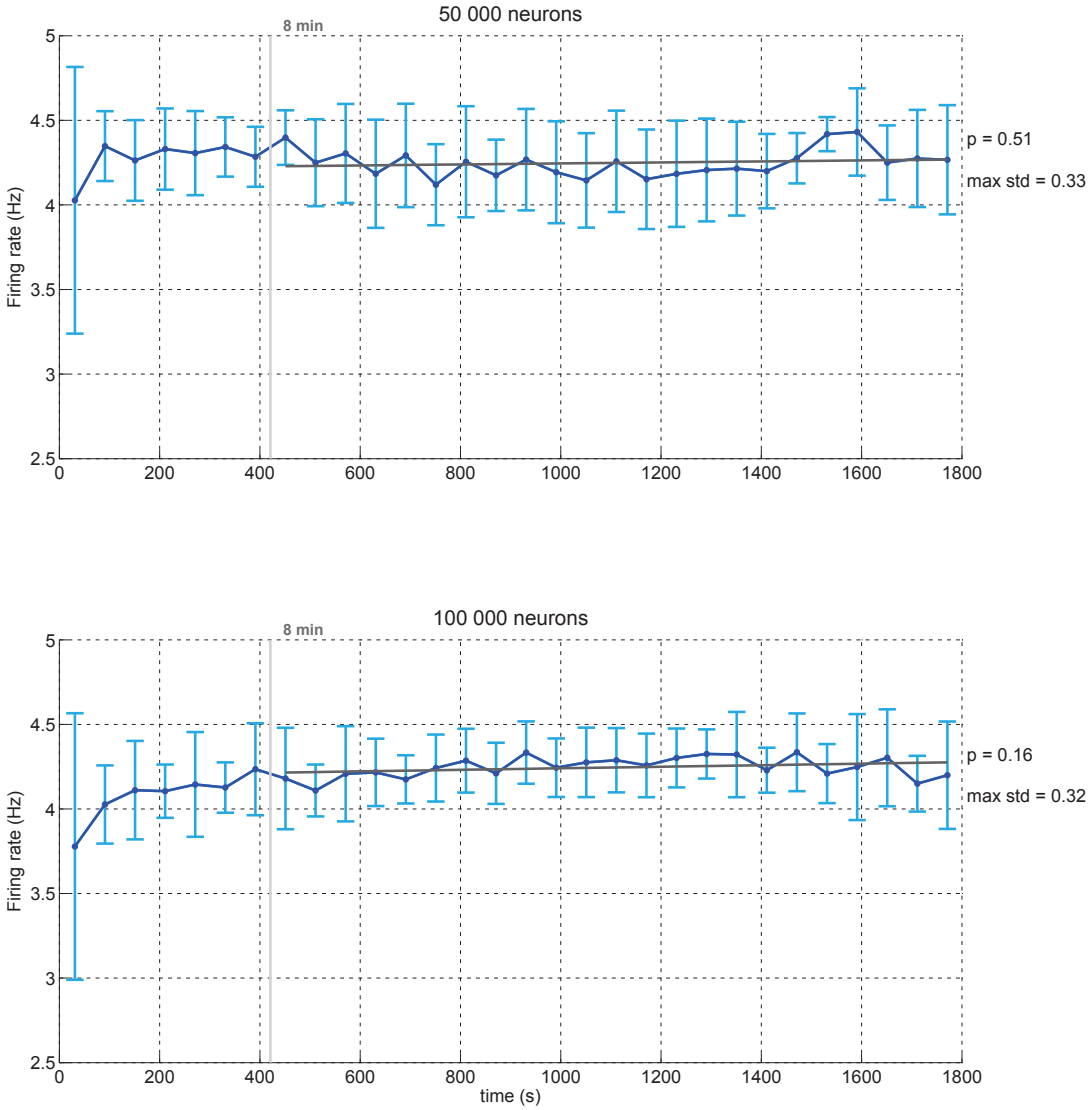

Figure 2.4: Evaluation of stability of the network activity simulated under spontaneous activity. The 30 min of simulation were binned into minute-long segments and the mean standard deviation of the network activity in these segments is plotted. After initial stabilisation (8 min), both networks reached a stereotypical dynamic state (non-significant slope and non-increasing standard deviation). To test if there was not a trend in firing rates, suggesting lack of stabilisation, a line was fitted through the 23 points of mean firing rate from 8th to 30th minute and the significance of its slope has been tested using a regression slope test. The resulting p-values and maximal standard deviations in this period are given on the right side of the graphs.

2.1.1 Evaluation of evoked activity

We also evaluated network behaviour under evoked activity using a network with 50 000 neurons which had been evolved for 12 hours with spontaneous activity (to get rid of as much randomness due to network initialisation as possible). This network was then stimulated with different intensities of noise (along with the inner spontaneous activity). We compared two intensities (0.1 and 0.5) and two durations of stimulation (20 ms and 500 ms). Each stimulation was followed by 1 s of silence and was repeated ten times. The spontaneous activity (i.e., minis) was present during the entire simulation and weights were fixed.

The propagation of the signal through the network in the z-axis is visualised in Fig. 2.5 and 2.6. The activity is gradually spread from input L4. Note the response adaptation in L4.

When comparing the four experimental conditions, both durations of the stimulus led to a similar reaction, especially in the first ca. 50 ms after the start of stimulation. After this time, the reactions in L2/3 and L5 differed (in the 500 ms stimulation, they were weaker, but longer and more gradual). The weaker stimulation led to weaker and less distinct reactions, especially in L6, but the general shape of the signal propagation was similar to the stronger stimulation propagation.

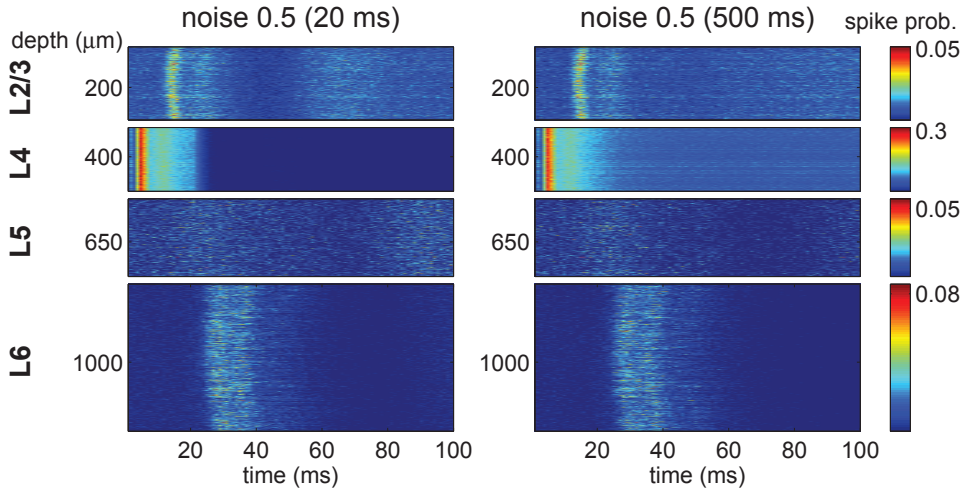

Figure 2.5: Evaluation of evoked activity (measured on 50 k network after 12 h of spontaneous activity) for stimulation with *noise0.5*. All of the values were averaged over ten stimulations. Spike probability as a function of depth and time. Each layer has its own colour-scale (but was common for both experiments).

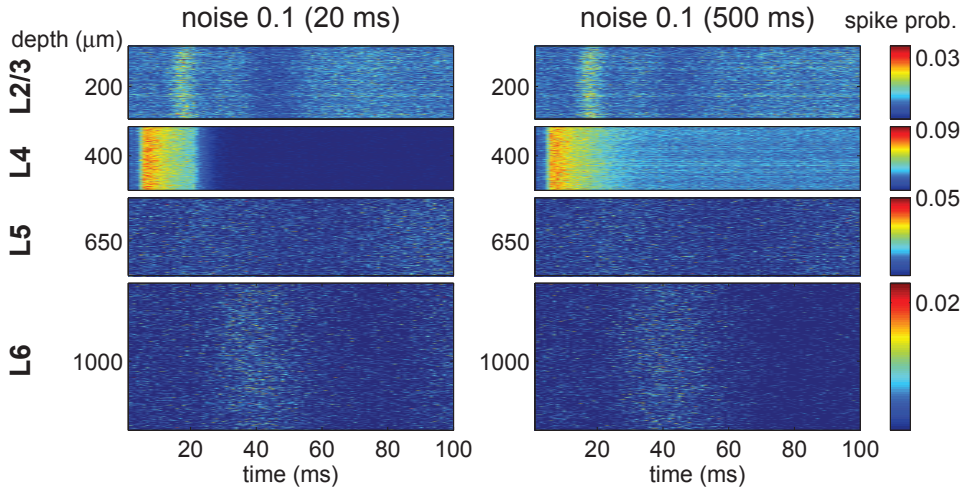

Figure 2.6: Evaluation of evoked activity (measured on 50 k network after 12 h of spontaneous activity) for stimulation with *noise0.1*. All of the values were averaged over ten stimulations. Spike probability as a function of depth and time. Each layer has its own colour-scale (but was common for both experiments).

2.1.2 I-E model of gamma oscillations

	Neuronal type	Contribution at gamma band (40–60 Hz) (%)
1	nb1	0.5
2	p2/3	3.16
3	b2/3	76.29
4	nb2/3	1.12
5	ss4(L4)	1.34
6	ss4(L2/3)	1
7	p4	1.13
8	b4	4
9	nb4	0.49
10	p5(L2/3)	1.98
11	p5(L5/6)	2.2
12	b5	4.41
13	nb5	0.9
14	p6(L4)	1.05
15	p6(L5/6)	0.17
16	b6	0.21
17	nb6	0.03

Table 2.1: Relative contribution of the populations of specific cell types to the potential oscillation at the gamma band.

2.2 Tonotopy-related experiments

This section contains additional figures depicting results from the tonotopy-related experiments: In Fig. 2.7, examples of receptive fields are shown. Figures 2.8, 2.9, 2.10 and 2.11 show spatial visualization over time, given different types of stimulation. It can be observed that the state of tonotopy is consistent over different seeds and network sizes, with the exception of the unstable state right after initialization of the network. Graphs in Fig. 2.12, 2.13, 2.14, 2.15 give the development of tonotopy over time for two different seeds and two different network sizes. In all four cases, it holds that *noise0.01* causes the highest tonotopy, *noise0.5* causes the lowest tonotopy and other types of stimulation lie between. The numerical results of tonotopy are given in Tab. 2.2, 2.3, 2.4, 2.5, 2.6 and 2.7.

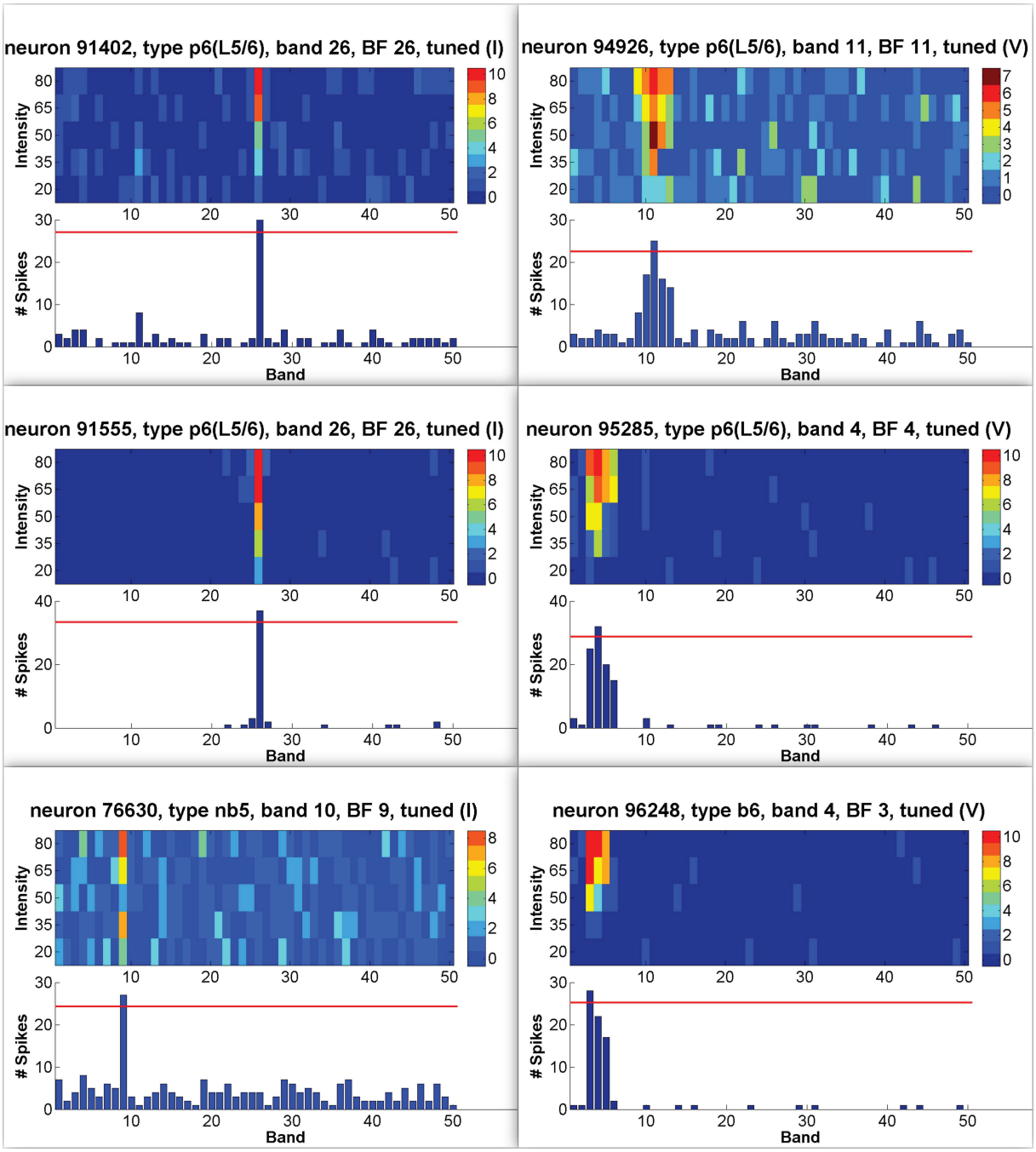

Figure 2.7: Examples of tuned neurons present in the networks, measured after 12 h of development: "I" shape (first column) and "V" shape (second column); excitatory neurons (first two rows) and inhibitory neurons (third row).

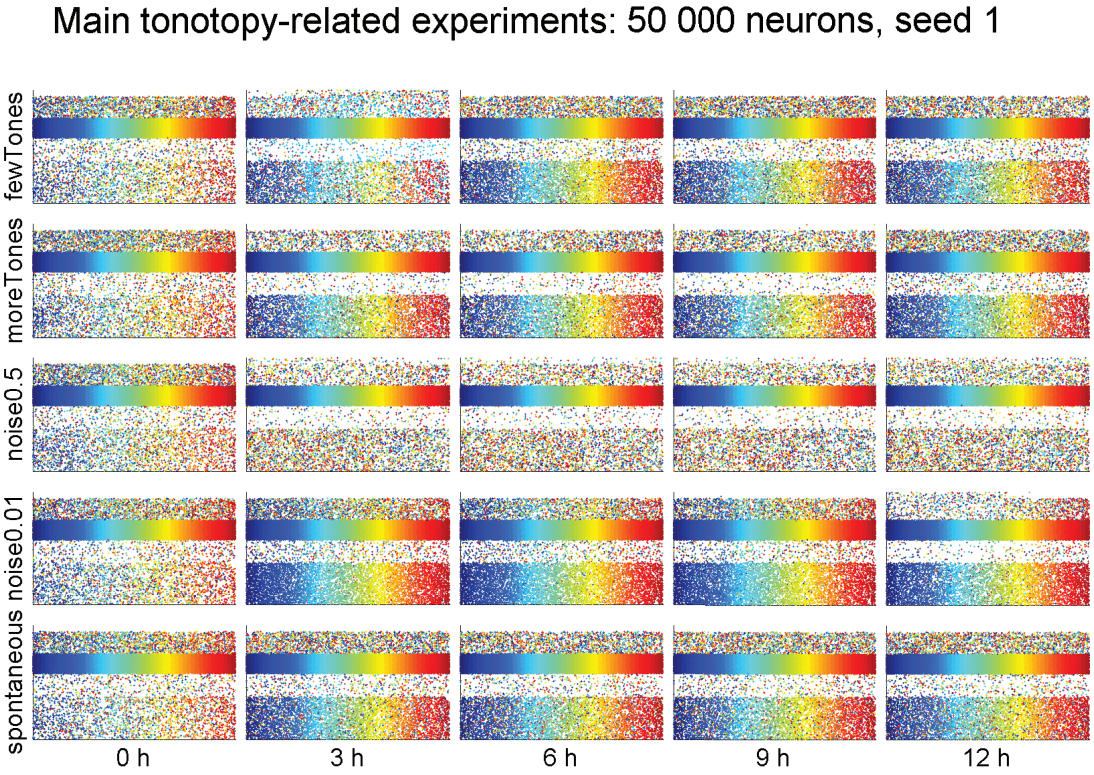

Figure 2.8: A network with 50 000 neurons, the first seed (333): a comparison of spatial visualisation of the network stimulated with five different input conditions (rows) in six time slices (columns). Only the tuned neurons are plotted, with the colour representing their best frequency.

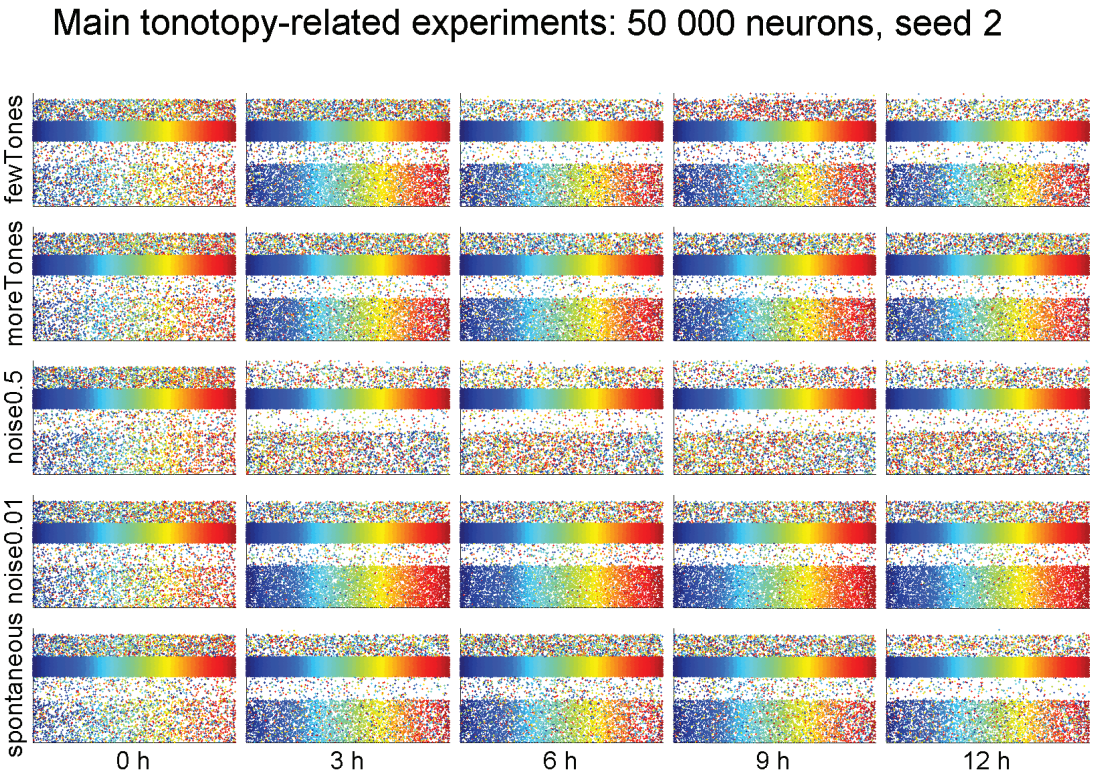

Figure 2.9: A network with 50 000 neurons, the second seed (444): a comparison of spatial visualisation of the network stimulated with five different input conditions (rows) in six time slices (columns). Only the tuned neurons are plotted, with the colour representing their best frequency.

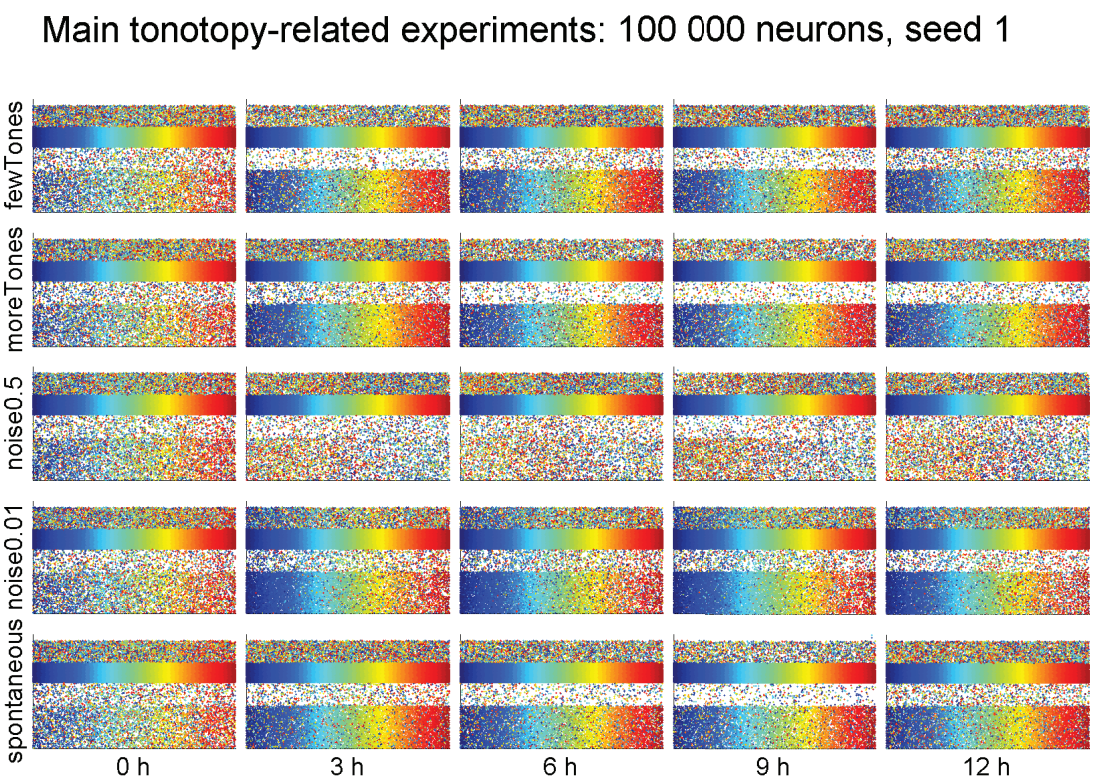

Figure 2.10: A network with 100 000 neurons, the first seed (333): a comparison of spatial visualisation of the network stimulated with five different input conditions (rows) in six time slices (columns). Only the tuned neurons are plotted, with the colour representing their best frequency.

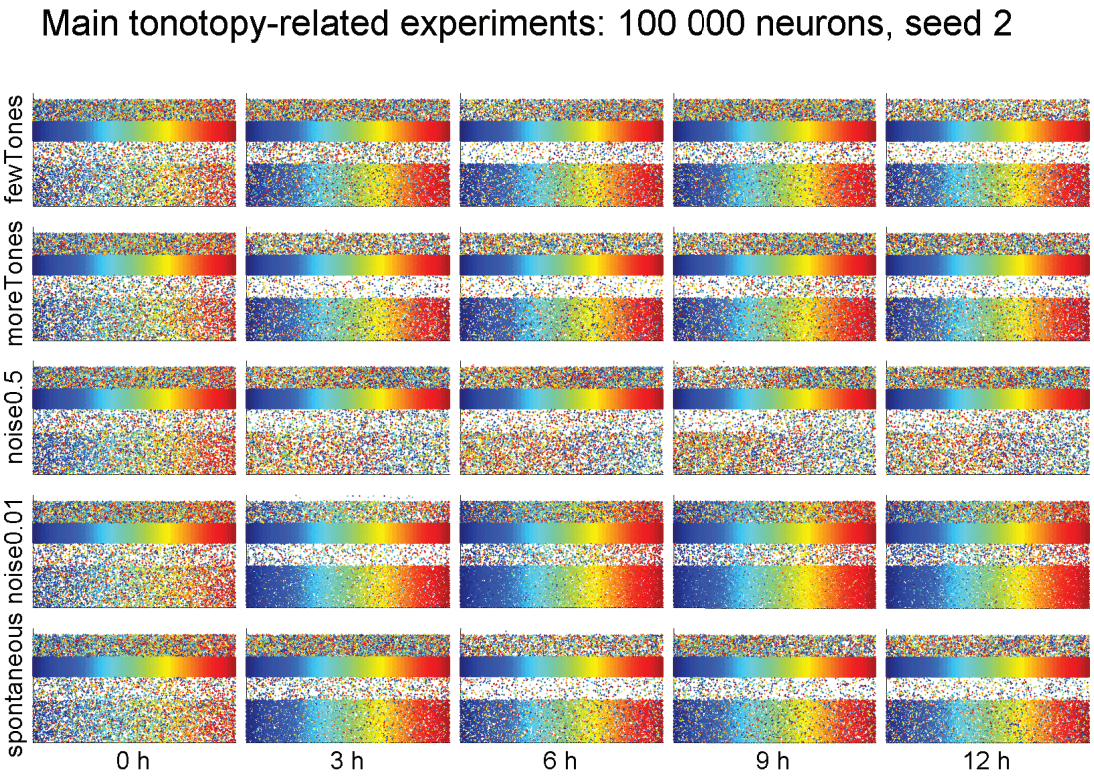

Figure 2.11: A network with 100 000 neurons, the second seed (444): a comparison of spatial visualisation of the network stimulated with five different input conditions (rows) in six time slices (columns). Only the tuned neurons are plotted, with the colour representing their best frequency.

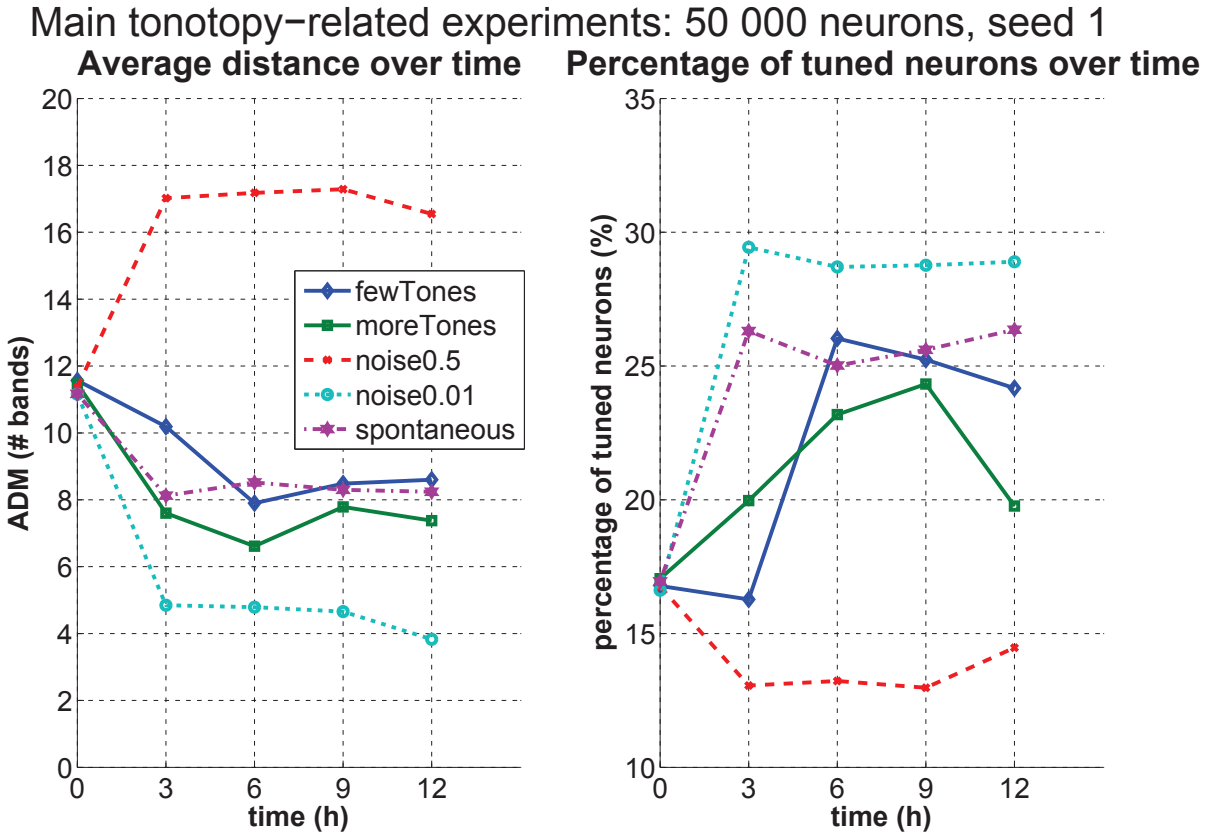

Figure 2.12: Development of tonotopy of non-input neurons over time in different input conditions for a network with 50 000 neurons and the first seed (333). Note that the lower ADM, the higher tonotopy.

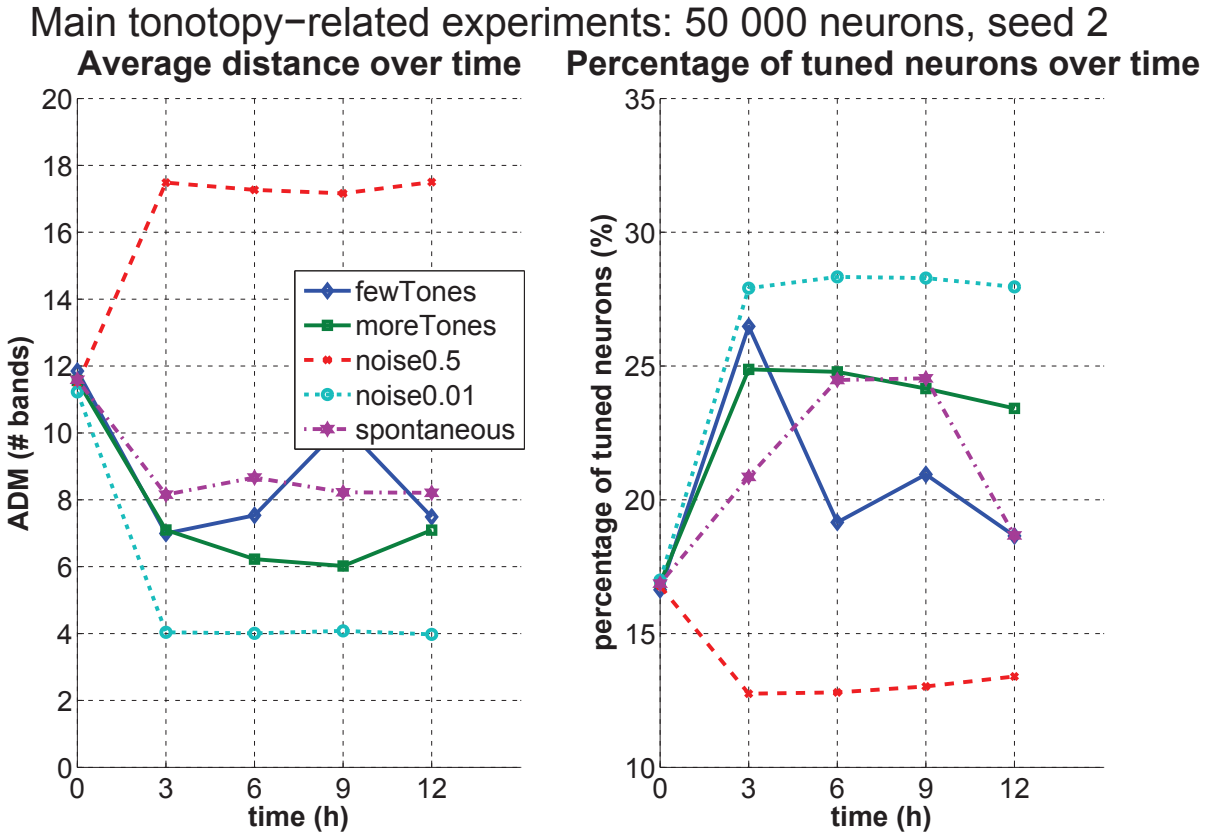

Figure 2.13: Development of tonotopy of non-input neurons over time in different input conditions for a network with 50 000 neurons and the second seed (444). Note that the lower ADM, the higher tonotopy.

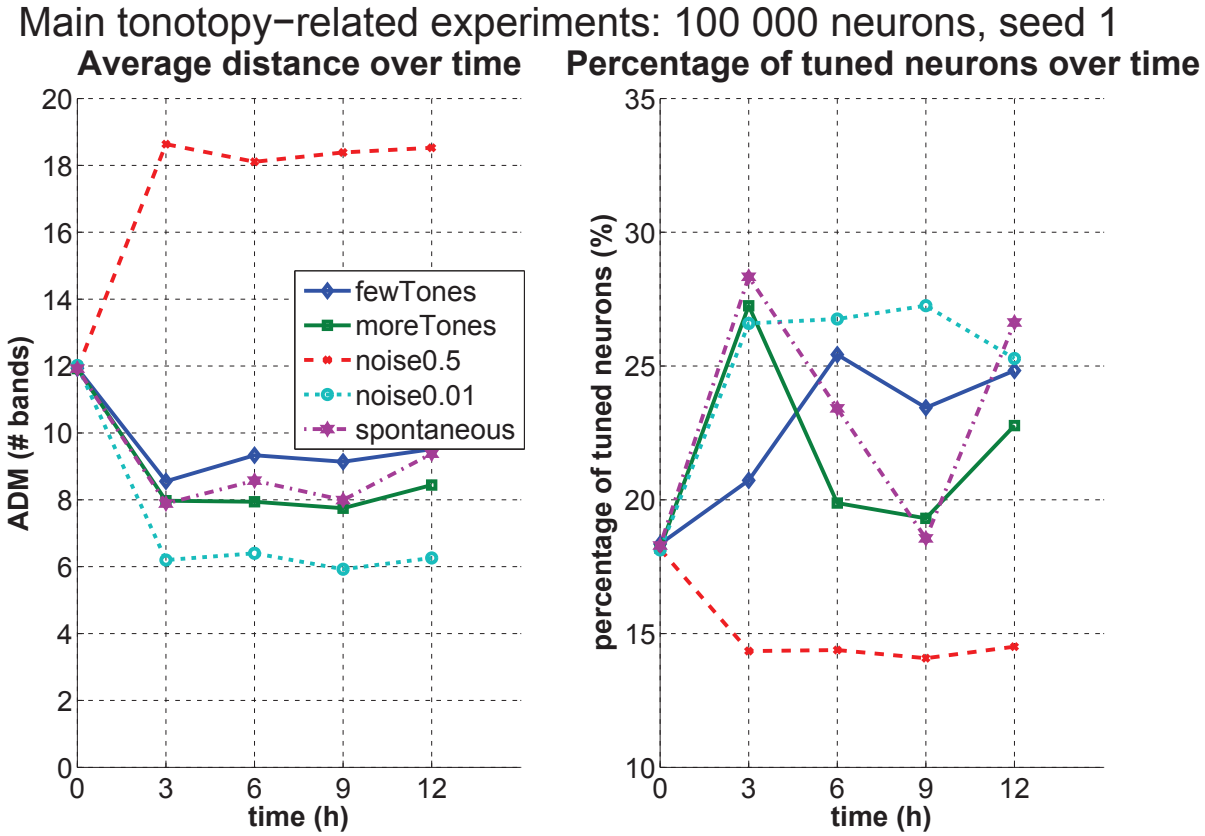

Figure 2.14: Development of tonotopy of non-input neurons over time in different input conditions for a network with 100 000 neurons and the first seed (333). Note that the lower ADM, the higher tonotopy.

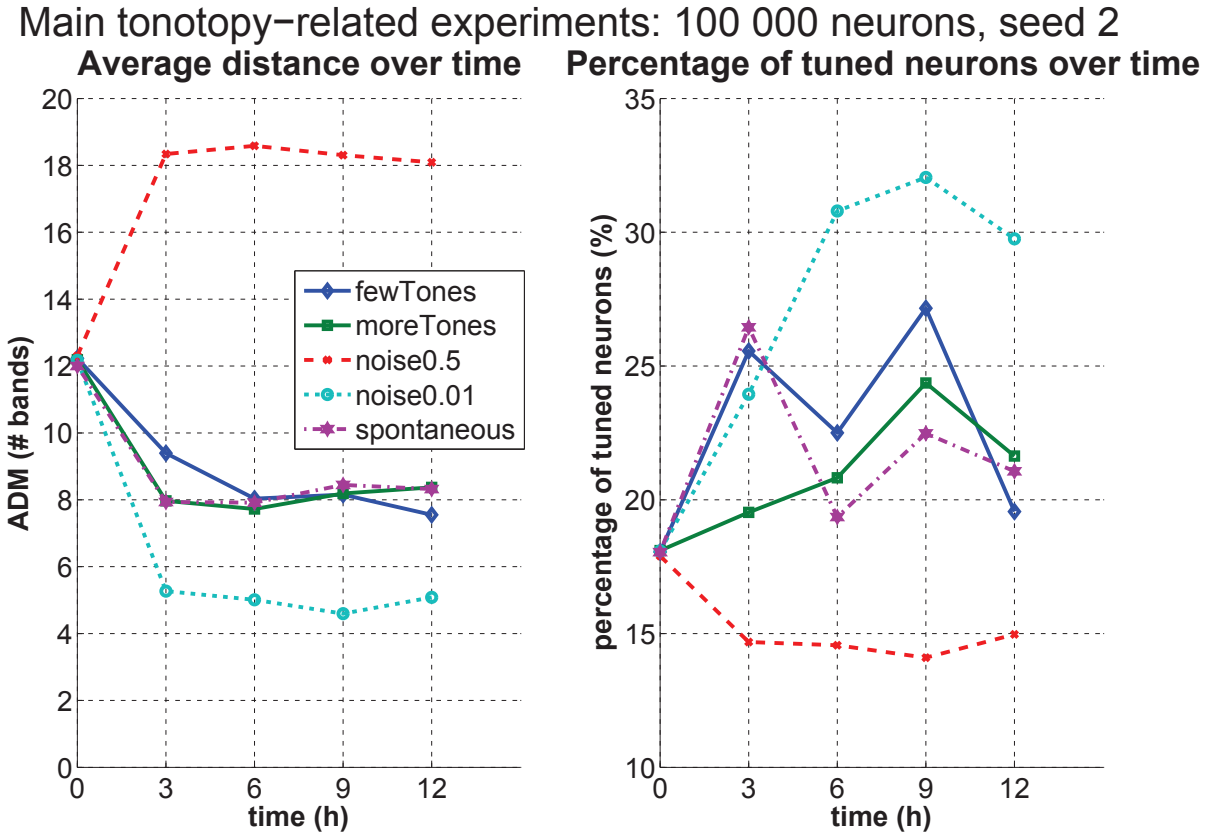

Figure 2.15: Development of tonotopy of non-input neurons over time in different input conditions for a network with 100 000 neurons and the second seed (444). Note that the lower ADM, the higher tonotopy.

		ADM			PTN		
	condition	mean	std	median	mean	std	median
1	fewTones	8.43	1.22	8.19	22.12	3.86	22.56
2	moreTones	6.98	0.64	7.09	23.06	2.06	23.79
3	noise0.5	17.18	0.30	17.22	13.21	0.55	13.04
4	noise0.01	4.28	0.41	4.06	28.54	0.52	28.52
5	spontaneous	8.31	0.19	8.23	23.98	2.76	24.78

Table 2.2: Numerical results from **50k network** computed from both seeds and all time slices except the initial one. ADM = average distance metric, PTN = percentage of tuned neurons (from all layers except L4).

		ADM			PTN		
	condition	mean	std	median	mean	std	median
1	fewTones	8.71	0.74	8.85	23.65	2.60	24.14
2	moreTones	8.04	0.27	7.97	21.95	2.75	21.23
3	noise0.5	18.37	0.20	18.36	14.45	0.30	14.45
4	noise0.01	5.59	0.68	5.60	27.80	2.80	27.01
5	spontaneous	8.31	0.51	8.16	23.29	3.59	22.95

Table 2.3: Numerical results from **100k network** computed from both seeds and all time slices except the initial one. ADM = average distance metric, PTN = percentage of tuned neurons (from all layers except L4).

***spontaneous* condition**							
		ADM			**PTN**		
	type	mean	std	median	mean	std	median
1	nb	8.44	2.42	9.30	7.62	3.54	9.09
2	b	1.54	0.39	1.51	29.03	2.72	30.22
3	p	5.97	0.35	5.94	34.82	3.08	36.03

***noise0.5* condition**							
		ADM			**PTN**		
	type	mean	std	median	mean	std	median
1	nb	18.47	1.32	18.19	4.23	1.59	3.83
2	b	10.96	0.32	10.88	19.12	1.76	18.84
3	p	17.31	0.37	17.34	20.38	0.53	20.16

***noise0.01* condition**							
		ADM			**PTN**		
	type	mean	std	median	mean	std	median
1	nb	3.32	2.95	2.38	10.08	3.51	9.97
2	b	0.89	0.26	0.79	37.22	6.84	40.05
3	p	2.59	0.40	2.58	43.14	2.79	44.00

***pureTones5* condition**							
		ADM			**PTN**		
	type	mean	std	median	mean	std	median
1	nb	8.93	3.22	9.40	8.58	6.07	8.91
2	b	1.90	1.09	1.41	30.51	2.38	30.48
3	p	6.42	1.35	6.27	32.05	5.41	32.43

***pureTones25* condition**							
		ADM			**PTN**		
	type	mean	std	median	mean	std	median
1	nb	4.94	1.88	4.11	4.04	3.04	3.78
2	b	1.19	0.15	1.17	30.53	2.58	30.86
3	p	4.92	0.69	4.86	34.62	2.43	35.41

Table 2.4: Numerical results from **50k network**, grouped by morphological neuron types (nb = inhibitory non-basket neurons, b = inhibitory basket neurons, p = excitatory pyramidal neurons); computed from both seeds and all time slices except the initial one. ADM = average distance metric, PTN = percentage of tuned neurons.

***spontaneous* condition**							
		ADM			**PTN**		
	type	mean	std	median	mean	std	median
1	nb	6.78	3.00	6.77	5.06	3.00	3.56
2	b	1.03	0.27	0.89	31.37	6.65	33.83
3	p	5.99	0.90	6.44	33.46	4.76	32.71

***noise0.5* condition**							
		ADM			**PTN**		
	type	mean	std	median	mean	std	median
1	nb	20.24	1.46	20.29	4.69	2.39	3.95
2	b	9.01	0.88	8.81	6.48	1.45	6.53
3	p	18.70	0.32	18.70	16.68	0.76	16.82

***noise0.01* condition**							
		ADM			**PTN**		
	type	mean	std	median	mean	std	median
1	nb	4.17	0.95	4.27	13.47	3.42	15.06
2	b	0.98	0.29	0.91	28.88	5.22	28.34
3	p	3.62	0.65	3.69	40.97	3.94	39.61

***pureTones5* condition**							
		ADM			**PTN**		
	type	mean	std	median	mean	std	median
1	nb	7.90	4.05	8.13	5.22	3.89	4.81
2	b	1.03	0.13	1.04	28.22	6.22	28.16
3	p	6.23	0.47	6.34	33.80	3.09	34.49

***pureTones25* condition**							
		ADM			**PTN**		
	type	mean	std	median	mean	std	median
1	nb	3.71	3.54	2.40	3.85	3.62	2.53
2	b	0.89	0.09	0.90	33.63	4.25	35.33
3	p	6.12	0.46	6.25	31.96	3.62	30.63

Table 2.5: Numerical results from **100k network**, grouped by morphological neuron types (nb = inhibitory non-basket neurons, b = inhibitory basket neurons, p = excitatory pyramidal neurons); computed from both seeds and all time slices except the initial one. ADM = average distance metric, PTN = percentage of tuned neurons.

***spontaneous* condition**							
		ADM			**PTN**		
	type	mean	std	median	mean	std	median
1	L1	15.78	0.04	15.78	0.15	0.28	0.00
2	L2/3	16.52	0.35	16.42	11.58	2.16	12.46
3	L4	0.00	0.00	0.00	100.00	0.00	100.00
4	L5	13.73	1.10	13.47	13.55	3.41	15.10
5	L6	4.70	0.33	4.65	46.48	3.75	47.60

***noise0.5* condition**							
		ADM			**PTN**		
	type	mean	std	median	mean	std	median
1	L1	18.49	1.37	18.18	11.97	4.68	10.85
2	L2/3	15.42	0.51	15.41	6.86	0.43	6.99
3	L4	0.00	0.00	0.00	100.00	0.00	100.00
4	L5	14.52	0.45	14.50	7.31	0.43	7.34
5	L6	18.07	0.43	18.09	24.82	0.89	24.73

***noise0.01* condition**							
		ADM			**PTN**		
	type	mean	std	median	mean	std	median
1	L1	8.74	9.54	8.74	2.46	6.91	0.00
2	L2/3	12.30	0.93	12.78	11.03	2.35	10.28
3	L4	0.00	0.00	0.00	100.00	0.00	100.00
4	L5	9.91	0.62	9.95	14.88	3.90	13.16
5	L6	1.73	0.37	1.67	58.13	4.09	59.03

***pureTones5* condition**							
		ADM			**PTN**		
	type	mean	std	median	mean	std	median
1	L1	18.14	3.57	16.92	4.84	10.23	0.20
2	L2/3	15.97	1.32	15.68	10.24	2.79	10.78
3	L4	0.00	0.00	0.00	100.00	0.00	100.00
4	L5	14.94	2.61	14.54	11.86	4.11	11.76
5	L6	5.08	1.33	4.86	43.40	6.39	43.97

***pureTones25* condition**							
		ADM			**PTN**		
	type	mean	std	median	mean	std	median
1	L1	15.33	0.00	15.33	0.05	0.14	0.00
2	L2/3	15.18	1.02	15.39	10.47	1.67	10.93
3	L4	0.00	0.00	0.00	100.00	0.00	100.00
4	L5	13.96	1.79	13.85	9.89	2.49	9.52
5	L6	3.74	0.52	3.72	47.16	2.68	47.66

Table 2.6: Numerical results from **50k network**, grouped by layers, computed from both seeds and all time slices except the initial one. ADM = average distance metric, PTN = percentage of tuned neurons.

***spontaneous* condition**							
		ADM			**PTN**		
	type	mean	std	median	mean	std	median
1	L1	25.00	14.85	25.00	0.03	0.06	0.00
2	L2/3	16.56	0.46	16.56	11.94	3.15	11.64
3	L4	0.00	0.00	0.00	100.00	0.00	100.00
4	L5	15.51	1.41	15.95	11.49	3.54	10.57
5	L6	4.45	0.67	4.78	45.12	4.56	44.83

***noise0.5* condition**							
		ADM			**PTN**		
	type	mean	std	median	mean	std	median
1	L1	26.00	12.26	25.50	0.12	0.27	0.00
2	L2/3	17.68	0.18	17.70	13.10	1.06	13.42
3	L4	0.00	0.00	0.00	100.00	0.00	100.00
4	L5	17.13	0.44	17.17	13.97	2.29	13.44
5	L6	19.50	0.32	19.57	17.12	1.23	16.80

***noise0.01* condition**							
		ADM			**PTN**		
	type	mean	std	median	mean	std	median
1	L1	15.89	0.00	15.89	0.16	0.44	0.00
2	L2/3	11.62	0.68	11.88	13.95	1.81	14.44
3	L4	0.00	0.00	0.00	100.00	0.00	100.00
4	L5	10.89	0.67	10.88	19.44	3.91	21.26
5	L6	2.46	0.61	2.63	52.32	5.09	49.99

***pureTones5* condition**							
		ADM			**PTN**		
	type	mean	std	median	mean	std	median
1	L1	NaN	NaN	NaN	0.00	0.00	0.00
2	L2/3	16.53	0.62	16.59	12.49	2.56	13.14
3	L4	0.00	0.00	0.00	100.00	0.00	100.00
4	L5	15.17	0.79	15.26	12.60	3.90	12.28
5	L6	4.75	0.43	4.93	44.52	2.76	44.42

***pureTones25* condition**							
		ADM			**PTN**		
	type	mean	std	median	mean	std	median
1	L1	27.83	21.33	30.00	0.04	0.06	0.00
2	L2/3	16.09	0.36	16.08	10.62	2.39	9.98
3	L4	0.00	0.00	0.00	100.00	0.00	100.00
4	L5	15.64	1.40	16.00	10.26	3.60	8.27
5	L6	4.51	0.33	4.59	43.81	3.35	43.10

Table 2.7: Numerical results from **100k network**, grouped by layers, computed from both seeds and all time slices except the initial one. ADM = average distance metric, PTN = percentage of tuned neurons.

Bibliography

Evgeniy Bart, Shaowen Bao, and David Holcman. Modeling the spontaneous activity of the auditory cortex. *Journal of Computational Neuroscience*, **19**(3):357–378, 2005. ISSN 0929-5313.

Michael Beierlein, Jay R. Gibson, and Barry W. Connors. Two dynamically distinct inhibitory networks in layer 4 of the neocortex. *Journal of Neurophysiology*, **90**(5):2987–3000, 2003. ISSN 0022-3077.

Tom Binzegger, Rodney J. Douglas, and Kevan A. C. Martin. A quantitative map of the circuit of cat primary visual cortex. *The Journal of Neuroscience*, **24**(39):8441–8453, 2004. ISSN 0270-6474.

Michael Chrostowski, Le Yang, Hugh R Wilson, Ian C Bruce, and Suzanna Becker. Can homeostatic plasticity in deafferented primary auditory cortex lead to travelling waves of excitation? *Journal of Computational Neuroscience*, **30**(2):279–299, 2011. ISSN 0929-5313.

Barry W. Connors and Michael J. Gutnick. Intrinsic firing patterns of diverse neocortical neurons. *Trends in Neurosciences*, **13**(3):99–104, 1990. ISSN 0166-2236.

Diego Contreras. Electrophysiological classes of neocortical neurons. *Neural Networks*, **17**(5):633–646, 2004. ISSN 0893-6080.

David E. Goldberg. Genetic algorithms in search, optimization, and machine learning. *Addion wesley*, 1989.

Eugene M. Izhikevich. Simple model of spiking neurons. *IEEE Transactions on Neural Networks*, **14**(6): 1569–1572, 2003. ISSN 1045-9227.

Eugene M. Izhikevich. Which model to use for cortical spiking neurons? *IEEE Transactions on Neural Networks*, **15**(5):1063–1070, 2004. ISSN 1045-9227.

Eugene M. Izhikevich. Polychronization: Computation with spikes. *Neural Computation*, **18**(2):245–282, 2006. ISSN 0899-7667.

Eugene M. Izhikevich. Solving the distal reward problem through linkage of stdp and dopamine signaling. *Cerebral Cortex*, **17**(10):2443–2452, 2007. ISSN 1047-3211.

Eugene M. Izhikevich and Gerald M. Edelman. Large-scale model of mammalian thalamocortical systems. *Proceedings of the National Academy of Sciences*, **105**(9):3593–3598, 2008. ISSN 0027-8424.

Yasuo Kawaguchi. Physiological subgroups of nonpyramidal cells with specific morphological characteristics in layer ii/iii of rat frontal cortex. *The Journal of Neuroscience*, **15**(4):2638–2655, 1995. ISSN 0270-6474.

Yasuo Kawaguchi and Yoshiyuki Kubota. Gabaergic cell subtypes and their synaptic connections in rat frontal cortex. *Cerebral Cortex*, **7**(6):476–486, 1997. ISSN 1047-3211.

Robert B. Levy and Alex D. Reyes. Spatial profile of excitatory and inhibitory synaptic connectivity in mouse primary auditory cortex. *The Journal of Neuroscience*, **32**(16):5609–5619, 2012. ISSN 0270-6474.

Henry Markram, Maria Toledo-Rodriguez, Yun Wang, Anirudh Gupta, Gilad Silberberg, and Caizhi Wu. Interneurons of the neocortical inhibitory system. *Nature Reviews Neuroscience*, **5**(10):793–807, 2004. ISSN 1471-003X.

Jiri Matousek and Jaroslav Nesetril. *Invitation to discrete mathematics*. Oxford University Press, 1998. ISBN 0198502079.

Carsten Mehring, Ulrich Hehl, Masayoshi Kubo, Markus Diesmann, and Ad Aertsen. Activity dynamics and propagation of synchronous spiking in locally connected random networks. *Biological Cybernetics*, **88**(5):395–408, 2003. ISSN 0340-1200.

Eilen Nordlie, Marc-Oliver Gewaltig, and Hans Ekkehard Plesser. Towards reproducible descriptions of neuronal network models. *PLoS Computational Biology*, **5**(8):e1000456, 2009. ISSN 1553-7358.

Bethany Percha, Rhonda Dzakpasu, Michal Zochowski, and Jack Parent. Transition from local to global phase synchrony in small world neural network and its possible implications for epilepsy. *Physical Review E*, **72**(3):031909, 2005.

Marketa Popelova. *Software tool for modelling coding and processing of information in auditorycortex of mice*. Master Thesis, Charles University in Prague, Faculty of Mathematics and Physics, 2013. URL `http://www.marketa.najevisti.info/dokumenty/master_thesis.pdf`.

Misha V. Tsodyks and Terrence Sejnowski. Rapid state switching in balanced cortical network models. *Network: Computation in Neural Systems*, **6**(2):111–124, 1995. ISSN 0954-898X.

Imre Vida, Marlene Bartos, and Peter Jonas. Shunting inhibition improves robustness of gamma oscillations in hippocampal interneuron networks by homogenizing firing rates. *Neuron*, **49**(1):107–118, 2006. ISSN 0896-6273.